Univerzita Karlova v Praze
Přírodovědecká fakulta

Studijní program: Vývojová a buněčná biologie
Studijní obor: Vývojová biologie

Mgr. Monika Šídová

Časo-prostorové utváření molekulárních gradientů v časném embryonálním vývoji *Xenopus laevis*

Formation of spatio-temporal molecular gradients in early embryonic development of *Xenopus laevis*

Disertační práce

Školitel: RNDr. Tereza Tlapáková, Ph.D.
Konzultant: Mgr. Radek Šindelka, Ph.D.

Praha, 2015

Prohlášení

Prohlašuji, že jsem závěrečnou práci zpracovala samostatně a že jsem uvedla všechny použité informační zdroje a literaturu. Tato práce ani její podstatná část nebyla předložena k získání jiného nebo stejného akademického titulu.

V Praze, 9.6. 2015

Podpis

Poděkování

Na tomto místě bych chtěla poděkovat všem, kteří mi během studia pomáhali a podporovali mě. Poděkování patří především mým školitelům RNDr. Tereze Tlapákové, Ph.D. a Mgr. Radku Šindelkovi, Ph.D. za odborné vedení práce, ochotu, trpělivost, cenné rady a zkušenosti, které se mi snažili předat po celou dobu vypracovávání této disertační práce. Poděkování si zaslouží členové kolektivu Laboratoře genové exprese, Biotechnologický ústav AV ČR, a Laboratoře vývojové biologie, Přírodovědecká fakulta UK, kteří po celou dobu vytvářeli příjemné pracovní prostředí a přátelskou atmosféru. Na závěr patří velké poděkování mé rodině a nejbližším, kteří mě celou dobu mého studia podporovali a vždy mi byli cennou oporovou v jakékoliv životní situaci.

Abstrakt

Detailní pochopení vývoje nového jedince zavisí na objasnění časo-prostorových mechanismů, které určují tělní plán. Z tohoto důvodu klíčovou otázkou časného embryonálního vývoje obratlovců stále zůstává, kdy a jak dochází k determinaci a diferenciaci jednotlivých buněk, což posléze vede ke specifikaci tělní osové polarity a založení základů všech orgánů a tkání. Odpověď na tuto otázku přinese nové možnosti využití nejen pro primární výzkum, ale i pro obor aplikované medicíny.

Hlavní cíl předkládané disertační práce spočíval ve stanovení časo-prostorových molekulárních gradientů buněčných determinantů v průběhu časného embryonálního vývoje. Jako modelový organismus byla zvolena africká drápkatá žába, druh *Xenopus laevis*, která disponuje dostatečně velkými oocyty a vnější embryogenezí. Vzhledem k pozdní aktivaci embryonálního genomu se předpokládá, že stěžejní mechanismus počáteční determinace buněk závisí na nerovnoměrné lokalizaci maternálních faktorů uvnitř oocytu a jejich asymetrické distribuci do dceřiných blastomer v průběhu rýhování. Pomocí metody qPCR tomografie byly identifikovány dva hlavní lokalizační gradienty s preferencí buď v animální, nebo vegetativní hemisféře zralého oocytu. Tyto gradienty se shodovaly jak pro maternální mRNA, tak i pro miRNA molekuly. U maternální mRNA navíc došlo k rozlišení dvou vegetativních podskupin s odlišným profilem gradientu. Determinanty zárodečné plazmy vykazovaly strmý gradient ve vegetativním pólu, zatímco ostatní vegetativní transkripty měly pozvolný gradient. Potvrzena byla i asymetrická distribuce maternální mRNA z oocytu do jednotlivých blastomer od vývojového stádia 8 buněk po 32 buněčné embryo, kde animální blastomery vykazovaly jiné zastoupení transkriptů než vegetativní blastomery. V jednotlivých blastomerách nebyl nalezen gradient mRNA, který by odpovídal specifikaci dorzo-ventrální a pravo-levé tělní osy během časného rýhování embrya.

Souhrnné výsledky předkládané práce představují první krok k sestavení časo-prostorové mapy klíčových biomolekul, které se podílejí na určení tělní osové polarity a tělního plánu během časného embryonálního vývoje obratlovců.

Abstract

Clarifying the underlying spatio-temporal mechanisms that determine body pattern is important for detailed understanding of embryonic development. A crucial question of vertebrate embryogenesis remains: when and how are single blastomeres determined for differentiation that subsequently leads to body axes specification and the formation of different tissues and organs? The answer to this question will be beneficial for primary research as well as in the field of applied medicine.

The main aim of the presented thesis was to study spatio-temporal molecular gradients of cell fate determinants during early embryonic development. The African clawed frog *Xenopus laevis* was used as a model organism because of their large size of oocytes and external embryonic development. Due to late activation of embryonic transcription, a crucial mechanism of early blastomeres determination is dependent on asymmetric localization of maternal factors within oocyte and their uneven distribution into single blastomeres during early cell division. Two main localization patterns were identified along the animal-vegetal axis of the mature *Xenopus* oocyte using qPCR tomography. The localization gradient with preference in either animal or vegetal hemisphere was found for maternal mRNA as well as miRNAs. Moreover, two vegetal subgroups were distinguished for maternal mRNAs, which differ in gradient pattern. Germ plasm determinants showed a very steep gradient towards the vegetal pole, whereas the other vegetal transcripts had a less steep spatial gradient towards the pole. We demonstrated that the animal-vegetal asymmetry within the mature oocyte is transferred to the single blastomeres of 8, 16 and 32-cell stage embryos during early cell division. No asymmetry of maternal mRNA distribution was found among single blastomeres that may be ascribed to the dorso-ventral specification and/or left-right body axis formation during early embryogenesis.

Summarizing the results of this thesis represents the first step of creating the spatio-temporal map of crucial biomolecules involved in body axis polarity formation and body pattern specification during early embryonic development in *Xenopus laevis*.

Obsah

1. Úvod

Nerovnoměrná distribuce buněčných determinantů představuje základní biologickou strategii, jak produkovat rozdílné buňky během buněčného dělení. Toto asymetrické dělení je pozorováno u mnoha biologických procesů, které zahrnují například diferenciaci a obnovu kmenových buněk (Blanpain *et al.*, 2004; Knoblich, 2008), nádorové bujení (Knoblich, 2010; Shahriyari and Komarova, 2013) či vývoj embrya (Schatten and Sun, 2010; Pereira and Yamashita, 2011). Z pohledu časné embryogeneze představuje vznik buněčné polarity, jejímž výsledkem dochází k asymetrickému dělení, zásadní mechanismus určení tělní osové polarity a celého tělního plánu.

Asymetrická lokalizace maternálních determinantů v konkrétních podoblastech uvnitř oocytu představuje vysoce konzervovanou strategii, která umožňuje nerovnoměrné rozdělení těchto maternálních biomolekul do dceřiných buněk během časného rýhování embrya. Nejenom přítomnost či absence konkrétního determinantu v buňce, ale i jeho množství může posléze ovlivnit celou řadu dalších genů nebo i celé signální dráhy. Bylo ukázáno, že již třínásobný rozdíl v koncentraci buněčného determinantu může vést ke kompletně odlišnému buněčnému osudu (Smith and Gurdon, 2004). Obecně se předpokládá, že mezi klíčové maternální determinanty buněčného osudu patří zejména mRNA (messenger ribonucleic acid) a proteiny. Maternálně uložená informace přetrvává u naprosté většiny obratlovců ve vyvíjejícím se embryu až do chvíle aktivace embryonálního genomu. U žab rodu *Xenopus* dochází ke spuštění embryonální transkripce až ve stádiu střední blastuly (MBT stage, mid-blastula transition), tj. v průběhu 12. buněčného dělení po oplození, kdy embryo obsahuje již tisíce buněk. Rýhováním vznikají kompletně oddělené blastomery, které nejsou propojené cytoplazmatickými můstky, a proto se maternální determinanty nemohou volně přesouvat mezi vzniklými dceřinými buňkami. Z tohoto důvodu je určení lokalizace maternálních determinantů uvnitř oocytu a jejich distribuce do dceřiných buněk v průběhu rýhování zcela zásadní pro objasnění mechanismů, které specifikují základní tělní osy a obecně tělní plán embrya. První osovou asymetrii u *Xenopus laevis* lze pozorovat ještě opřed oplozením. V průběhu

oogeneze dochází k vytvoření animálně-vegetativní osy, která odpovídá hlavo-ocasní tělní ose. Další dvě tělní osy jsou určené v průběhu časného embryonálního vývoje. První rýha rozděluje embryo na budoucí pravou a levou část, kdežto druhá rýha určuje dorzo-ventrální (hřbeto-břišní) tělní osu.

V předkládané dizertační práci byla pro určení lokalizačních profilů maternální mRNA a miRNA (micro ribonucleic acid; microRNA) uvnitř zralého oocytu *Xenopus laevis* použita metoda RT-qPCR (reverse transcriptase quantitative polymerase chain reaction) tomografie. Tato metoda umožňující měření prostorové lokalizace transkriptů podél osy zájmu uvnitř biologického vzorku byla zcela poprvé aplikována v Laboratoři genové exprese Biotechnologického ústavu Akademie Věd ČR. Kvantifikace miRNA byla provedena pomocí unikátní metody zvané RT-miQPCR (reverse transcriptase miRNA quantitative polymerase chain reaction) ve spolupráci s Dr. Vladimírem Benešem a Dr. Mirco Castoldi (EMBL Genomics Core Facility, Heidelberg, Německo) (Benes *et al.*, 2015). Tato metoda využívá univerzální adaptor neboli miLINKER, který prodlouží 3´ konec jednovláknové RNA. Toto prodloužení umožní přepis miRNA do cDNA a posléze i její kvantifikaci standardní qPCR metodou (quantitative polymerase chain reaction).

2. Cíle disertační práce

Cílem disertační práce bylo studium časo-prostorové lokalizace klíčových maternálních biomolekul, které zajišťují determinaci a diferenciaci jednotlivých blastomer v průběhu časného embryonálního vývoje. Modelovým organismem byla zvolena africká drápkatá žába, druh *Xenopus laevis*.

Stanovené cíle:

1. Stanovit lokalizační profily maternálních mRNA podél animálně-vegetativní osy zralého oocytu *Xenopus laevis* pomocí vysokorozlišovací qPCR tomografie.

2. Určit distribuci maternálních mRNA do jednotlivých blastomer v průběhu časného rýhování se zaměřením na specifikaci animálně-vegetativní, dorzo-ventrální a pravo-levé tělní osy.

3. Popsat lokalizační profily regulačních molekul miRNA podél animálně-vegetativní osy zralého oocytu *Xenopus laevis*.

4. Ověřit vliv teplotní degradace a enzymatické degradace *post mortem* na kvalitu vzorků RNA.

5. Vyhodnotit základní faktory, které ovlivňují efektivitu pre-amplifikační reakce, jenž je nezbytná pro kvantifikaci genové exprese prostřednictvím vysokokapacitního qPCR BioMark^{TM} systému (Fluidigm).

3. Literární přehled

3.1. *Xenopus* – modelový organismus

V současné době představují obojživelníci rodu *Xenopus* jeden z nejvýznamnějších modelových organismů vývojové biologie. V porovnání s ostatními modelovými organismy embryonálního vývoje obratlovců nabízejí hned několik nesporných výhod, které je činí unikátními. Hlavními přednostmi oproti savčímu modelu je bezpochyby velký počet oocytů ve snůšce (řádově tisíce), vnější oplození a následný, již od první rýhy dobře pozorovatelný embryonální vývoj. Z hlediska mikromanipulací mezi výhody patří dostatečná velikost oocytů a embryí, které upřednostňují tyto obojživelníky před myším modelem (*Mus musculus*) (Beck and Slack, 2001). Dalším modelem z pohledu embryologie je Dánio pruhované (*Danio rerio*), které vykazuje podobné výhody jako žáby rodu *Xenopus*. Avšak z hlediska mikromanipulací a mikroinjikací do blastomer vykazují embrya Dánia značnou křehkost, čímž dochází k výrazné redukci úspěšnosti tohoto typu manipulací (Hirsch *et al.*, 2002). Oproti tomu embrya žab rodu *Xenopus* disponují nezvykle vysokou regenerační schopností a navíc po strávení části žloutkových granul se ve stádiu plovacího pulce stávají transparentními (okolo vývojového stádia 35). Průhlednost embryí poté umožňuje využívání fluorescenčních reportérových genů jako visuálních markerů během studia vývojových procesů a signálních kaskád.

3.1.1. Význam rodu *Xenopus*

Význam obojživelníků rodu *Xenopus* je podtrhnut faktem, že v souvislosti se studium tohoto modelového organismu byly uděleny dvě Nobelovy ceny. Roku 1935 získal Nobelovu cenu v oboru fyziologie a lékařství německý zoolog Hans Spemann za objev dorzálního rtu blastoporu u obojživelníků, též označovaný jako „Spemannův organizátor“. Organizátor představuje klíčovou oblast gastrulace a diferenciace buněk všech tří zárodečných listů (Sander and Faessler, 2001). Funkčně stejné struktury se utvářejí v časném embryonálním vývoji u všech obratlovců. U savců se tato oblast nazývá Hensenův uzel a u ptáků embryonální štít

(Boettger *et al.*, 2001; Viebahn, 2001). Dalším významným nositelem Nobelovy ceny za fyziologii a lékařství se stal v roce 2012 britský vývojový biolog Sir John Gurdon, který v 50. letech 20. století studoval přenos jader somatických buněk. Gurdon *et al.* (1958) naklonoval 10 pulců *Xenopus laevis* z jader střevních buněk, které vložil do enukleovaných zralých oocytů. Dokázal, že jádra diferencovaných buněk jsou schopná se ve vhodném prostředí reprogramovat do stádia pluripotentní kmenové buňky (Gurdon, 1962).

3.1.2. *Xenopus laevis* vs. *Xenopus tropicalis*

Obecně se *Xenopus* řadí mezi drápkaté žáby, které pocházejí z mokřad a bažin střední a jižní Afriky. Systematicky spadají do čeledi *Pipidae*, kde je rozlišováno několik rodů. Drápkaté žáby jsou pak dle ploidie jednotlivých druhů přiřazovány ke dvěma rodům. První z nich se označuje *Silurana* a zahrnuje diploidní druh *Silurana tropicalis*, častěji označovaný jako *Xenopus tropicalis* (drápatka tropická). Druhý rod *Xenopus* zahrnuje většinu tetraploidních, oktopoidních a dodekaploidních druhů, včetně druhu *Xenopus laevis* (drápatka vodní) (Evans *et al.*, 2004). Evoluční oddělení těchto dvou rodů proběhlo zhruba před 30 miliony lety (Bisbee *et al.*, 1977). Dnes jsou oba dva druhy vnímány jako klíčové modelové organismy experimentální biologie, avšak jejich využití se liší v závislosti na jejich genomu, generační době a velikosti (Tab. 1.). *X. tropicalis* představuje diploidní druh s 10 páry chromozomů, které lze rozdělit do šesti morfologicky odlišných skupin (Tymowska, 1973). Menší velikost dospělých jedinců (dorůstají velikosti 4 - 5 cm), menší velikost oocytů (0,7 – 0,8 mm) a kratší generační doba (4 - 6 měsíců) předurčují tento druh k využití pro multigenerační genetické a genomické studie (Amaya *et al.*, 1998; Hirsch *et al.*, 2002). Vzhledem k diploidnímu genomu lze snadněji využít metody transgeneze či genetického mapování (Goda *et al.*, 2006). Oproti tomu druh *X. laevis* je allotetraploidní s duplikovaným genomem obsahující čtyři kopie většiny genů (Thiebaud and Fischberg, 1977). Karyotyp tvoří 18 párů chromozomů, které jsou rozděleny do sedmi morfologických skupin a v průběhu meiózy tvoří tyto chromozomy bivalenty (Tymowska and Fischberg, 1973). Relativně dlouhá

generační doba (1 – 2 roky) společně s tetraploidním genomem činí tento druh nevhodným pro genetické analýzy a transgenní postupy. Nicméně větší velikost dospělých jedinců (dorůstají do velikosti kolem 10 cm), větší rozměry nakladených oocytů (1 – 1,3 mm) a posléze i větší velikost vyvíjejících se embryí zvýhodňují tento druh jako modelový organismus pro experimentální embryologii a výzkum časného embryonálního vývoje (Hirsch *et al.*, 2002).

	Xenopus tropicalis	***Xenopus laevis***
Ploidie	Diploid	Allotetraploid
Počet chromozomů (n)	10	18
Velikost genomu	1,7 x 10^9 bp	3,1 x 10^9 bp
Velikost dospělce	4 – 5 cm	10 cm
Generační doba	3 – 5 měsíců	8 – 12 měsíců a déle
Velikost oocytů	0,7 – 0,8 mm	1 – 1,3 mm
Počet oocytů ve snůšce	300 – 1000	1000 - 9000

Tab. 1. Základní údaje popisující druhy *Xenopus tropicalis* a *Xenopus laevis* (upraveno podle Hirsch *et al.*, 2002).

3.1.3. *Xenopus laevis* (drápatka vodní)

Druh *Xenopus laevis* (Obr. 1.) se do popředí zájmů dostal ve 30. letech 20. století, kdy bylo zjištěno, že lze u samice stimulovat ovulaci oocytů lidským choriogonádotropním hormonem (hCG). Injekční podání tohoto hormonu pod kůži do lymfatických vaků na hřbetní straně vyvolává kdykoliv během roku, nezávisle na ročním období, do 12 hodin ovulaci. Zpočátku byly samice *X. laevis* využívány na testy těhotenství. Těhotné ženy ve své moči vylučují hCG, a tudíž její injekční podání do lymfatických vaků samic vede k ovulaci oocytů (Bellerby, 1934; Shapiro and Zwarenstein, 1934). Díky tomuto faktu došlo v 50. letech k masivnímu rozšíření

tohoto modelového organismu do klinických laboratoří po celém světě (Gurdon and Hopwood, 2000). V dnešní době je stimulace samic pomocí hCG v laboratořích využívána rutinně, a tudíž byl eliminován problém spojený s nedostatkem experimentálního materiálu. V jedné snůšce samice *X. laevis* naklade řádově tisíce oocytů (Hirsch *et al.*, 2002) a stejná samice může být využívána k opětovné stimulaci jednou za 3 měsíce.

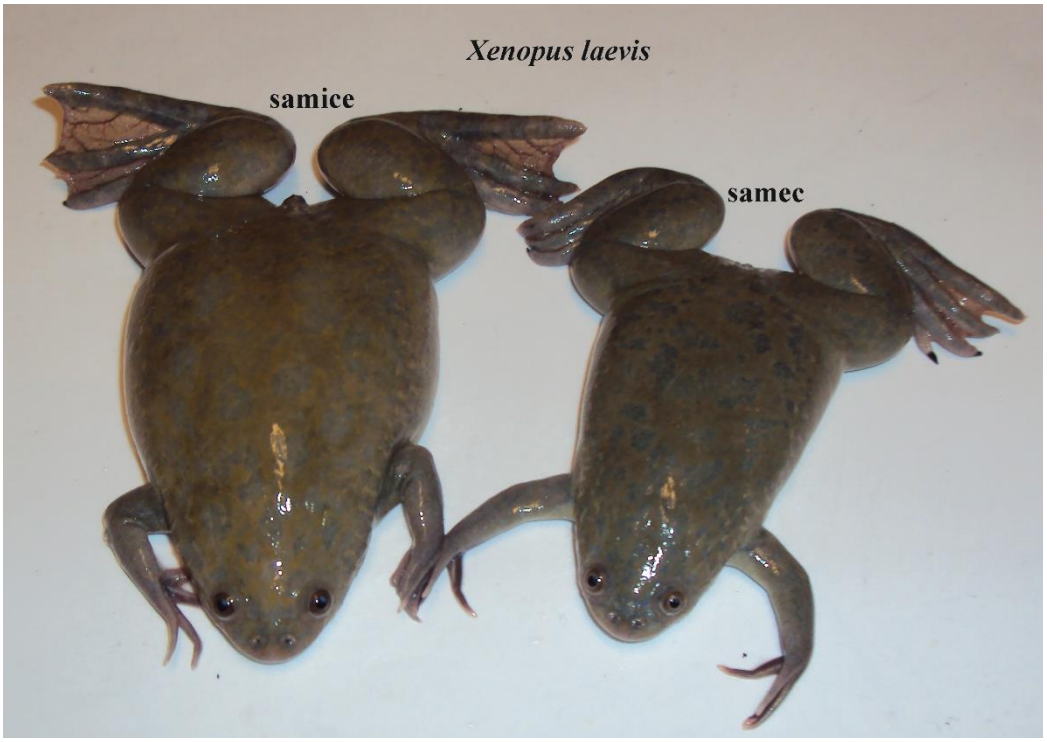

Obr. 1. Dospělý pár *Xenopus laevis* z chovů Biotechnologického ústavu AV ČR. Samice dorůstají velikosti 10 až 13 cm, zatímco samci dosahují zhruba o jednu třetinu menšího vzrůstu.

Možnosti využití *X. laevis* jako modelového organismu jsou široké a zahrnují studium jak na poli buněčné biologie, tak v rámci časného embryonálního vývoje obratlovců. Již v 70. letech 20. století Sir John Gurdon využíval oocyty *X. laevis* k translačním pokusům. Dokázal, že oocyt disponuje schopností translatovat mikroinjikovanou exogenní mRNA a následně syntetizovat odpovídající protein

(Gurdon *et al.*, 1971). Posléze se oocyty začaly používat pro *in vivo* studium biologických makromolekul (Gurdon, 1975). Další možné využití tohoto modelového organismu představuje studium funkce genů v průběhu časného embryonálního vývoje. V tomto přístupu se nejčastěji používá blokace exprese zkoumaného genu pomocí mikroinjekce antisense morpholino oligonukleotidů (MO) do cytoplazmy oocytu, kde MO specificky a účinně blokuje translaci transkriptu (Heasman *et al.*, 2000; Heasman, 2002). Nevýhoda této metody je pouze přechodný účinek MO. Oproti tomu trvalou změnu genomu, a tím i stálou změnu exprese konkrétního genu, umožňují transgenní metody (Kroll and Amaya, 1996; Werdien *et al.*, 2001). Z hlediska časné embryogeneze umožňuje modelový organismus *X. laevis* studovat nejenom funkci jednotlivých genů během vývoje, ale i ostatní procesy a biomolekuly.

3.2. Časný embryonální vývoj *Xenopus laevis*

Klíčovou otázkou vývojových biologů stále zůstává jak na počátku jedna buňka, tedy oocyt, může vést ke vzniku komplexního organismu, který má určenou tělní osovou polaritu a obsahuje různé typy tkání. Prvním a zároveň stěžejním krokem embryogeneze je oplození. Ačkoliv vznik dospělého jedince závisí na genetické informaci z obou rodičovských jader, základní informace pro časnou fázi embryonálního vývoje lze najít již ve zralém oocytu. Tato maternální informace přetrvává ve vyvíjejícím se embryu až do doby aktivace embryonálního genomu, respektive zahájení embryonální transkripce (Schier, 2007; Langley *et al.*, 2014). Napříč různými druhy obratlovců dochází k aktivaci embryonální transkripce v odlišných fázích rýhování časného embrya.

3.2.1. Oogeneze a struktura oocytu *Xenopus laevis*

Produkce zralých oocytů je zajištěna souvisle po celou dobu reprodukčního života dospělé samice *X. laevis*. Oogeneze trvá 6 – 8 měsíců a probíhá asynchronně. Z tohoto důvodu se v ovariích nacházejí vždy všechna vývojová stádia zrání oocytu. Významnou roli v procesu zrání zajišťují folikulární buňky, které v jedné vrstvě

obklopují rostoucí oocyt. Jejich funkce spočívá v syntéze mukopolysacharidového obalu a pomocí mezerového spojení (z angl. gap junction) regulují meiózu a ukládání žloutku v oocytu (Houston, 2013).

Vlastní oogenezi lze rozdělit do šesti po sobě následujících stádií (stádium I – VI), kdy na začátku oocyt vykazuje jiné morfologické vlastnosti než na konci procesu zrání. Ve stádiu I je oocyt průhledný, s jádrem orientovaným uprostřed a zcela bez vnějších znaků polarity. Akumulace pigmentových granul a žloutku uvnitř oocytu se odehrává až v průběhu stádia III (Dumont, 1972; Danilchik and Gerhart, 1987; Kloc *et al.*, 2001). Zralý oocyt *X. laevis* (stádium VI) se skládá ze dvou barevně odlišitelných hemisfér, které určují animálně-vegetativní osu. Tmavé zbarvení animální poloviny je způsobeno nahromaděním značného množství pigmentových granul neboli melanozómů v této oblasti. Oproti tomu obsah světle zbarvené vegetativní hemisféry vyplňuje žloutek (Danilchik and Gerhart, 1987) (Obr. 2.). Asymetrickou lokalizaci podél animálně-vegetativní osy vykazují i buněčné organely. Jádro zralého oocytu není umístěné uprostřed, ale dochází k jeho posunu směrem k animální hemisféře (Gurdon, 1968; Jullien *et al.*, 2011). Golgiho aparát, část endoplazmatického retikula a mitochondrie lze naopak najít ve větším množství ve vegetativní hemisféře (Kloc *et al.*, 2001).

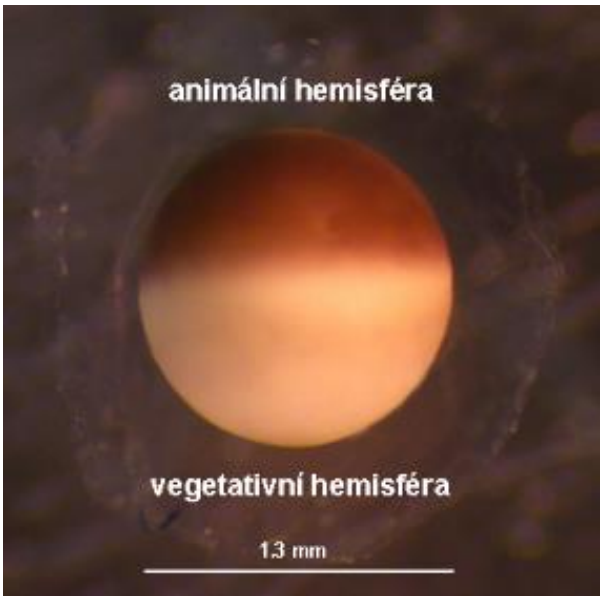

Obr. 2. Zralý oocyt *Xenopus laevis*. Určení animálně-vegetativní osy probíhá během oogeneze. Tmavé zbarvení animální hemisféry způsobuje nahromadění pigmentových granul v této oblasti. Oproti tomu světlá vegetativní hemisféra obsahuje žloutek. Průhledný, rosolovitý obal kolem oocytuplní funkci mechanické ochrany (upraveno z www.xenbase.org).

Z hlediska vývojové biologie se rozlišuje několik typů oocytů v závislosti na množství a distribuci žloutku. Oocyty obojživelníků se řadí do skupiny mezolecitálních oocytů, které obsahují střední množství žloutku s lokalizací ve vegetativní hemisféře. Kromě žloutku a buněčných organel se ve zralém oocytu *X. laevis* vyskytuje značné množství proteinů a nezvykle velké množství RNA, které se v rámci jedné buňky pohybuje okolo 4 µg. Vzhledem k tomuto faktu jsou oocyty drápatek s výhodou používány ke studiu těchto biomolekul, jak na úrovni jedné buňky (Smits *et al.*, 2014; Sun *et al.*, 2014), tak v případě RNA dokonce i na úrovni vnitrobuněčné (Sindelka *et al.*, 2008).

3.2.1.1. Maternální faktory

Oocyty žab rodu *Xenopus* obsahují kompletní informaci nezbytnou k proliferaci a následnou diferenciaci dceřiných buněk v průběhu časného embryonálního vývoje. Rozdílná distribuce maternálních faktorů v oocytu

představuje vysoce konzervovanou strategii, která buňce umožňuje vytvářet lokální asymetrii v konkrétních podoblastech cytoplazmy. Z hlediska diferenciace a pozdější specializace buněk je klíčová právě distribuce maternálních faktorů uvnitř oocytu (Shav-Tal and Singer, 2005). Bylo ukázáno, že mezi tyto klíčové determinanty buněčného osudu patří hlavně molekuly mRNA a různorodé proteiny (Houston, 2013).

3.2.1.2. Maternální transkripce

Zralé oocyty *X. laevis* obsahují tzv. maternální mRNA, která je syntetizovaná v průběhu oogeneze a jako předloha transkripce slouží maternální chromozomy (Heasman, 2006). Maternální mRNA se nachází ve vyvíjejícím se embryu až do 12. buněčného dělení po oplození, kdy embryo obsahuje více než 4000 buněk (vývojové stádium označované jako stádium 8). Tato hranice se u embrya označuje jako MBT stádium (stádium střední blastuly) a jejím klíčovým bodem je spuštění embryonální transkripce (Newport and Kirschner, 1982; Etkin and Balcells, 1985). Do MBT stádia probíhá pouze translace a veškeré transkripty nezbytné pro časný embryonální vývoj musí být přítomny již ve zralém oocytu.

3.2.2. Určení tělních os v časném embryonálním vývoji *Xenopus laevis*

Z pohledu tělního plánu obratlovců rozlišujeme tři základní tělní osy: anterio-posteriorní (též označovaná jako kranio-kaudální, hlavo-ocasní), dorzo-ventrální (hřbeto-břišní) a pravo-levou. Animálně-vegetativní osa, která se formuje ještě před oplozením oocytu odpovídá anterior-posteriorní ose. Vytvoření základů všech tří výše zmíněných tělních os lze pozorovat již v průběhu časného embryonálního vývoje.

První fáze embryonálního vývoje po oplození se nazývá rýhování a u *X. laevis* probíhá úplně a radiálně symetricky. První rýha se objevuje 90 min po oplození a označuje se jako meridionální. Tato rýha začíná na animálním pólu a prodlužuje se směrem k vegetativnímu pólu rychlostí 1 mm/1 min. Prochází místem průniku

spermie do oocytu a na opačné straně i středem šedého srpku a tím určuje budoucí pravo-levou tělní osu embrya. Oblast šedého srpku určuje dorzální části embrya (na opačné straně vůči místu průniku spermie do oocytu) a je rozhodující pro vznik blastoporu (prvoúst) a následnou gastrulaci. Následující druhou rýhu lze pozorovat 30 min po zahájení prvního rýhování. Druhá rýha je kolmá na předchozí a nazývá se také meridionální. Postupuje opět směrem od animálního pólu k vegetativnímu, avšak rozděluje embryo na dorzální a ventrální část. Ve vzniklém 4-buněčném stádiu všechny čtyři blastomery obsahují cytoplazmu jak z animální, tak vegetativní oblasti. Teprve třetí, ekvatoriální rýha rozděluje embryo na animální a vegetativní část. Třetí rýha vzniká 15 min po druhé rýze a je kolmá na obě předcházející rýhy. Přítomnost žloutku ve vegetativní oblasti částečně inhibuje rýhování a z tohoto důvodu ve stádiu 8 buněk vznikají dva odlišně velké typy blastomer, tzv. vegetativní makromery a animální mikromery (Obr. 3.). Následný embryonální vývoj *X. laevis* je označovaný jako regulační a jeho podstatu tvoří induktivní interakce buněk.

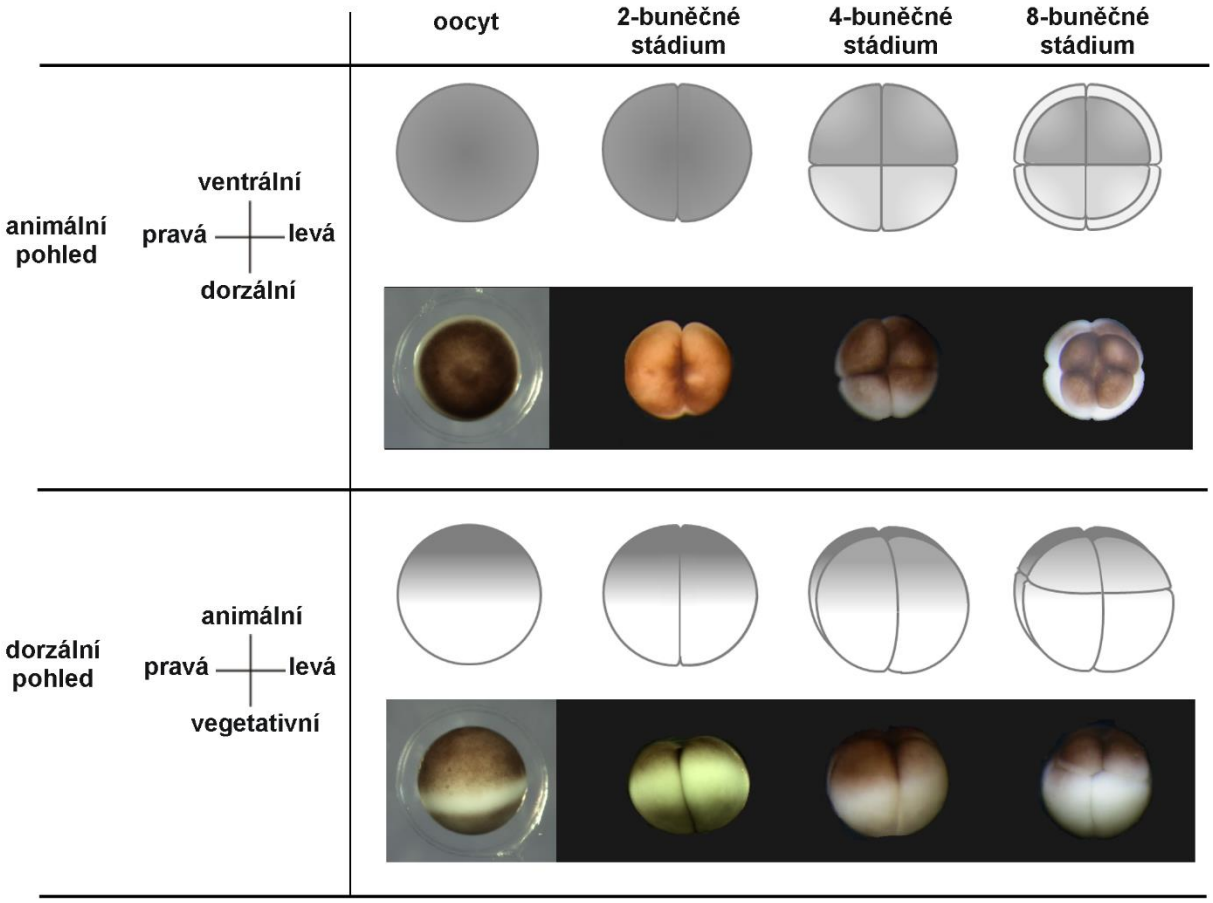

Obr. 3. Schématické (horní řada) a reálné (spodní řada) znázornění časného embryonálního vývoje a formování základních tělních os u *Xenopus laevis* z animálního a dorzálního pohledu. Rýhování oplozeného oocytu je zahájeno 90 min po oplození. První rýha vzniká na animálním pólu, prodlužuje se směrem k vegetativnímu pólu a určuje budoucí pravo-levou tělní osu embrya. Druhá rýha probíhá kolmo k první rýze a rozděluje embryo na ventrální a dorzální část. Třetí rýha je kolmá na obě předcházející rýhy a odděluje animální mikromery od vegetativních makromer. Reálné obrázky rýhování použity z www.xenbase.org, oocyt a časné embryo odpovídá velikosti 1,3 mm.

3.2.2.1. Animálně-vegetativní osa

První asymetrická distribuce maternálních faktorů uvnitř oocytu probíhá již v průběhu oogeneze (Deshler *et al.*, 1997; King *et al.*, 2005). Vnější znaky této asymetrie se projevují v období střední a pozdní oogeneze (stádium III – VI), kdy dochází k nahromadění pigmentových granul v animální hemisféře a žloutkové masy ve vegetativní hemisféře (Danilchik and Gerhart, 1987). Animálně-vegetativní asymetrii uvnitř oocytu lze sledovat i na úrovni biomolekul. Kódující maternální mRNA, ale i nekódující RNA utvářejí gradient podél této osy s preferencí buď

v animální, nebo vegetativní hemisféře. Nedávná analýza transkriptomu odhalila zhruba 300 molekul, které jsou lokalizované ve vegetativním kortexu oocytu, což představuje 2-3% maternálně exprimovaných genů (Cuykendall and Houston, 2010). K lokalizaci maternálních transkriptů do vegetativní hemisféry jsou využity dvě odlišné transportní dráhy (Kloc and Etkin, 1995).

3.2.2.1.1. Časná transportní dráha (METRO)

Časná dráha označována také jako METRO (messenger transport organizer) je asociovaná s tzv. mitochondriálním mrakem, který je také nazýván jako Balbianiho tělíska. Mitochondriální mrak se utváří již v průběhu časné oogeneze (ve stádiu I) v oblasti na vegetativní straně zárodečného váčku (angl. germinal vesicle; označení jádra oocytu před meiotickým dělením) a obsahuje značné množství mitochondrií, hladké endoplazmatické retikulum a elektron-denzní granulo-fibrilární materiál (budoucí zárodečná plazma) (Heasman *et al.*, 1984). Syntéza maternálních transkriptů probíhá v zárodečném váčku, ze kterého jsou následně transportovány do cytoplazmy. Krátké nukleotidové repetice na cis a trans regulačních elementech těchto transkriptů umožňují navázání na RNA-vazebné proteiny a ty poté zprostředkují vazbu do mitochondriálního mraku (Snedden *et al.*, 2013). V časné fázi oogeneze (stádium II) dochází k rozpadu mitochondriálního mraku na jednotlivé ostrůvky zárodečné plazmy a následné translokaci maternálních transkriptů asociovaných s těmito ostrůvky do vegetativního kortexu (Heasman *et al.*, 1984). Byly identifikovány dva nezávislé lokalizační signály na 3´ UTR (untranslated region) oblasti mRNA. První signál zprostředkovává lokalizaci do mitochondriálního mraku a druhý umožňuje lokalizaci do vegetativního kortexu (Kloc *et al.*, 1993; Zhou and King, 1996a; Zhou and King, 1996b).

Časná dráha transportuje především maternální faktory asociované se zárodečnou plazmou. Transkripty *cdx1* (caudal type homeobox 1, *nanos* homolog, dříve označován *xcad2*), *dazl* (deleted in azoospermia-like) a *ddx25* (deadsouth) se přímo podílejí na určení zárodečných buněk, a tudíž je lze detekovat v zárodečných granulích oocytu (Kloc *et al.*, 2002; Zhou and King, 2004). Oproti tomu transkripty

pgat (primordial germ cell-associated transcript, dříve označovaný jako *xpat*) a *wnt11* (wingless-type member 11) jsou spojené s fibrilární sítí zárodečné plazmy (Kloc *et al.*, 1998). Zároveň pomocí této dráhy lze transportovat i funkční RNA. Transkript *Xlsirt* (*Xenopus laevis* short interspersed repeat transcripts) spadá do skupiny netranslatovaných funkčních RNA, které se pravděpodobně podílí na strukturní funkci cytoskeletální sítě ve vegetativním pólu (Kloc and Etkin, 1994). Nicméně METRO transportní dráha maternálních faktorů vykazuje nezávislost na cytoskeletálním aparátu. Depolymerace mikrotubulů a mikrofilament pomocí nokodazolu a cytochalasinu B nevede ke zhroucení časného transportu (Kloc and Etkin, 1995; Kloc *et al.*, 1996) a dokonce nevede ani ke snížení integrity mitochondriálního mraku (Heasman *et al.*, 1984). Oproti tomu vlastní uchycení maternálních transkriptů ve vegetativním kortexu však vyžaduje mikrofilamentární aparát. Tento fakt vyplývá ze studie, kdy po ošetření oocytů cytochalasinem B došlo k uvolnění molekul RNA z vegetativního kortexu (Kloc and Etkin, 1995).

3.2.2.1.2. Pozdní transportní dráha

Druhá lokalizační dráha se nazývá pozdní. K její aktivaci dochází v době střední a pozdní oogeneze (stádium III – IV) a využívá transportu pomocí cytoskeletu (Yisraeli *et al.*, 1990). Touto dráhou nejsou transkripty směrovány do mitochondriálního mraku či jeho obdoby, ale dochází k jejich přímému hromadění ve vegetativní ooplazmě (Deshler *et al.*, 1997; Gautreau *et al.*, 1997). Pozdní dráha lokalizuje mRNA maternálních transkripčních faktorů *gdf1* (growth differentiation factor 1, dříve používané označení *vg1*) a *vegt* (vegetal T-box transcription factor), které jsou nezbytné pro specifikaci a následné utvoření zárodečných listů (White and Heasman, 2008). Transport těchto transkriptů do vegetativní hemisféry je kódován prostřednictvím UUUCU a UUCAC lokalizačních sekvencí v 3´ UTR oblasti (Bubunenko *et al.*, 2002; Kwon *et al.*, 2002; Lewis *et al.*, 2004). Mechanismus transportu pravděpodobně závisí na speciální populaci váčků z endoplazmatického retikula. Maternální transkripty se vážou na tyto váčky prostřednictvím Vera proteinu a následný transport do vegetativního pólu je zprostředkován mikrotubulárními

vlákny (Deshler *et al.*, 1997; Etkin, 1997; Kwon *et al.*, 2002). Následné uchycení ve vegetativním pólu vyžaduje mikrofilamentární síť. Depolymerace mikrotubulů nokodazolem ve stádiu III oogeneze způsobí rozptýlení *gdf1* transkriptu v cytoplazmě oocytu. Avšak působení nokodazolu nemá žádný efekt ve stádiu IV, protože zde již dochází k uchycení maternálních transkriptů na mikrofilamenta vegetativního pólu. Uvolnění transkriptu *gdf1* z tohoto místa pak lze ve stádiu IV navodit cytochalasinem B, který se využívá k destabilizaci mikrofilamentární sítě. Na druhou stranu stejný postup s použitím cytochalasinu B nemá žádný vliv ve stádiu III (Yisraeli *et al.*, 1990). Ukazuje se, že vlastní polarizace mikrotubulů v oocytu *X. laevis* představuje důležitý aspekt vegetativního transportu. Naprostá většina plus konců směřuje do středu (95% v animální hemisféře a 80% ve vegetativní hemisféře), zatímco mínus konce se přichytávají v blízkosti kortexu (Pfeiffer and Gard, 1999). Tato orientace představuje opačný mechanismus polarizace než u většiny somatických buněk. Nicméně studie vegetativního transportu naznačují, že tento transport závisí na minoritní subpopulaci mikrofilamentárních vláken, které vykazují orientaci plus koncem k vegetativnímu kortexu a jsou propojené s kinesinovými molekulárními motory (Messitt *et al.*, 2008).

3.2.2.1.3. Animální transport

Mechanismus aktivního transportu maternální RNA do animální poloviny není zatím objasněn. Dosud nebyla prokázána závislost cis/trans regulačních faktorů nebo zapojení cytoskeletálního aparátu na vzniku animálního gradientu. Předpokládá se však, že tyto transkripty nevyžadují aktivní transport. Vzhledem k faktu, že je jádro umístěné v animální polovině oocytu, pasivní pohyb a prostá difúze maternálních transkriptů přirozeně vede k animálnímu gradientu.

3.2.2.1.4. Vliv animálně-vegetativní osy na určení zárodečných listů

Výsledkem asymetrické lokalizace maternálních faktorů podél animálně-vegetativní osy je nerovnoměrné rozdělení těchto transkriptů do dceřiných buněk, což vede v průběhu časného embryonálního vývoje k založení všech tří zárodečných listů (Obr. 4.). Vnější zárodeční list (ektoderm) vzniká z buněk animální hemisféry a určuje formování pokožky, nervového systému a sliznic začátku a konce trávicí trubice. Vnitřní zárodeční list (endoderm) pochází z buněk vegetativní hemisféry a v průběhu embryonálního vývoje vytváří trávicí soustavu. Zároveň buňky vegetativní oblasti obsahují i maternální determinanty, které jsou klíčové v určení středního zárodečného listu (mezoderm). Mezi tyto determinanty patří maternální proteiny Gdf1 a Vegt. Funkce Vegt transkripčního faktoru spočívá v indukci exprese *xnr* transkriptů (*Xenopus* nodal related). Ty následně aktivují *xbra* (*Xenopus* brachyury) expresi v buňkách ležících nad nimi, respektive v tzv. ekvatoriálních buňkách (někdy také označované jako buňky marginální zóny). Protein Xbra řídí expresi dalších mezodermálních genů, které přímo ovlivňují tvorbu mezodermu. Klíčovou úlohu Vegt maternálního proteinu ve specifikaci endodermu a zároveň mezodermu potvrzuje studie, kde účinek tohoto transkripčního faktoru byl eliminován antisense oligonukleotidy (Zhang and King, 1996). Obecným důkazem mezodermální indukce je přímé spojení buněk animální čepičky s vegetativními buňkami, kdy dojde ke konverzi presumptivního ektodermu na mezoderm. Oproti tomu odstranění ekvatoriálních blastomer blastuly má za následek úplnou ztrátu mezodermální tkáně (Nieuwkoop, 1969; Sudarwati and Nieuwkoop, 1971; Nieuwkoop, 1973). Buňky mezodermu stojí za vznikem struny hřbetní, vylučovací soustavy, cévní soustavy, svalů a kostí (Dale and Slack, 1987).

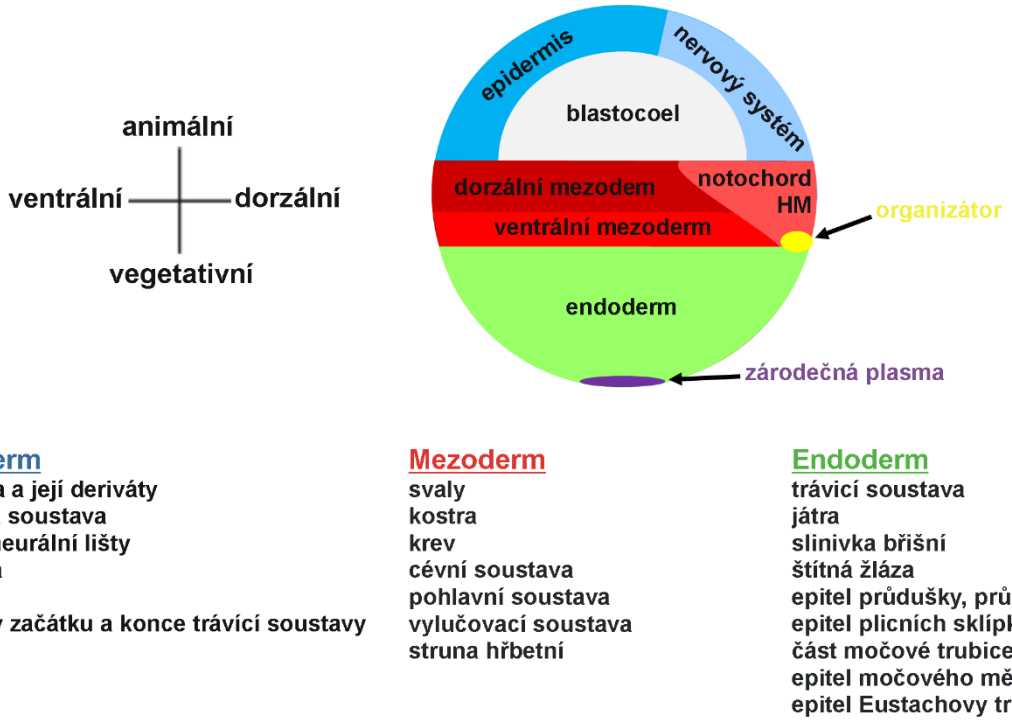

Obr. 4. Mapa původu buněk zárodečných listů ve stádiu blastuly. Ektoderm (vnější zárodečný list, označeno modře) vzniká z buněk animální čepičky. V průběhu vývoje dochází k rozdělení presumptivního ektodermu na linii buněk, která formuje pokožku a její deriváty (tmavá modrá) a na tzv. neuroektoderm (světle modrá). Presumptivní mezoderm (střední zárodečný list, označeno červeně) je lokalizován do buněk marginální zóny a posléze dochází k jeho diferenciaci na dorzální mezoderm (tmavě červená), ventrální mezoderm (červená) a notochord/hlavový mezoderm (HM, růžová). Endoderm (vnitřní zárodečný list, označeno zeleně) vzniká z buněk vegetativní hemisféry. Znázorněný je i dorzální ret blastoporu (žlutá) a umístění zárodečné plazmy ve vegetativním kortexu (fialová).

3.2.2.2. Dorzo-ventrální osa

Určení dorzo-ventrální tělní osy závisí hned na dvou procesech, které probíhají v různých fázích embryonálního vývoje. Kortikální rotace představuje časný krok a specifikace dorzálních struktur organizátorem zastupuje pozdější krok vývoje dorzo-ventrální asymetrie.

3.2.2.2.1. Vliv kortikální rotace na dorzo-ventrální osu

První asymetrická distribuce maternálních faktorů a utváření jejich gradientů podél animálně-vegetativní osy probíhá již během oogeneze. Další přesuny těchto faktorů lze pozorovat v oocytu bezprostředně po oplození. Spermie proniká do oocytu v jeho animální polovině a místo průniku definuje ventrální stranu budoucího embrya. Přibližně 20 min po oplození dochází k tzv. kortikální rotaci, kdy se vnější (kortikální) cytoplazma pootočí vůči vnitřní cytoplazmě oocytu o 30^{o} v opačném směru od místa průniku spermie do oocytu (Vincent and Gerhard, 1987; Denegre and Danilchik, 1993) (Obr. 5.). Tato rotace je zprostředkována pomocí mikrotubulární sítě vegetativního kortexu a na uspořádání této sítě mají vliv i mikrotubuly pocházející ze spermie (Vincent *et al.*, 1987; Schroeder and Gard, 1992). Výsledkem kortikální rotace je opět asymetrie, která v tomto případě odráží dorzo-ventrální tělní osu embrya. Toto tvrzení podporují studie, kdy bylo zabráněno kortikální rotaci ozářením oplozeného oocytu UV světlem. Následkem ozáření nedošlo k vývoji dorzální osy a embrya vykazovala pouze ventralizovaný fenotyp (Vincent and Gerhart, 1987; Elinson and Pasceri 1989). Oproti tomu indukcí druhé kortikální rotace u oplozeného oocytu vznikla embrya, ve kterých došlo k vývoji dvou dorzálních os (Gerhart *et al.*, 1989; Sive, 1993). Výskyt specifických dorzálních determinantů lze detekovat v oblasti vegetativní kortikální cytoplazmy zralého oocytu. Důkazem je vývoj ektopické dorzální osy u recipientního embrya, kterému bylo transplantováno malé množství této cytoplazmy (Fujisue *et al.*, 1993). Na druhou stranu, delece kortikální cytoplazmy způsobuje ventralizaci embrya. Důsledkem kortikální rotace dochází k nahromadění specifických dorzálních determinantů v budoucí dorzální části embrya, tzn. v místě zhruba 180^{o} proti místu oplození (tzv. oblast šedého srpku) (Weaver and Kimelman, 2004; White and Heasman, 2008). Konkrétně dochází k přesunu maternálního proteinu Dvl (Dishevelled) z vegetativního kortexu do dorzální oblasti (Miller *et al.*, 1999), kde tento protein inaktivuje protein Gsk3β (glycogen synthase kinase 3 beta) a tím zabrání degradaci β-kateninu (neboli Ctnnb1)(Yost *et al.*, 1996). Nahromaděný β-katenin v dorzální části způsobuje aktivaci lokální Wnt dráhy (Wingless/Int-1). Tato Wnt/β-kateninová signální dráha poté reguluje transkripci již zygotických transkriptů *xnr3*

(*Xenopus* nodal related 3), *siamois* a *goosecoid*, kteří určují dorzální fenotyp (Darras *et al.*, 1997; Marikawa *et al.*, 1997).

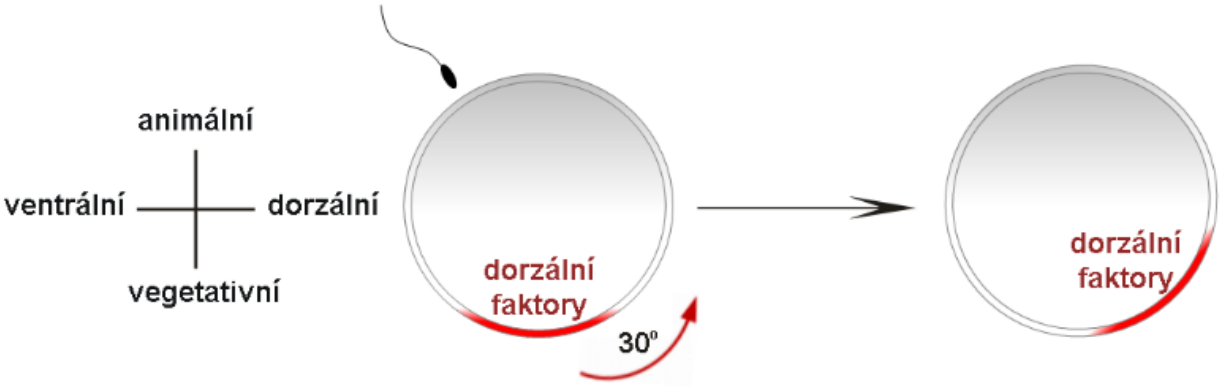

Obr. 5. Schématické znázornění kortikální rotace. Spermie proniká do oocytu v oblasti animální hemisféry a toto místo určuje budoucí ventrální stranu embrya. Po uplynutí 20 min od oplození dochází k pootočení kortikální cytoplazmy vůči vnitřní mase cytoplazmy o 30°. Tento proces se nazývá kortikální rotace a zajišťuje nahromadění dorzálních maternálních faktorů na budoucí dorzální straně embrya, která se nachází naproti místu průniku spermie do oocytu.

Výsledek kortikální rotace, respektive dorzo-ventrální asymetrie, se na povrchu embrya projevuje již ve 4-buněčném vývojovém stádiu. Na základě odlišné velikosti a intenzity pigmentace lze odlišit dva typy blastomer (Sive *et al.*, 2000; Blum *et al.*, 2014). Dorzální blastomery vykazují menší velikost a světlejší pigmentaci. Ventrální blastomery se pak jeví velikostně větší a s tmavší pigmentací (Obr. 3.). Nejen vizuální odlišnost dorzo-ventrálních blastomer, ale i buněčný obsah určuje tuto osu již v průběhu rýhování embrya. Po kortikální rotaci lze detekovat větší množství proteinů Ctnnb1 a Dvl v dorzálních blastomerách (Rowning *et al.*, 1997; Miller *et al.*, 1999). Ve vegetativních blastomerách na dorzální straně embrya dochází přednostně k translaci maternální *wnt11* mRNA (Schroeder *et al.*, 1999) a zároveň zde probíhají i posttranslační úpravy proteinu Gdf1, který zde vykazuje vyšší aktivitu (Thomsen and Melton, 1993). Naproti tomu ventrální blastomery animální části embrya disponují větším množstvím maternální mRNA *wnt8b*, jejíž funkce spočívá v represi dorzálního fenotypu (Pandur *et al.*, 2002). Odstranění dorzálních blastomer časným embryím způsobilo deficienci dorzálních struktur a následné selhání

normálního vývoje embrya. Na druhé straně odstranění ventrálních blastomer vedlo k vývoji hyperdorzalizovaných fenotypů (Cooke, 1985; Sive, 1993).

3.2.2.2.2. Specifikace dorzálních struktur v průběhu gastrulace

Výše zmíněná Wnt/β-kateninová signální dráha je stěžejní i k vytvoření center, které určují dorzo-ventrální asymetrii a následně organizují gastrulaci a potažmo diferenciaci dorzálních a ventrálních struktur. Ve vegetativních blastomerách na budoucí dorzální straně, kde se protíná lokalizace Gdf1, Vegt společně s Ctnnb1 vzniká tzv. Nieukoopovo centrum. Přítomnost tohoto centra indukuje diferenciaci nad ním ležících buněk (oblast šedého srpku) v organizátor (Moon and Kimelman, 1998). Organizátor (označovaný také jako Spemannův organizátor nebo dorzální ret blastoporu) vzniká ve stádiu blastuly a jeho funkce spočívá ve schopnosti zahájit gastrulační pohyby a následně dorzalizovat migrující buňky. V průběhu migrace dochází k diferenciaci dorzálního mezodermu, paraxiální mezodemu (somitů) a k dorzalizaci ektodermu, ze kterého se posléze vyvine neurální trubice. Tuto funkci organizátoru dokazují pokusy objevitele organizátoru Hanse Spemanna, který rozděloval časná embrya na dvě části a sledoval jejich vývoj. Rozdělení embrya napříč šedým srpkem vedlo k vývoji dvou normálních jedinců. Zatímco rozdělení mimo šedý srpek mělo za následek vývoj pouze jednoho fenotypově normálního embrya (Sander and Faessler, 2001).

3.2.2.3. Pravo-levá osa

Na rozdíl od výše zmíněné animálně-vegetativní a dorzo-ventrální osy, pravo-levá tělní osa vykazuje vedle asymetrických projevů i znaky souměrnosti. Obecnou vlastností obratlovců je bilaterální symetrie, kdy jejich tělem lze vést jednu rovinu souměrnosti. Tato rovina představuje právě pravo-levou tělní osu. Tuto symetrii však lze pozorovat pouze na úrovni vnějších znaků. Vzhledem k uložení vnitřních orgánů a rozložení trávicí soustavy se i pravo-levá tělní osa projevuje asymetricky.

3.2.2.3.1. Pravo-levá osa v průběhu rýhování

Rozdělení časného embrya na pravou a levou část je již určeno prvním buněčným dělením po oplození oocytu (Obr. 3.). Ve stádiu 2-4 buněk dochází k nerovnoměrné distribuci komponentů H+/K+-ATPázové (Levin *et al.*, 2002) a H+-V-ATPázové iontové pumpy (Adams *et al.*, 2006). Předpokládá se, že rozdílný iontový tok a vznik odlišného napětí na membráně vede k ovlivnění distribuce pravo-levých determinantů. Blastomery na pravé straně embrya disponují ATPázovými pumpami, což má za následek jejich záporný náboj. Tento náboj představuje hybnou sílu pro transport malých nabitých molekul přes gap-spojení mezi jednotlivými blastomerami (Levin *et al.*, 2002; Vandenberg and Levin, 2010) (Obr. 6.). Serotonin představuje kandidátní morfogen pravo-levé asymetrie, který podléhá tomuto transportu a v průběhu časného embryonálního vývoje se hromadí v pravých, ventrálních blastomerách (Fukumoto *et al.*, 2005a). Byly také identifikovány dva transportéry serotoninu, membránový transportér serotoninu a vezikulární monoamin transportér, jejichž funkce je klíčová pro zformování pravo-levé tělní osy (Fukumoto *et al.*, 2005b). Zablokováním těchto transportérů, ATPázových pump či samotného transportu serotoninu vede k tzv. heterotaxii, neboli k náhodnému uložení srdce a vnitřních orgánů podél pravo-levé tělní osy (Levin *et al.*, 2002; Fukumoto *et al.*, 2005b; Adams *et al.*, 2006). Na úrovni proteinů byl dosud popsán protein 14-3-3E, který vykazuje asymetrickou lokalizaci v blastomerách 2-buněčného stádia. Protein 14-3-3 aktivuje transport H+ iontů přes cytoplazmatickou membránu a zablokování distribuce tohoto proteinu pomocí fusicoccinu A opět vyústilo ve vývoj embryí s heterotaxí (Bunney *et al.*, 2003).

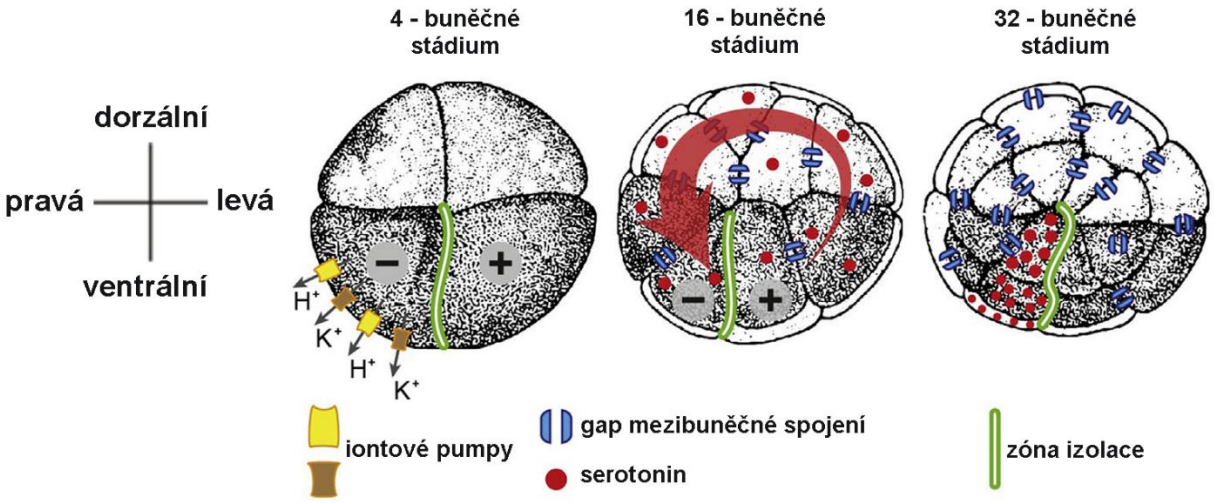

Obr. 6. Model iontového toku při určení pravo-levé tělní osy (upraveno podle Blum *et al.*, 2014). Odlišný iontový tok a membránové napětí ovlivňuje distribuci pravo-levých determinantů. Nerovnoměrná distribuce komponentů H+/K+-ATPázové a H+-V-ATPázové iontové pumpy do pravé, ventrální blastomery ve 4-buněčném stádiu vede ke vzniku záporného náboje. Tento náboj následně umožňuje transport serotoninu mezi jednotlivými blastomerami, čímž dochází k jeho hromadění v pravých, ventrálních blastomerách.

3.2.2.3.2. Pravo-levá osa v průběhu neurulace

V průběhu časného embryonálního vývoje se pravo-levá tělní asymetrie fenotypově neprojevuje, ale začíná se uplatňovat až po aktivaci embryonální transkripce, konkrétně během neurulace. Ciliární buňky na horní straně gastrocoelu (oblast GRP - gastrocoel roof plate) usměrňují proudění extracelulární tekutiny zprava doleva. Tímto dochází k represi proteinu Coco a následné aktivaci Nodal signální dráhy na levé straně embrya (oblast LPM – lateral plate mesoderm) (Schweickert *et al.*, 2010; Hatayama *et al.*, 2011). Prozatím však nebyl objasněn mechanismus, jak směr pohybu cilií ovlivňuje aktivaci genové exprese. Nodal signální dráhu ovlivňuje i maternální protein Gdf1. Tento protein vykazuje vyšší aktivitu na levé straně embrya, a tím pozitivně ovlivňuje expresi embryonálního *xnr1* (*Xenopus* nodal-related 1) transkriptu. Protein Xnr1 přímo aktivuje produkci proteinu Pitx2 (paired-like homeodomain 2), který je zřejmě nezbytný pro utvoření fenotypu levé strany (Toyoizumi *et al.*, 2005). Pokud byl protein Gdf1 injikován do budoucí

pravé části embrya, došlo k náhodnému uložení srdce, sleziny a trávicí soustavy podél pravo-levé tělní osy (Hyatt *et al.*, 1996).

3.3. Regulace maternální mRNA

Maternální mRNA kóduje specifické transkripční faktory, které v průběhu časného embryonálního vývoje určují diferenciaci jednotlivých buněk nebo celých částí embrya. Nicméně tato diferenciace a určení tělního plánu není odrazem pouze přítomnosti či nepřítomnosti konkrétní maternální mRNA, ale závisí i na působení regulačních molekul, popřípadě regulačních sekvencí uvnitř transkriptu. Translace maternální mRNA může být posttranskripčně regulována, přičemž mezi nejvýznamnější mechanismy regulace patří adenylace/deadenylace poly(A) konce nebo regulace pomocí molekul miRNA.

3.3.1. Regulace translace prostřednictvím poly(A) konce

Poly(A) konec označuje sekvenci několika desítek až stovek adeninových nukleotidů poskládaných za sebou na 3´ UTR konci mRNA. Tato sekvence zvyšuje stabilitu mRNA, a tím i možnost vyššího obratu translace daného transkriptu. Oproti tomu deadenylovaná mRNA není chráněná proti exonukleázám, a tudíž je přednostně určena k degradaci. Mechanismus kontroly translace pomocí poly(A) konce závisí na jaderném polyadenylačním signálu. Tento signál se skládá ze sekvence AAUAAA a spouští polyadenylaci během úprav pre-mRNA. Další stupeň kontroly translace poskytuje cytoplazmatický polyadenylační element (CPE) se sekvencí $UUUUA_{1-2}U$ na 3´ UTR oblasti mRNA. Vazba CPE vazebného proteinu na tuto regulační oblast umožňuje prodlužování poly(A) konce a ve výsledku aktivuje translaci mRNA (Preiss *et al.*, 1998). Vlastní délka poly(A) konce představuje významný ukazatel nejen stability, ale i translační aktivity maternální mRNA. U žab rodu *Xenopus* maternální mRNA, které obsahují CPE sekvenci podstupují cytoplazmatickou polyadenylaci, zatímco maternální transkripty jsou bez CPE signálu deadenylovány (Lagagneux *et al.*, 1995; Meric *et al.*, 1996). V průběhu procesu zrání oocytu dochází

prostřednictvím CPE sekvence k polyadenylaci a následné transkripční aktivaci klíčových maternálních mRNA. Mezi tyto transkripty patří i *c-mos* a *cyklin B1*, které udržují oocyt v bloku metafáze II (de Moor and Richter**,** 1997; de Moor and Richter**,** 1999). Pandur *et al.* (2002) ukázali, že maternální mRNA z dorzální blastomery označené D1 ve vývojovém stádiu 8 buněk nevykazuje schopnost dorzalizovat embryo, ale její linie ve vývojovém stádiu 16 buněk tuto schopnost již má. Schopnost indukce dorzálního fenotypu ve stádiu 16 buněk je dána polyadenylací specifických maternálních mRNA v cytoplazmě. Naproti tomu proces deadenylace vede ke snížení translační aktivity některých maternálních transkriptů, což je uplatňováno již ve zralém oocytu *X. laevis* nebo bezprostředně po jeho oplození (Paris and Philippe, 1990; Varnum and Wormington, 1990; Wickens, 1990). Zároveň bylo dokázáno, že rozdílná translační aktivita umožňuje gradientové rozmístění proteinu v embryu. Maternální mRNA *wnt11* je rovnoměrně distribuována podél dorzo-ventrální osy embrya. Na druhou stranu deadenylace poly(A) konce transkriptu *wnt11* na ventrální straně vede ke snížení množství proteinu Wnt11, a tím i k nerovnoměrnému rozložení tohoto proteinu podél dorzo-ventrální osy (Schroeder *et al.*, 1999).

3.3.2. Regulace translace prostřednictvím mikroRNA

Translaci mRNA lze regulovat i nezávisle na poly(A) konci a to s využitím molekul miRNA. Tyto krátké, jednovláknové nekódující RNA endogenního původu mají průměrnou délku 22 nukleotidů (v rozmezí 19-25 nukleotidů) a vznikají během několikastupňového procesu. Molekuly miRNA bývají často kódovány oblastmi uvnitř intronů genů kódujících protein (Tang and Maxwell, 2008) a přepis probíhá pomocí RNA polymerázy II (Lee *et al.*, 2004). Výsledkem transkripce je dlouhá smyčka, tzv. pri-miRNA, která nese na svém 5´ konci methylguanosinovou čepičku a na 3´ konci poly(A) řetězec a je sestřihována stejně jako mRNA (Cai *et al.*, 2004). Ke štěpení pri-miRNA enzymem Drosha (RNáza III) dochází ještě v jádře a vzniká vlásenka o velikosti zhruba 70 nukleotidů s přesahem dvou nukleotidů na jejím 3´ konci, tzv. pre-miRNA (Lee *et al.*, 2003). Protein Exportin 5 poté rozpozná tento nukleotidový přesah a společně s proteinem Ran-GTP umožní transport pre-miRNA

z jádra do cytoplazmy (Bohnsack *et al.*, 2004; Wang *et al.*, 2011). V cytoplazmě pak dochází k dalšímu sestřihu pre-miRNA enzymem Dicer (RNazá III). Vzniká 19 až 25 nukleotidů dlouhá dvouřetězcová RNA, neboli miRNA/miRNA* duplex. Dvouřetězcová miRNA je rozpoznána proteinovým komplexem RISC (RNA-induced silencing complex), který naváže funkční jednovláknovou miRNA a degraduje druhé miRNA* vlákno (Bartel, 2004) (Obr. 7.). Za klíčovou složku RISC komplexu lze považovat protein Argonaute (Ago). Tento protein obsahuje dvě RNA vazebné domény a přímo zprostředkovává interakci mezi miRNA a 3´ UTR oblastí mRNA (Hammell, 2008; Iwasaki and Tomari, 2009). Ukazuje se, že vlastní interakci miRNA a cílové mRNA zásadně ovlivňuje tzv. seed sekvence, která představuje úsek od 2. po 8. nukleotid na 5´ konci miRNA (Hibio *et al.*, 2012).

Regulace translace prostřednictvím miRNA, respektive potlačení translace, může být uskutečněno buď degradací mRNA, nebo její inhibicí. První způsob zahrnuje perfektní komplementaritu bazí mezi vláknem miRNA a cílovou mRNA. V takovém případě dochází ke štěpení dané mRNA. Druhý způsob umožňuje regulovat translaci i v případě pouze částečné shody sekvencí miRNA s cílovou mRNA. Nedokonalé párování vede k formování miRNA/mRNA komplexu, který se váže s dalšími proteiny za vzniku mRNP komplexu (mRNA and protein complex). Posléze dochází k hromadění těchto mRNP komplexů v cytoplazmě a tyto oblasti se pak označují P-bodies (processing bodies) (Liu *et al.*, 2005). Tento mechanismus potlačení translace mRNA představuje vratný proces, který umožňuje opětovné obnovení translační aktivity cílové mRNA (Brengues *et al.*, 2005; Parker and Sheth, 2007).

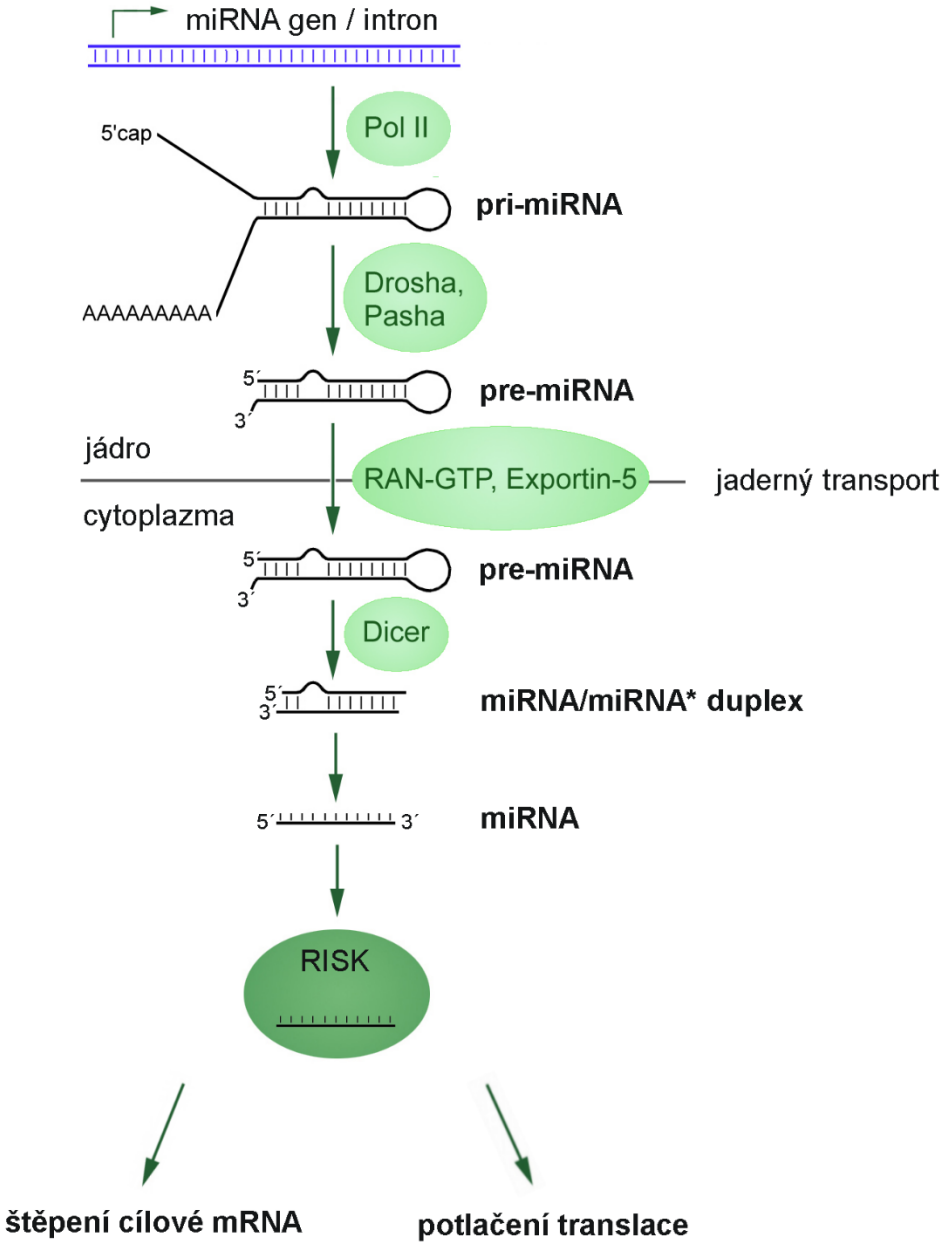

Obr. 7. Biogeneze miRNA. Přepis genu pro miRNA probíhá pomocí RNA polymerázy II za vzniku pri-miRNA. Tato dlouhá smyčka nese na svém 5´ konci methylguanosinovou čepičku a na 3´ konci poly(A) řetězec a je štěpena enzymem Drosha. Vzniká pre-miRNA vlásenka, která má velikost 70 nukleotidů s dvounukleotidový přesahem na 3´ konci. Transport pre-miRNA z jádra do cytoplazmy zajišťuje exportin 5/Ran-GTP. V cytoplazmě dochází k druhému enzymatickému sestřihu (enzym Dicer). Výsledkem štěpení je 19-25 nukleotidů dlouhá dvouřetězcová RNA (miRNA/miRNA* duplex). Tento duplex je rozpoznán RISC komplexem, který váže funkční miRNA vlákno a degraduje miRNA* řetězec. Zároveň RISC komplex umožňuje interakci s cílovou mRNA. Úplná komplementarita bází mezi miRNA a mRNA vede ke štěpení cílové mRNA, zatímco nedokonalá komplementarita bází nezničí cílovou mRNA, ale pouze zabrání translaci. Upraveno podle Esquela-Kerscher and Slack, 2006.

4. Seznam publikací

Na základě „*Xenopus* Gene Nomenclature Committee“ došlo v roce 2013 ke změně názvosloví genů u žab rodu *Xenopus*. Z tohoto důvodu označení genů v publikaci 4.1. (Spatial expression profiles in the *Xenopus laevis* oocytes measured with qPCR tomography) nemusí vždy odpovídat označení transkriptů v ostatních publikacích (Tab. 2.). Kompletní seznam aktuálních názvů genů, včetně jejich dříve používaných synonym, lze dohledat na stránkách www.xenbase.org.

staré / nové označení	**staré / nové označení**
alpha-actin / *acta*	Oct60 / *pou5f3.3*
An1 / *zfand4*	Otx1 / *otx1*
An2 / *pax6*	RNA pol. II / *polr2k*
APC / *apc*	Stat3 / *stat3.1*
axin / *axin1*	Tcf-3 / *tcf3*
beta-tubulin / *tubb*	U3 snoRNA / *imp3*
DeadSouth / *ddx25*	VegT / *vegt*
EF-1alpha / *eef1a1*	Vg1 / *gdf1*
Eg6 / *spire1*	Wnt11 / *wnt11*
Est1/ *est1*	Xcad2 / *cdx1*
FoxH1 / *foxh1*	Xdazl / *dazl*
Fz7 / *fzd7*	Xmam1 / *maml1*
GAPDH / *gapdh*	Xpar1 / *mark3*
GSK-3beta / *gsk3b*	ZPC / *zp3*
mtcytc / *cyc1*	Zp3 / *zp3.2*

Tab. 2. Přehled nové nomenklatury genů žab rodu *Xenopus*. Uvedené geny se vztahují k publikaci 4.1. (Spatial expression profiles in the *Xenopus laevis* oocytes measured with qPCR tomography).

4.1. Spatial expression profiles in the *Xenopus laevis* oocytes measured with qPCR tomography

Sindelka R., **Sidova M.**, Svec D. a Kubista M. *Methods* 2010, 51: 87-91. IF 3.221

Laboratoř genové exprese vyvinula metodu qPCR tomografie, která umožňuje stanovit lokalizaci mRNA podél konktrétní osy zájmu uvnitř biologického vzorku (Sindelka *et al.*, 2008). V tomto případě byla studována lokalizace maternálních mRNA podél animálně-vegetativní osy zralého oocytu *X. laevis*. V prvním kroku byly oocyty umístěny do kapky média OCT (optimum cutting temperature). Poté byly z těchto oocytů pomocí kryomikrotomu připraveny 30 μm silné řezy vedené podél jejich animálně-vegetativní osy. Velké množství RNA v jednom oocytu (~ 4 μg) umožnilo připravit celkem 45 řezů, které byly rozděleny do 15 zkumavek tak, že každá zkumavka obsahovala vždy 3 po sobě jdoucí řezy oocytu podél animálně-vegetativní osy. Z každého vzorku byla izolována celková RNA a reverzní transkripcí byla připravena cDNA. Následující genově specifická pre-amplifikace umožnila zvýšit množství cílových templátových molekul, což bylo nezbytné pro použití vysokokapacitního qPCR BioMark™ systému. Vlastní kvantifikace maternálních transkriptů probíhala v rámci mikrofluidního čipu, na kterém lze současně analyzovat 48 vzorků proti 48 genům. Výsledek této studie dokázal, že maternální RNA lze rozdělit do dvou skupin podle profilu lokalizace podél animálně-vegetativní osy oocytu. První skupina RNA (*zfand4, pax6, apc, axin1, est1, fzd7, zp3, zp3.2, maml1, mark3, stat3.1, pou5f3.3, tcf3, gsk3b, foxh1, gapdh, eef1a1, tubb, acta, polr2k, imp3* a *cyc1*) vykazovala lokalizaci v animální hemisféře. Na rozdíl od druhé skupiny transkriptů, která měla nejvyšší zastoupení ve vegetativní hemisféře. Vysoké rozlišení řezů oocytem (15 vzorků) navíc umožnilo identifikovat dvě vegetativní podskupiny, které se liší profilem gradientu. Gradient *gdf1, vegt, otx1, spire1* a *wnt11* transkriptů se objevoval v celé vegetativní hemisféře a pozvolna narůstal směrem k vegetativnímu pólu, kdežto *cdx1, dazl* a *ddx25* RNA byly strmě lokalizovány ve vegetativním pólu.

Methods 51 (2010) 87–91

Contents lists available at ScienceDirect

Methods

journal homepage: www.elsevier.com/locate/ymeth

Spatial expression profiles in the *Xenopus laevis* oocytes measured with qPCR tomography

Radek Sindelka [a], Monika Sidova [b,c], David Svec [b], Mikael Kubista [b,d,*]

[a] *Whitehead Institute, Cambridge, USA*
[b] *Laboratory of Gene Expression, Institute of Biotechnology, Academy of Sciences of the Czech Republic, Prague, Czech Republic*
[c] *Charles University in Prague, Faculty of Science, Department of Cell Biology, Czech Republic*
[d] *TATAA Biocenter AB, Odinsgatan 28, 411 03 Göteborg, Sweden*

ARTICLE INFO

Article history:
Accepted 18 December 2009
Available online 4 January 2010

Keywords:
Xenopus
Oocyte
qPCR tomography
Expression profiling

ABSTRACT

qPCR tomography was developed to study mRNA localization in complex biological samples that are embedded and cryo-sectioned. After total RNA extraction and reverse transcription, the spatial profiles of mRNAs and other functional RNAs were determined by qPCR. The *Xenopus laevis* oocyte was selected as model, because of its large size (more than 1 mm) and large amount of total RNA (~5 μg). Fifteen sections along the animal–vegetal axis were cut and prepared for quantification of 31 RNA targets using the high-throughput real-time RT-PCR (qPCR) BioMark™ platform. mRNAs were found to have two localization patterns, animal/central or vegetal. Because of the high resolution in sectioning, it was possible to distinguish two subgroups of the vegetal gene patterns: germ plasm determinant pattern and profile of other vegetal genes.

1. Introduction

The early development of a multicellular organism is a complex process in which each step must be precisely controlled. Each cell has unique expression of genes and the spatial gene expression patterns within the growing embryo depend on the cells' position.

In situ hybridization, microarray analyses, RNA protection assays, RT-PCR, Illumina sequencing and real-time quantitative PCR (qPCR) are among the most frequently used methods for gene expression analysis. Each method has its limitations and comparison of results between laboratories using different methods including different conditions and protocols is difficult. For example, while whole mount *in situ* hybridization is standard for spatial analysis in developmental biology, quantification of gene expression is at best qualitative. On the other hand, high-throughput quantitative methods such as microarrays and Illumina sequencing can produce large amounts of quantitative expression data. However, spatial resolution is limited using these methods since they require large amounts of pure and high quality RNA. qPCR is in-between; quantification is highly precise and minute amounts of RNA can be used, which allows for spatial profiling. Tens of genes can be conveniently quantified in each sample.

Oogenesis in *Xenopus laevis* results in oocytes with 1.3 mm in diameter [1]. Mature oocytes have differently colored hemispheres that specify the developmental animal–vegetal axis. Pigmentation of the animal hemisphere is caused by accumulation of melanosomes. The animal hemisphere also contains the germinal vesicle. The light color of the vegetal hemisphere is due to storage of yolk platelets [2].

mRNA molecules synthesized during oogenesis are termed maternal, because the template for their transcription is solely maternal chromosomes (reviewed in [3]). Two groups of maternal transcripts have been identified that differ in their spatial distribution in the *Xenopus* oocyte (reviewed in [4–6]). One group is called vegetal. These genes are expressed during the early stages of oogenesis and the corresponding mRNA molecules are actively transported from the nucleus to the vegetal pole. Two different transport pathways have been identified. DEADSouth, Xcad2, Xdazl and Xpat transcripts are transported by the early METRO (message transport organizer) pathway [7,8] and they accumulate in the primordial germ cells formed in later developmental stages. The second pathway is active later during oogenesis and transports mRNA molecules, such as VegT and Vg1, that are important for germ layer determination. The vegetal hemisphere gives rise to the endoderm cell layer in later stages of development and stimulates the formation of the mesodermal layer. mRNAs encoded by many maternal genes including An1, An2, An3, Tcf-1, axin, Xpar1 localize predominantly in the animal hemisphere [4–6,9].

The distribution of mRNAs along the animal–vegetal axis in the *Xenopus* oocyte is critical for successful development. The second

* Corresponding author. Address: Laboratory of Gene Expression, Institute of Biotechnology, Academy of Sciences of the Czech Republic, Prague, Czech Republic. Fax: +46 31 152890.
E-mail address: mikael.kubista@tataa.com (M. Kubista).

1046-2023/$ - see front matter © 2010 Elsevier Inc. All rights reserved.
doi:10.1016/j.ymeth.2009.12.011

developmental axis, the dorsal–ventral, can be distinguished at the 4-cell stage in *Xenopus*. The sperm enters the oocyte at a random position in the animal pole. This is followed by the cortical rotation approximately 20 min after the fertilization [10–12], during which the vegetal cortex layer moves approximately 30° in the opposite direction to the sperm's entry. This results in the accumulation of beta-catenin and some yet unknown stabilizing factors into the forthcoming dorsal side of the embryo. Surprisingly, the cortical rotation does not significantly change the distribution of maternal mRNAs along the A–V axis [9].

In this paper we present the high resolution qPCR tomography technique for spatiotemporal analysis of mRNAs in the *X. laevis* oocyte. We present the entire procedure from sample preparation, embedding, slicing, RNA extraction, reverse transcription, preamplification, qPCR to data analysis. In our study, *X. laevis* oocytes were sectioned into 15 segments across the animal–vegetal (A–V) axis and the levels of 31 maternal transcripts, mitochondrial RNAs, and nucleus specific RNAs were quantified using the high-throughput real-time RT-PCR microfluidic BioMark™ platform (www.fluidigm.com).

2. Materials and methods

2.1. Embryo fixation and sectioning

Xenopus laevis females were stimulated with 500 U of hCG (human chorionic gonadotrophin) and kept overnight in room temperature. Oocytes were obtained by gentle squeezing. They were not treated with cysteine, which is common procedure, because the treatment compromises the subsequent cryo sectioning of the samples. Three oocytes from the same female were used in our study. The oocytes were embedded in a drop of optimum cutting temperature (OCT) on a pre-cooled dissection block (Microm HM560). The block was placed for 5 min at −20 °C in the cryostat chamber and the samples were dissected into 45 slices each 30 μm thick along the animal–vegetal (A–V) axis (Fig. 1). Consecutive slices were pooled into fifteen tubes with three slices in each. Hence, the first tube contained the first three animal sections, the second tube contained sections 4–6, etc., and tube fifteen contained the last three vegetal sections.

2.2. Extraction of total RNA and quality control

The RNeasy Micro kit (Qiagen) was used for total RNA extraction. RLT (350 μl) RNeasy lysis buffer with 1% mercaptoethanol and RNA carrier was added to each tube, which were immediately stored at −80 °C. After thawing of the samples they were vortexed for at least 1 min in lysis buffer. The mercaptoethanol added and the long vortexing were found to be essential for efficient removal of inhibitors. Yolk platelets localized in the vegetal part of the oocyte were found serious inhibitor of reverse transcription and qPCR. RNA concentrations were measured with the Nanodrop® ND1000 quantification system (Nanodrop Inc., Fig. 1).

Quality of the extracted RNA was assessed by running 10 randomly selected samples on the capillary electrophoresis system Experion (Bio-Rad). Total RNA (50 ng) was denatured and loaded into the HighSense chip and run according to the manufacturer's protocol (Fig. 2). An 18S to 28S ribosomal RNA ratio of 1:2 indicated high quality RNA. High quality RNA is further supported by the absence of short RNA fragments that would indicate degradation.

2.3. Reverse transcription

cDNA was produced starting with 30 ng of total RNA, 1.5 μl of a (1:1) mixture of 10 μM oligo-dT and 10 μM random hexamers and water. Total reaction volume was 8.5 μl. After 10 min incubation at 72 °C, 100 U of MMLV reverse transcriptase (Promega), 12 U of RNasin (Promega), 5 nmol of dNTP and 2 μl of buffer (5×) were added to a total volume of 11.8 μl. The mixture was incubated for 60 min at 37 °C. The cDNA product was diluted to 60 μl and stored at −20 °C.

2.4. Primer design and preamplification

Primers for the amplification of the 31 selected maternal genes were designed with Primer3 [http://frodo.wi.mit.edu/primer3/]. Primer specificity and assay efficiency was tested on control cDNA (mixture of cDNA from different *Xenopus* developmental stages). Acceptance criteria were: specific amplification of control cDNA with a Cq lower than 35, a single dominant peak in the derivative of the melting curve, and no amplification of non-template controls.

Preamplification was used to increase the number of template molecules. This is needed because the cDNA synthesis does not yield sufficient number of molecular copies of the template molecules that they can be analyzed with confidence in parallel singleplex reactions. Preamplification PCR was run in 20 μl containing 4 μl of cDNA, 2 μl of a mixture of all forward and reverse primers (500 nM each), 10 μl of Sigma JumpStart mastermix (Sigma, cus-

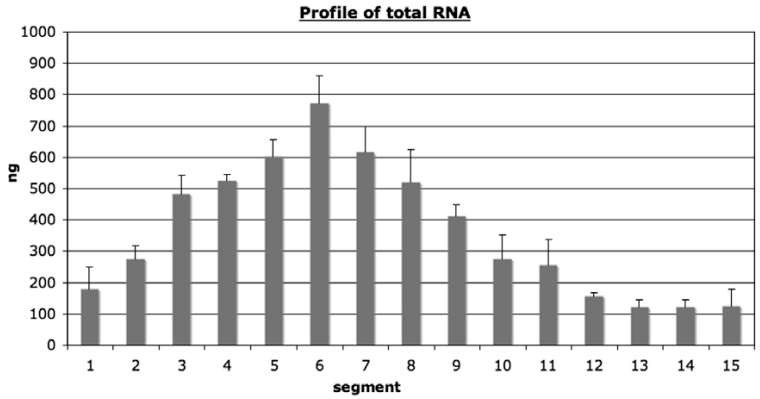

Fig. 1. Spatial distribution of total RNA in the *Xenopus laevis* oocyte. Oocytes were sectioned across the A–V axis. Total RNA was extracted and quantified using the Nanodrop. Each bar represents a 90 μm section.

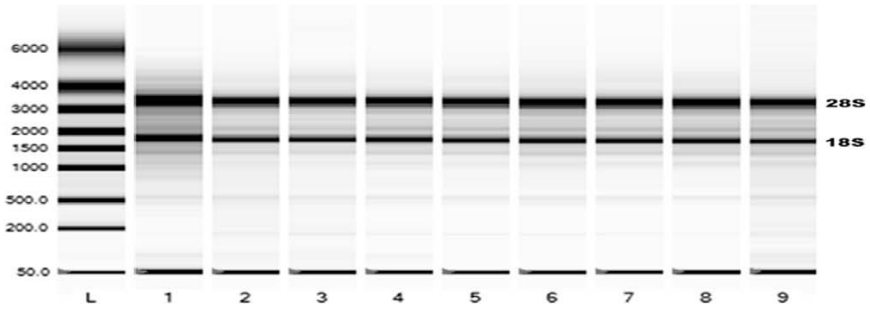

Fig. 2. The quality of the extracted RNA was assessed with capillary electrophoresis (Experion, Bio-Rad). Total RNA (100 ng) from 11 sections were analyzed on high sense chip.

tomized product) and water. A CFX 96 cycler (Bio-Rad) was used for the preamplification with the cycling conditions: polymerase activation at 95 °C for 2 min, followed by 18 cycles (95 °C 15 s, 59 °C 1 min and 72 °C 1 min). The product of the preamplification reaction was diluted to 80 μl and stored at −20 °C. The robustness of the preamplification was validated by comparing qPCR expression levels of the genes Xmam1 and Vg1 that were analyzed with and without preamplification. The relative expression of the two genes was similar when analyzing data with and without preamplification (Fig. 3).

2.5. High-throughput qPCR performed on Biomark system

The high throughput microfluidic qPCR platform BioMark™ (Fluidigm) was used for qPCR analysis running the 48.48 dynamic array. The sample reaction mixtures had a final volume of 5.3 μl made up of 1.2 μl preamplified cDNA, 0.6 μl of SYBR Green Sample Loading reagent (Fluidigm), 2.77 μl Sigma A mastermix (Sigma, custom product), 0.165 μl of Chromophy, diluted 1:25 (TATAA Biocenter), 0.025 μl of ROX (Invitrogen) and 0.1 μl of JumpStart DNA Taq polymerase (Sigma). The primer reaction mixtures had also a final volume of 6 μl and were made up of 3 μl Assay Loading reagent (Fluidigm) and 3 μl of a mixture of reverse and forward primers (10 μM). The empty dynamic array was first primed with oil solution in the NanoFlex™ 4-IFC Controller (Fluidigm) to fill its control valves. Sample reaction mixtures were loaded into the sample wells carefully avoiding any bubbles, and primer reaction mixtures were loaded into the assay wells. The dynamic array was then placed again into the NanoFlex™ 4-IFC Controller for loading and mixing. The mixing takes place by diffusion between the reaction chambers filled with sample reagent and adjacent containers filled with the appropriate primer and probe mix, between which a channel is opened. After about 55 min the dynamic array was transferred to the BioMark™. The qPCR cycling program was 3 min at 95 °C for activation of the hot-start enzyme, followed by 30 cycles of denaturation at 95 °C for 15 s, annealing at 60 °C for 20 s, and elongation at 72 °C for 20 s. Melting curves analysis was performed after completed qPCR collecting fluorescence between 60 and 95 °C at 0.5 °C increments.

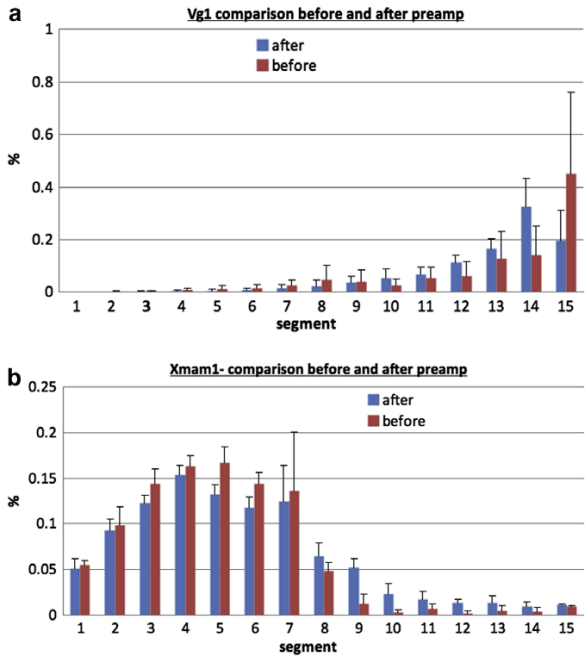

Fig. 3. Comparison of the spatial expression profiles of Vg1 (vegetal gene) and Xmam1 (animal genes) measured with and without preamplification.

2.6. Data analysis

Specific amplification of each targeted cDNA was confirmed by melt curve analysis. Measured Cq values were exported from the BioMark™ platform software to Excel for data analysis. qPCR technical replicates of samples were averaged. Expression ratios were calculated by the delta Cq method normalized to the first animal tube (containing sections 1–3). This artificially sets the expression of all genes in the first segment to 1, relative to which all other segments are expressed. For each oocyte and separately for every gene the relative expressions in all segments were summed, and the data were divided with the sum. This resulted in expression of each gene being presented as the percentage of its total expression. The percentage values for the three oocytes were finally averaged. The averaged values and associated standard deviations are presented. The standard deviations were in general very small and cannot be seen in the plot.

3. Results

During optimization of sample collection and preparation for cryosectioning we found that extensive cysteine treatment, which is common in many protocols, makes oocytes fragile and lowers the quality of the RNA. Because of the large size (1.3 mm in diameter) of the *X. laevis* oocyte, different thickness of the cryostat sections is possible. We found that 30 μm sections, which is the maximum width possible with our cryostat (Microm), worked very well and most oocytes gave the same number of sections. We also

found that pre-incubation of the samples in the cryostat chamber for at least 10 min was important for smooth sectioning. Mercaptoethanol (1%) was critical not only for reducing the activity of RNases, but also for removal of the yolk and other lipids from the vegetal pole. Once the protocol was optimized, the variability in total RNA concentration between segments cut from different oocytes was very low, evidencing precise and reproducible sectioning and RNA extraction (Fig. 1). The quality of the extracted RNA was assessed with capillary electrophoresis using the Experion system (Bio-Rad), and indicated high quality RNA (Fig. 2).

The reaction chambers in the BioMark™ platform are only 10 nl and the loaded cDNA is automatically aliquoted into 48 chambers. For each chamber to contain sufficient cDNA for reliable quantification the material must be preamplified. The performance of the preamplification was tested by comparing one vegetal gene (Vg1) and one animal gene (Xmam1) with and without preamplification. The relative expression of the two genes was the same suggesting that preamplification introduces minimal bias (Fig. 3).

Two main spatial expression profiles were found for the 31 maternal genes studied. Most were abundant in the upper third of the oocyte, which is in the animal hemisphere probably close to the oocyte nucleus. Genes frequently used for normalization of expression in *X. laevis* [13], such as EF-1alpha, GAPDH, beta-tubulin, alpha-actin and RNA polymerase II had this localization. Mitochondrial cytochrome C mRNAs and U3 snoRNA, which is located in the nucleolus, were also localized to the animal hemisphere (Figs. 4 and 5). The high resolution of qPCR tomography allowed two subgroups within the vegetal genes to be distinguished (Fig. 6). The spatial distribution of germ plasm determinants such as Xdazl, DEADSouth and Xcad2 shows a very steep gradient toward the vegetal pole, suggesting that these mRNAs are localized densely close to the pole itself [14]. Vg1, VegT, Otx1, Eg6 and Wnt11 are also localized vegetal, but with a less steep spatial gradient toward the pole.

4. Conclusions

qPCR tomography was introduced by Sindelka et al., in 2008. In the pioneer work *X. laevis* oocytes were sectioned into five segments across the animal–vegetal axis and expression levels of 18 maternal genes were measured by qPCR. Two distinct expression patterns were found that were referred to as animal and vegetal. In the presented study, we refine the qPCR tomography technique to increase its resolution to 15 segments. This allowed us to distinguish two subgroups of the vegetal genes.

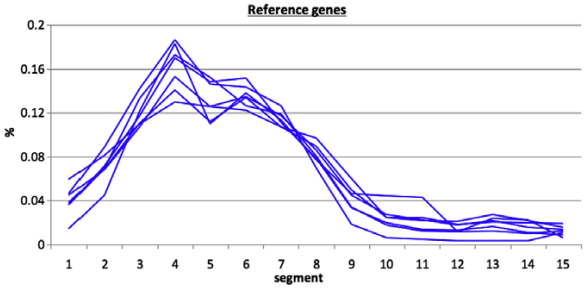

Fig. 4. Spatial expression profiles of common reference genes, mitochondrial RNA, reflecting the distribution of mitochondria in the cell, and nucleolar RNA, reflecting the position of the nucleus, along the A–V axis of the *X. laevis* oocyte. Distributions of mRNA coding RNA polymerase 2, mitochondrial cytochrome C, GAPDH, EF-1alpha, beta-tubulin, alpha-actin and U3 snoRNA was determined in 15 serial segments.

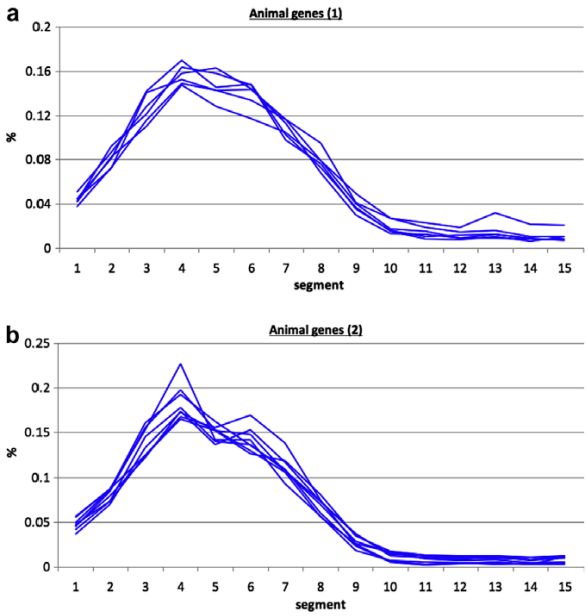

Fig. 5. Expression profiles of animal genes along the A–V axis of *X. laevis* oocyte. The distribution of mRNAs coding for An1, An2, APC, axin, Est1, Fz7, Zp3 and ZPC (1) and Xmam1, XPar1, Tcf-3, Stat3, Oct60, GSK-3beta and FoxH1 (2) was determined in 15 serial segments.

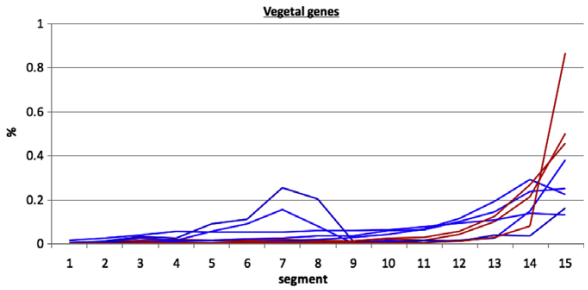

Fig. 6. Expression profiles of vegetal genes along the A–V axis of the *X. laevis* oocyte. The distribution of mRNA coding germ plasm factors Deadsouth, Xdazl and Xcad2 (in red) and other vegetal genes Otx1, Eg6, Vg1, VegT and Wnt11 (in blue) was determined in 15 serial segments.

The majority of mRNA molecules encoded by animal genes were found in sections 3–8. This is where the oocyte nucleus is expected to be located. This may indicate that animal transcripts are localized in the nucleus or stored somewhere near it. Interestingly, common reference genes used in *Xenopus* expression studies, such as EF-1alpha, GAPDH, beta-tubulin and alpha-actin, have animal localization. Clearly, they would not be suitable for normalization of spatial expression in the *Xenopus* oocyte and not even in early blastomere stages, where the original spatial distribution remains (unpublished data).

The higher sensitivity, better specificity and wider dynamic range of qPCR tomography compared to other RNA based methods allow spatial expression profiles to be measured with higher resolution than has been possible. Previous studies on single cell expression profiling have indicated large variations in the mRNA levels among cells [15,16]. This does not seem to apply to the *Xenopus* oocyte. The intracellular expression profiles seem to be highly conserved among the oocytes, indicating that mRNA spatial distribution is critical for the early development.

Acknowledgments

This work was supported by Grant agency of Academy of Science Czech Republic (IAA500970904) and research goal AV0Z50520701 granted by Ministry of Youth, Education and Sports of the Czech republic, together with support from Grant agency of Czech Republic (GACR 301/09/1752).

References

[1] P. Chang, D. Perez-Mongiovi, E. Houliston, Microsc. Res. Tech. 44 (1999) 415–429.
[2] M.V. Danilchik, J.C. Gerhart, Dev. Biol. 122 (1987) 101–112.
[3] J. Heasman, Semin. Cell Dev. Biol. 17 (2006) 93–98.
[4] M.L. King, T.J. Messitt, K.L. Mowry, Biol. Cell 97 (2005) 19–33.
[5] Y. Zhou, M.L. King, IUBMB Life 56 (2004) 19–27.
[6] K.L. Mowry, C.A. Cote, FASEB J. 13 (1999) 435–445.
[7] H. MacArthur, M. Bubunenko, D.W. Houston, M.L. King, Mech. Dev. 84 (1999) 75–88.
[8] H. MacArthur, D.W. Houston, M. Bubunenko, L. Mosquera, M.L. King, Mech. Dev. 95 (2000) 291–295.
[9] R. Sindelka, J. Jonak, R. Hands, S.A. Bustin, M. Kubista, Nucleic Acids Res. 36 (2) (2008) 387–392.
[10] J. Gerhart, M. Danilchik, T. Doniach, S. Roberts, B. Rowning, R. Stewart, Development 107 (1989) 37–51.
[11] J.C. Gerhart, J.P. Vincent, S.R. Scharf, S.D. Black, R.L. Gimlich, M. Danilchik, Philos. Trans. R. Soc. Lond. B Biol. Sci. 307 (1984) 319–330.
[12] J.P. Vincent, J.C. Gerhart, Dev. Biol. 123 (1987) 526–539.
[13] R. Sindelka, Z. Ferjentsik, J. Jonak, Dev. Dyn. 235 (2006) 754–758.
[14] F. Nishiumi, T. Komiya, K. Ikenishi, Dev. Growth Differ. 47 (1) (2005) 37–48.
[15] M. Bengtsson, A. Stahlberg, P. Rorsman, M. Kubista, Genome Res. 15 (2005) 1388–1392.
[16] A. Tichopad, R. Kitchen, I. Riedmaier, C. Becker, A. Ståhlberg, M. Kubista, Clin. Chem. 55 (10) (2009) 1816–1823.

4.2. Single blastomere expression profiling of *Xenopus laevis* embryos of 8 to 32-cells reveals developmental asymmetry

Flachsova M., Sindelka R. a Kubista M. *Scientific Reports* 2013, 3:2278. IF 5.078

Asymetrická distribuce maternálních faktorů uvnitř oocytu a jejich následné nerovnoměrné rozdělení do dceřiných buněk představuje klíčový mechanismus determinace a diferenciace v časném embryonálním vývoji. Předmětem této studie byla distribuce 41 maternálních mRNA (*fzd7, otx1, bmp2, pias1, dvl2, dvl3, lrp6, trim36, foxr1, frat1, mapk8, odc1, 18S rRNA, 5S rRNA, cyc1, acta, tubb, gapdh, maml1, eef1a1, RNA pol. II, U3 snoRNA, par1, oct60, ddx25, dazl, cdx1, wnt11, vg1, vegt, axin1, est1, apc, tcf3, zpc, gsk3b, ctnnb1, mos, foxh1, stat3, pax6*) do jednotlivých blastomer od vývojového stádia 8 buněk až po stádium 32 buněk u *X. laevis*. Účelem bylo vytvoření distribuční mapy maternálních transkriptů, které předurčují formování základních tělních os (animálně-vegetativní, dorzo-ventrální a pravo-levé tělní osy) v průběhu rýhování. Naše předchozí studie prokázala, že dochází k nerovnoměrné distribuci maternálních transkriptů uvnitř oocytu podél animálně-vegetativní osy. V této studii výsledek analýzy maternálních transkriptů v jednotlivých blastomerách dokazuje, že dochází k zachování této animálně-vegetativní asymetrie i v průběhu rýhování a animální blastomery vykazují jiné zastoupení transkriptů než vegetativní blastomery. Nicméně nebyl nalezen žádný mRNA gradient, který by odpovídal formování dorzo-ventrální a/nebo pravo-levé tělní osy. Všechny studované transkripty vykazovaly rovnoměrnou distribuci uvnitř animální a vegetativní skupiny buněk. Z tohoto faktu byla vyvozena hypotéza, že ačkoliv animálně-vegetativní asymetrie vzniká důsledkem nerovnoměrné distribuce maternálních mRNA, dorzo-ventrální a pravo-levé určení tělního plánu bude zřejmě závislé na asymetrické lokalizaci jiných maternálních biomolekul. Mezi tyto biomolekuly patří zejména proteiny. Nerovnoměrná lokalizace maternálních proteinů může být způsobena jejich přímou distribucí do konkrétní části časného embrya anebo prostorově regulovanou translací maternálních mRNA.

SCIENTIFIC REPORTS

OPEN

SUBJECT AREAS:
CELL LINEAGE
DIFFERENTIATION
EMBRYONIC INDUCTION
BODY PATTERNING

Received
13 May 2013

Accepted
5 July 2013

Published
24 July 2013

Correspondence and requests for materials should be addressed to M.K. (mikael.kubista@img.cas.cz)

Single blastomere expression profiling of *Xenopus laevis* embryos of 8 to 32-cells reveals developmental asymmetry

Monika Flachsova[1,2], Radek Sindelka[1] & Mikael Kubista[1,3]

[1]Laboratory of Gene Expression, Institute of Biotechnology, Academy of Sciences of the Czech Republic, Prague, Czech Republic, [2]Charles University in Prague, Faculty of Science, Department of Cell Biology, Prague, Czech Republic, [3]TATAA Biocenter AB, Göteborg, Sweden.

We have measured the expression of 41 maternal mRNAs in individual blastomeres collected from the 8 to 32-cell *Xenopus laevis* embryos to determine when and how asymmetry in the body plan is introduced. We demonstrate that the asymmetry along the animal-vegetal axis in the oocyte is transferred to the daughter cells during early cell divisions. All studied mRNAs are distributed evenly among the set of animal as well as vegetal blastomeres. We find no asymmetry in mRNA levels that might be ascribed to the dorso-ventral specification or the left-right axis formation. We hypothesize that while the animal-vegetal asymmetry is a consequence of mRNA gradients, the dorso-ventral and left-right axes specifications are induced by asymmetric distribution of other biomolecules, probably proteins.

Understanding the formation of the embryonic body plan is essential in developmental biology. It is generally accepted that mechanisms of cellular differentiation driving development are based on differential transcription and translation of key regulatory elements. Recent development of highly sensitive and reliable molecular diagnostic methods allows for precise measurements of genes' transcriptional activities in very small samples including single cells[1]. In an excellent study by Guo *et al.*, mouse embryos from 8 to 64 cells were dissociated into individual blastomeres and gene expression profiles were measured using the high-throughput microfluidic quantitative real-time PCR (qPCR) system BioMark[2]. They found early mouse embryos are composed of three types of cells representing the trophoectoderm, epiblast, and primitive endoderm. The three cell types were readily distinguished by the expression profile of 48 genes. Pluripotency of mouse single blastomeres from preimplantation embryos (1 to 16-cell stages) was also demonstrated with multiplex RT-PCR expression analysis by May *et al.*[3]. Expression profiles of trophoectoderm markers, inner cell mass markers and stemness markers have also been measured on human single blastomeres from 5 to 8-cell embryos by Galan et al., using microarray[4] and in single putative stem cells from human adult ovarian surface epithelium[5].

The *Xenopus* oocyte has two differentially colored hemispheres known as animal and vegetal. The separation into the hemispheres creates the first developmental axis of the embryo referred to as animal-vegetal. The darker color of the animal hemisphere is due to accumulation of pigmented granules called melanosomes. The vegetal hemisphere stores yolk and has light color[6]. *De novo* transcription in the developing *Xenopus* embryo is silenced until the mid-blastula transition stage (MBT), which takes place after twelve cell divisions post fertilization. All mRNA molecules required for the development into MBT must be present in the oocyte. These were transcribed during oogenesis from solely maternal chromosomes. The maternal mRNAs are asymmetrically distributed along the animal-vegetal axis of the oocyte and direct the specialization of the animal and vegetal parts[7–9]. The second embryonic body axis is formed after fertilization and separates the embryo into a dorsal and a ventral part. In *Drosophila* embryos the mechanism determining the dorsal-ventral axis is triggered by a concentration gradient of *gurken* maternal mRNA, which is accumulated at the future dorsal site. Absence of *gurken* mRNA at the ventral site leads to translocation of transcription factor Dorsal from the cytoplasm into the nuclei, where the Dorsal activates genes that specify the ventral part[10]. The mechanistic details of the dorso-ventral axis formation in zebrafish are not known, but differences between the dorsal and ventral parts appear during the gastrula stage, when the ventral side of the embryo gets thinner than the dorsal side[11]. The formation of the dorso-ventral axis in *Xenopus laevis* embryo can be discerned already at the 4-cell stage[12]. The sperm enters the oocyte through the animal hemisphere and in about 25 minutes the cortical cytoplasm of the oocyte rotates some 30 degrees relative to the inner cytoplasmic mass in opposite direction to the sperm's entrance[13,14]. Dorsal maternal factors, such as

the Dishevelled protein (Dvl), move to the future dorsal side in the vegetal hemisphere of the oocyte[15]. Dvl inactivates gsk3β protein and protects β-catenin from degradation. The accumulation of β-catenin in the dorsal site of the embryo promotes local Wnt signaling, which regulates transcription of zygotic *xnr3* and *siamois*, leading to dorsalization of the embryo[16,17]. The first cell division cuts the oocyte through the point of sperm entrance in the animal pole and the groove elongates to the vegetal pole. The second cell division is perpendicular to the first and separates the embryo into the future dorsal and ventral halves. All four blastomeres contain cytoplasm from both the animal and vegetal hemispheres, but vary in size and pigmentation[12]. The third and last important body axis of *Xenopus laevis* embryos creates the right-left asymmetry, which manifests at the gastrula stage when the production of embryonic mRNAs has been initiated. Maternal vg1 protein is more active in the left side of the embryo and activates the expression of *xnr1* (*Xenopus* nodal-related 1). Xnr1 induces pitx2 production, which is required for the left side formation. Injection of vg1 protein to the future right side of the embryo causes left-right deformation manifested by random localization of the heart and of the digestive tube[18].

We have previously used quantitative real-time PCR (qPCR) expression profiling of cryostat sections (qPCR tomography) of a single oocyte to identify transcripts that form gradients along the animal-vegetal axis[8,9]. These transcripts will become differentially distributed among the animal and the vegetal blastomeres formed at the third cell division. The purpose of the present study is to elucidate if there are expression gradients throughout the embryo that also reflect the dorsal-ventral axis specification and the left-right axis formation by measuring expression of selected 41 maternal genes in individual blastomeres collected from *Xenopus* embryos between 8 to 32-cell stages.

Results

First we extensively optimized our experimental procedure for high extraction and reverse transcription yields, and high qPCR efficiencies. We standardized the protocol for minimum technical variation for the expression profiling of single blastomeres. The vegetal blastomeres store yolk, which is strong inhibitor of biochemical reactions and can induce high variation in the reverse transcription yield and compromise qPCR efficiencies. An RNA spike (*in vitro* transcribed artificial RNA with 3′ polyA tail and 5′ cap, TATAA Biocenter) was used to validate the reverse transcription reaction and the qPCR. The spike was added to the RNA extracted from the samples together with the random sequence hexamers and oligo-dT primers for reverse transcription. The amount of reverse transcribed spike was then measured along with the endogenous transcripts. For the optimized protocol the standard deviation of the RNA spike Cq values across all samples was below 0.20 cycles, which evidences excellent reproducibility between sample preparations. Embryos from the same mother also showed high concordance. Our protocol for expression profiling is based on collecting the individual blastomeres in random order and we can only keep track from which hemisphere (animal or vegetal) the different blastomeres originated. This was necessary to avoid introducing bias during collection. With this protocol any dorso-ventral (or possibly left-right) asymmetry would be reflected by heterogeneity in expression profiles among the blastomeres collected from the same hemisphere. As markers to probe the formation of the three developmental axes we chose ten maternal transcripts that have been implicated in the dorso-ventral patterning: *dvl2, dvl3, lrp6, wnt11, tcf3, gsk3b, ctnnb1(=β-catenin), foxh1, trim36* and *axin1*[16,19–21], one important marker for left-right specification: *vg1*[18], and nine genes implicated in animal-vegetal orientation: *dazl, cdx1 (=xcad2), wnt11, vg1, vegt, trim36, ddx25 (=deadsouth), otx1*, and *maml1*[9,19,22,23]. We also included 25 mRNAs that have previously been observed in the mature oocyte: *fzd7, bmp2, pias1, foxr1, frat1, mapk8, odc1, 18S rRNA, 5S rRNA, cyc1, acta, tubb, gapdh, eef1a1, RNA polymerase II, U3 snoRNA, par1, oct60, est1, apc, zpc, mos, stat3*, and *pax6*[8,9].

Expression data were collected for a total of 224 single blastomeres. The data were analyzed with principal component analysis (PCA) and hierarchical clustering, which are the most powerful multivariate methods to classify samples based on the collective expression of multiple genes[24]. PCA clearly separated cells originating from the animal and from the vegetal hemispheres into clusters (Fig. 1), and indicated that the vegetal blastomeres are more heterogeneous than the animal blastomeres. Neither of the clusters, however, divided into subgroups that would indicate additional asymmetry that could be ascribed to the formation of the other body axes (e.g. dorsal-ventral and left-right asymmetry). The PCA results were confirmed by classifications using SOM (not shown) and hierarchical clustering. The hierarchical clustering is presented in a

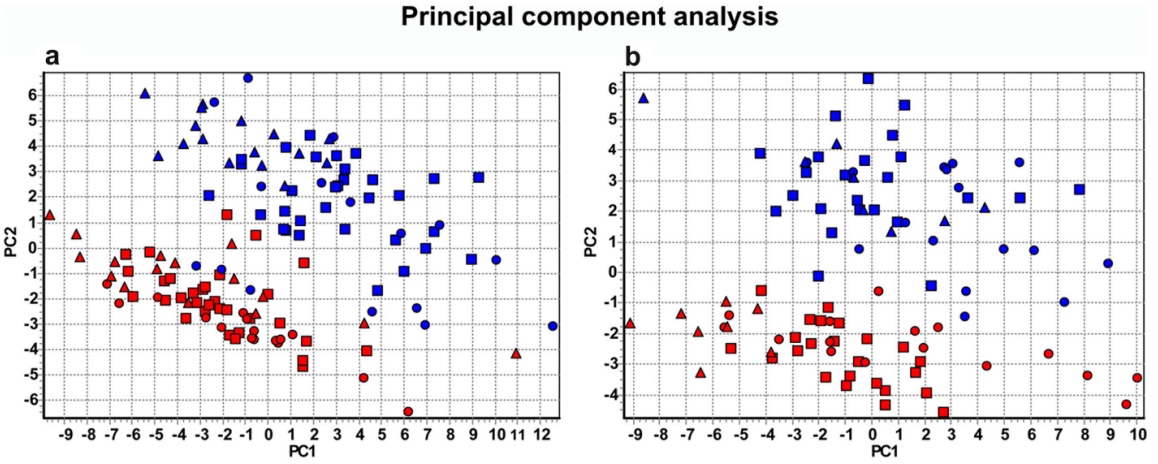

Figure 1 | PCA of profiled blastomeres collected from early developmental stages of *Xenopus laevis*. Triangles indicate blastomeres from the 8-cell stage; squares from the 16-cell stage, and circles from the 32-cell stage. Blastomeres originating from the animal hemisphere are shown in red and those from the vegetal hemisphere are shown in blue. Left and right graphs are data from two different females (left: four embryos from 8-cell stage, four embryos from 16-cell stage, and one 32-cell stage embryo, in total 128 blastomeres; right: two embryos from 8-cell stage, three from 16-cell stage, and one from 32-cell stage, in total 96 blastomeres).

heatmap (Fig. 2), which is a graphical illustration of all the genes' expressions in all the blastomeres with the level indicated by color, and dendrograms clustering the blastomeres and the genes, respectively, shown on the top and left side. Separate heatmaps were calculated for each embryo from 8-cell (six embryos), 16-cell (seven embryos), and 32-cell (two embryos) stages. Blastomeres of 8 and 16-cell stages separated into well-defined animal and vegetal clusters, but no subclusters that could be ascribed to the formation of dorsal-ventral or left-right body axes can be discerned. Blastomeres from the 32-cell stage also divided into an animal and a vegetal cluster. The 32-cell stage vegetal cluster was diffuse, reflecting heterogeneity among the vegetal blastomeres possibly caused by the blastomeres being arranged into two ventral layers and some transcripts, such as germ plasm determinants, being concentrated in the extreme ventral cortical layer. The genes cluster into four well separated groups at all the developmental stages studied. The first group contains ubiquitously expressed genes represented by *18S rRNA*, *5S rRNA*, and *cyc1*. These genes are expressed at high level in all the blastomeres at all stages. A second group is composed of *vg1*, *cdx1*, *vegt*, *dazl*, *wnt11*, *otx1*, *trim36*, and *ddx25*, which are most abundant in the vegetal blastomeres. Several of these transcripts have previously been found in the vegetal part of the mature oocyte[9]. Third and fourth groups of transcripts are more abundant in the animal blastomeres, but subtle difference in expression patterns separate them into two clusters. *Fzd7*, *bmp2*, *pias1*, *dvl2*, *dvl3*, *lrp6*, *frat1*, *mapk8*, *axin1*, *est1*, and *U3 snoRNA* are expressed at slightly lower level (indicated by the green shade in the heatmap in Fig. 2). Than the fourth set of genes; *ctnnb1*, *foxh1*, *odc1*, *zpc*, *mos*, *maml1*, *eef1a1*, *RNA polymerase II*, *foxr1*, *tcf3*, *gsk3b*, *oct60*, *stat3*, *par1*, *acta*, *tubb*, *gapdh*, *apc*, and *pax6* (indicated by the green shade turning to light red in the heatmap in Fig. 2). The separation of genes into these two groups shows some variability across embryos (data not shown). The separation of the gene transcripts into clusters is even more evident in the principal component analysis (PCA) (Fig. 3). One cluster characterizing genes expressed in animal blastomeres: *fzd7*, *bmp2*, *pias1*, *dvl2*, *dvl3*, *lrp6*, *frat1*, *mapk8*, *axin1*, *est1*, *U3 snoRNA*, *ctnnb1*, *foxh1*, *odc1*, *zpc*, *mos*, *maml1*, *eef1a1*, *RNA polymerase II*, *foxr1*, *tcf3*, *gsk3b*, *oct60*, *stat3*, *par1*, *acta*, *tubb*, *gapdh*, *apc*, and *pax6*; a second cluster of genes expressed in vegatal blastomeres: *vg1*, *cdx1*, *vegt*, *dazl*, *wnt11*, *otx1*, *trim36*, and *ddx25*; a third cluster of high expressed genes: *18S rRNA*, *5S rRNA*, and *cyc1*.

Discussion

Maternal mRNAs are synthesized during oogenesis and translated during the early development of *Xenopus laevis*. It is generally accepted that the temporal regulation and the spatial distribution of these maternal mRNAs are important for the establishment of the body axes and subsequently the whole body pattern. The animal-vegetal asymmetry is the first body axis formed during oogenesis. The germ layers, endoderm, mesoderm, and ectoderm, are formed along the animal-vegetal axis such that the vegetal part of the oocyte becomes the endoderm and the most distal animal part of the oocyte gives rise to the ectoderm[25,26]. Transcripts of genes coding specific endodermal and mesodermal factors, such as *vg1*, *wnt11*, and *vegt*, are localized in the vegetal hemisphere[8,9,22]. Genes responsible for primordial germ cell formation, such as *dazl* and *cdx1*, are localized towards the extreme vegetal pole[9]. Previously we described the new method qPCR tomography to quantify maternal mRNA distribution along the animal-vegetal axis formed during oogenesis, and found two dominant profiles: one with animal and one with vegetal mRNA localization[8]. Subsequent high-resolution qPCR tomography allowed us to discern two vegetal profiles; one encompassing germ plasm determinants (*dazl, cdx1, ddx25*) and one encompassing the other vegetal genes investigated (*vg1, vegt, wnt11, otx1, eg6*)[9]. In this study we show that the animal-vegetal polarizations observed in the oocyte remain in the 8, 16, and 32-cell stage embryos. The vegetal blastomeres had higher levels of *dazl, cdx1, ddx25, vg1, vegt, wnt11, otx1,* as well as *trim36*, which was not included in the oocyte study. At the 8 and 16-cell stages the vegetal mRNAs were distributed evenly among the vegetal blastomeres; the determinants of the germ plasm being present in all the vegetal cells. At the 32-cell stage, when the vegetal blastomeres form two layers, heterogeneity among the vegetal blastomers was introduced. *18S rRNA, 5S rRNA, cyc1, acta, tubb, gapdh, eef1a1, RNA polymerase II, U3 snoRNA, oct60, axin1, est1, apc, tcf3, zpc, gsk3b, maml1, ctnnb1, mos, foxh1, stat3, fzd7, par7, bmp2, pias1, dvl2, dvl3, lrp6, foxr1, frat1, mapk8, odc1* and *pax6* transcripts were more abundant in the animal blastomeres, and were evenly distributed among the individual cells. Multivariate statistical analysis revealed higher variability among the vegetal blastomeres than among the animal. The difference was particularly pronounced at the 32-cell stage. The heterogeneity seems random, possibly caused by yolk platelets that may interfere with PCR inducing technical noise or introduced by the formation of two ventral layers; but we find no evidence for systematic distribution of transcripts neither along the dorsal-ventral axis nor the left-right axis.

An essential question in developmental biology is how amphibians establish the dorsal-ventral axis. The site of sperm entry determines the future ventral half of the embryo. The dorsal part forms on the opposite side and is determined by the accumulation of maternal dorsal determinants during the cortical rotation[27–29]. Consequently, blastomeres of the early *Xenopus* embryos can be separated into a dorsal and a ventral group with equal number of animal and vegetal cells in each. In Drosophila the dorsalizing determinants have been shown to be maternal mRNA molecules that are asymmetrically distributed within the oocyte and regulate translation that leads to the polarization of the embryo[30,31]. In our study we tested if the dorsalizing factors in *Xenopus* embryogenesis are also mRNAs coding for dorsal specific proteins within the Wnt pathway. We found that among the maternal transcripts that have been implicated in the induction of dorso-ventral asymmetry *ctnnb1, dvl2, dvl3, lrp6, gsk3b, tcf3, foxh1,* and *axin1,* are present predominantly in the animal blastomeres, while *trim36* and *xwnt11* are more abundant in the vegetal blastomeres. This supports the idea that the majority of the dorsal-ventral inducing molecules is localized in the dorsal animal blastomeres of the 16-cell stage embryo[32], although we found no evidence of asymmetric distribution of maternal mRNAs among the dorsal or ventral blastomeres. In contrast to Tao *et al.*[33], we found *wnt11* distributed evenly between the dorsal and ventral cells. Our results rather support the finding of Schroeder *et al.*[34], who found maternal *wnt11* mRNA symmetrically distributed along the dorsal-ventral axis, and proposed that spatially regulated translation leads to asymmetric distribution of the Wnt11 protein. None of the 41 maternal mRNAs included in this study shows dorso-ventral polarization, although dorso-ventral asymmetry is observed starting from the 4-cell stage[12]. Of course, the dorso-ventral asymmetry could be induced by entirely different genes, but since our panel includes ten genes (*dvl2, dvl3, lrp6, wnt11, tcf3, gsk3b, ctnnb1, foxh1, trim36, and axin1*) previously implicated in dorsal-ventral patterning[16,19–21], this would be surprising. Rather, we suggest the dorsal-ventral asymmetry in *Xenopus laevis* is due to early accumulation of dorsal proteins that regulate signaling pathways, which after the midblastula transition activate the expression of downstream dorsalizing factors at the dorsal site of the embryo. We speculate these proteins are present already in the oocyte and accumulate in the future dorsal site during the cortical rotation. Our set includes only one, gene (vg1) previously shown to be involved in the left-right specification[18]. We find no evidence of asymmetric distribution of vg1 or of any other of the studied transcripts that could be implicated in left-right specification.

Methods

Ethics statement. This study was carried out in accordance with the Act No 246/1992 Coll., on the protection of animals against cruelty. Official permission was issued to Faculty of Science, Charles University in Prague by the Central Commission for

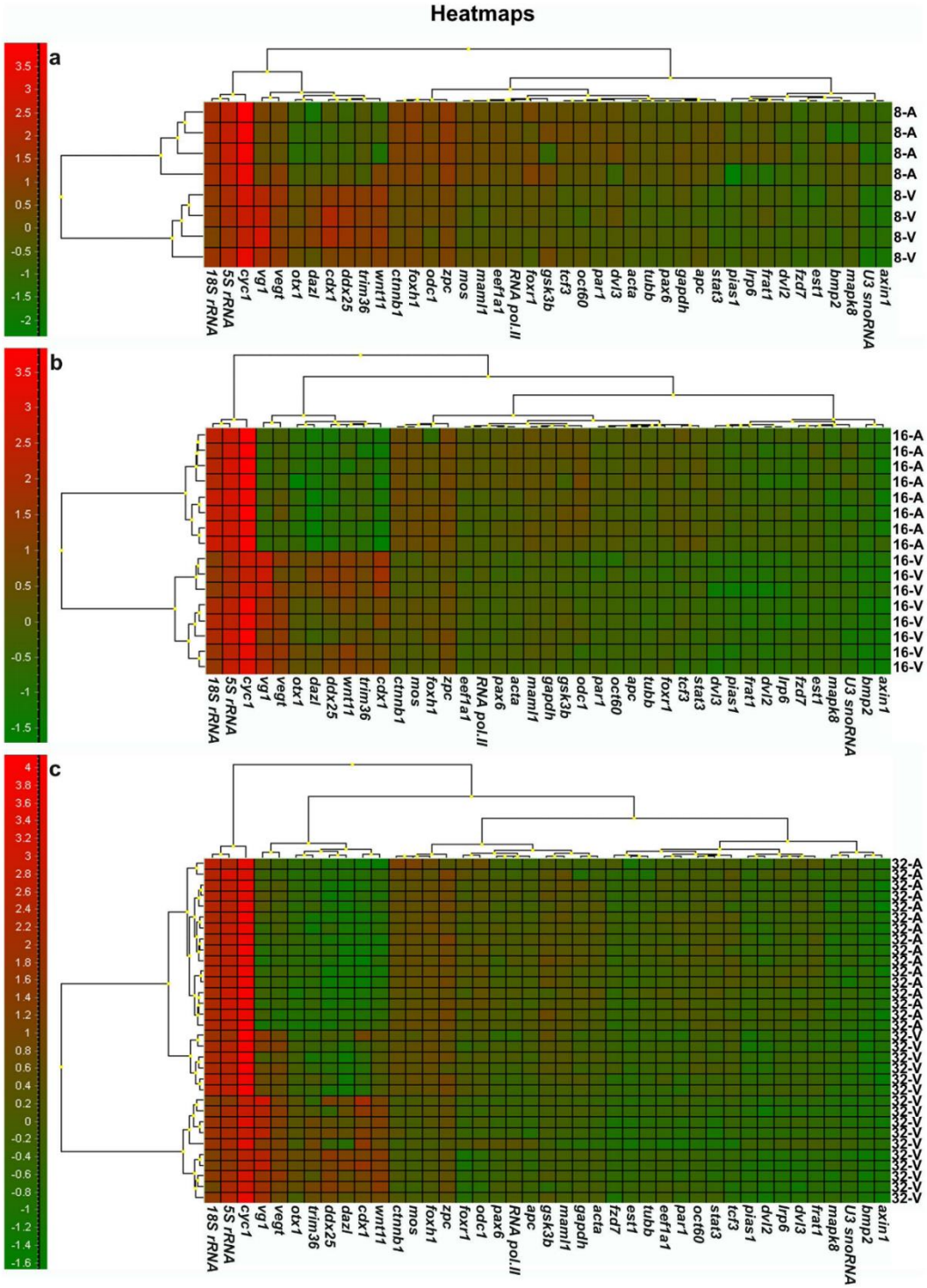

Figure 2 | Hierarchical clustering of blastomeres and mRNAs of *Xenopus laevis* early embryos presented as heatmaps. One embryo from each developmental stage was arbitrarily chosen for the cluster analysis. (A) 8-cell, (B) 16-cell and (C) 32-cell embryo. Green color indicates low expression and red high expression. The dendrograms clustering blastomeres and genes are shown in the top and left side of the heatmap, respectively. In the dendrograms similarity between blastomeres/genes is indicated by the height at which they are joined.

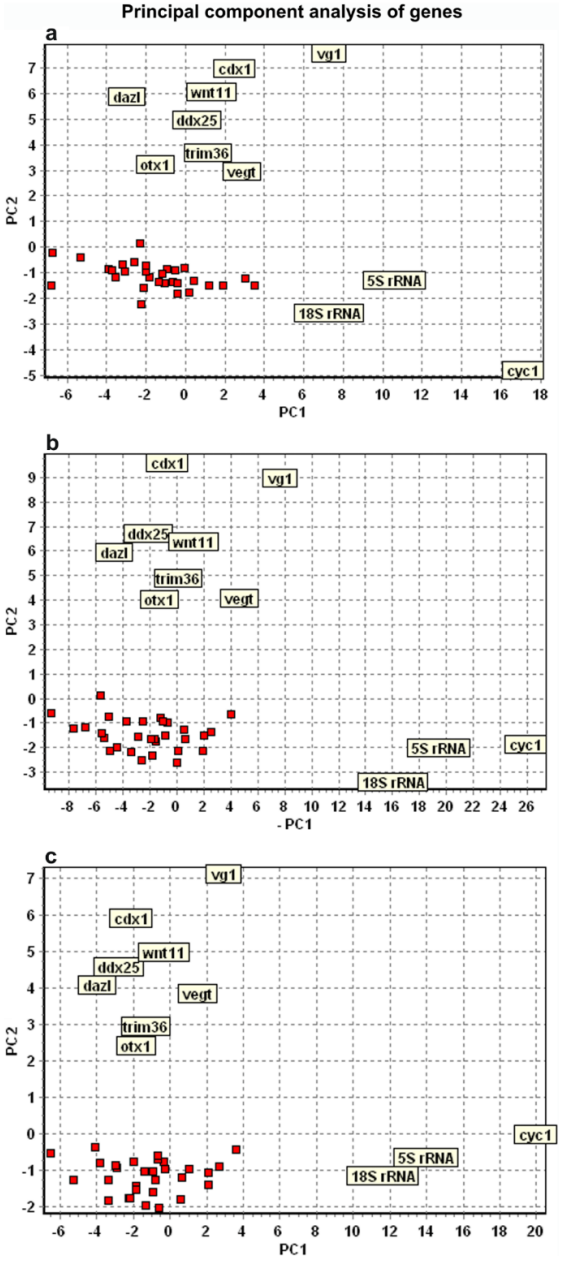

Figure 3 | Principal component analysis of maternal genes. (A) 8-cell stage (four embryos/32 cells analyzed), (B) 16-cell stage (four embryos/64 cells analyzed), and (C) 32-cell stage (32 cells analyzed) embryos. Three clusters are seen in all the developmental stages. First cluster comprises *18S rRNA, 5S rRNA,* and *cyc1(mitochondrial cytochrome c)*; second cluster *vg1, cdx1 (xcad2), wnt11, dazl, vegt, ddx25 (deadsouth), otx1,* and *trim36;* third cluster (red squares) *fzd7, par1, bmp2, pias1, dvl2, dvl3, lrp6, foxr1, fart1, mapk8, odc1, axin1, est1, U3 snoRNA, apc, gapdh, acta, eef1a1, tcf3, zpc, RNA polymerase II, gsk3b, maml1, tubb, ctnnb1 (β-catenin), mos, oct60, foxh1, stat3,* and *pax6.* The animal-vegetal distinction is found along the y-axis (PC2), while differences in expression level of the maternal transcripts is reflected along the x-axis (PC1).

Animal Welfare under the Ministry of Agriculture of Czech Republic (accreditation No.24773/2008-10001, date of expiry 10.12.2013). The experiment was also approved by the institutional ethics committee.

***In vitro* fertilization and collection of single blastomeres.** Two *Xenopus laevis* females were injected with 450 U of human chorionic gonadotrophin hormone (hCG) and kept overnight at room temperature. Ovulated oocytes were obtained 12 hours after stimulation by manual squeezing. Testes of *Xenopus laevis* males were removed and homogenized in L-15 Leibowitźs medium with 15% of fetal bovine serum. Oocytes were *in vitro* fertilized by sperm suspension and 1× MMR medium (Marćs Modified Ringers medium: 0.1 M NaCl, 2.0 mM KCl, 1 mM $MgCl_2$, 2 mM $CaCl_2$, 5 mM HEPES, pH 7.7) was added to cover the fertilized oocytes. Jelly coats were removed by cysteine treatment (2.2% in MMR, for 8 minutes) at 20 minutes after fertilization. During cell division the embryos were transferred to Ca^{2+} and Mg^{2+} free medium (88 mM NaCl, 1 mM KCl, 2.4 mM $NaHCO_3$, 7.5 mM Tris, pH 7.7) and kept there for 60 minutes in order to separate single blastomeres. Vitelline membranes of the embryos containing 8, 16, and 32 cells were manually torn and individual blastomeres were collected. The blastomeres were collected separately from animal and vegetal hemispheres, but in random order to avoid introducing any technical bias and subjective dorso-ventral specification before measurement.

Isolation of total RNA and reverse transcription. The individual blastomeres collected from the 8 and 16-cell stages were homogenized in 200 µl and blastomeres from the 32-cell stage in 100 µl of TRIzol reagent (Invitrogen), and immediately frozen at −80°C. After thawing, the samples were carefully vortexed for 2 minutes to pulp yolk. Manufacturer's instructions were followed during isolation of total RNA, and glycogen was added to enhance RNA precipitation yield. RNA from individual cells from the 8 and 16-cell stages was dissolved in 20 µl of RNase-DNase free water. Samples from the 32-cell stage were dissolved in 12 µl of water. RNA concentration was measured using the Nanodrop ND1000 quantification system. cDNA was produced with SuperScript™ III Reverse transcriptase kit (Invitrogen). 10 ng of total RNA, 0.5 µl of a mixture of oligo-dT and random hexamers (mixture 1 : 1, 50 µM each), 0.5 µl of dNTPs (10 mM each), and 0.5 µl of RNA spike (*in vitro* transcribed artificial RNA with 3′ polyA tail and 5′ cap, TATAA Biocenter) were mixed with sterile water to a total volume of 6.5 µl. Samples were incubated for 5 min at 70°C, followed by 20 sec at 25°C, and then cooled at 4°C for 1 min. 100 U of SuperScript III reverse transcriptase, 20 U of RNaseOUT™ (recombinant ribonuclease inhibitor, Invitrogen), 0.5 µl of 0.1 M DTT and 2 µl of 5× first strand synthesis buffer was added to a final volume of 10 µl. The following temperature gradient profile was used to synthesize cDNA: 5 min at 25°C, 60 min at 50°C, 15 min at 55°C, and 15 min at 75°C. cDNA samples were diluted 8 times to a final volume of 80 µl and were stored at −20°C.

Primer design and quantitative PCR. Primer assays for the selected 41 maternal genes (fzd7, otx1, bmp2, pias1, dvl2, dvl3, lrp6, trim36, foxr1, frat1, mapk8, odc1, 18S rRNA, 5S rRNA, cyc1, acta, tubb, gapdh, maml1, eef1a1, RNA polymerase II, U3 snoRNA, par1, oct60, ddx25, dazl, cdx1, wnt11, vg1, vegt, axin1, est1, apc, tcf3, zpc, gsk3b, ctnnb1, mos, foxh1, stat3, pax6) were designed with Primer3Plus (http://www.bioinformatics.nl/cgi-bin/primer3plus/primer3plus.cgi). Annealing temperature was set to 60°C and the length of qPCR products was around 120bp. Specificity of the assays was tested in silico using blast (http://blast.ncbi.nlm.nih.gov/Blast.cgi). Primer sequences are available upon request. qPCR and melting curve validations were measured on the real-time CFX384 cycler system (BioRad). qPCR mix contained 2 µl of cDNA, 0.5 µl of forward and reverse primers (mixture 1 : 1, 10 µM each), 5 µl of SYBR Green JumpStart™ Taq Ready Mix™ (Sigma), and water in a total volume of 10 µl. The cycling program was: 2 min at 95°C for activation of the polymerase, followed by 40 cycles of denaturation at 95°C for 15 sec, annealing at 60°C for 20 sec and elongation at 72°C for 30 sec. Post PCR melting curves were measured from 65 to 95°C in 0.5°C intervals to validate the formation of expected PCR products.

Data analysis. Data were analyzed with GenEx (MultiD, version 5.3.). Off scale data were removed during pre-processing using a cut off at 36 cycles and outliers were identified with Grubb's test. Missing data were imputed using the average Cq of the other blastomeres from the same hemisphere in the same embryo (roughly 6% of the data was imputed). All data were normalized to the spike and converted to relative quantities (relative to the highest Cq for each gene, corresponding to arbitrary assigning an expression of 1 to the least expressed sample). Last step of the pre-processing was to transform the data to log2 scale. 8-cell, 16-cell and 32-cell embryos were analyzed separately. The combined expression of the individual blastomeres adds up to the expression of the original oocyte, which is expected, since de novo expression does not start until MBT. Three multivariate statistical methods were used for classification: principal component analysis (PCA), Kohonen self-organizing map (SOM), and hierarchical clustering presented as heatmaps. PCA of individual blastomeres (Fig. 1) was performed on data autoscaled along genes, while heatmaps (Fig. 2) and PCA of genes (Fig. 3) were performed on data autoscaled along samples[35].

1. Bengtsson, M., Ståhlberg, A., Rorsman, P. & Kubista, M. Gene expression profiling in single cells from the pancreatic islets of Langerhans reveals lognormal distribution of mRNA levels. *Genome Res.* **15**, 1388–1392 (2005).

2. Guo, G. *et al.* Resolution of cell fate decisions revealed by single-cell gene expression analysis from zygote to blastocyst. *Dev. Cell* **18**, 675–685 (2010).
3. May, A. *et al.* Multiplex RT-PCR expression analysis of developmentally important genes in individual mouse preimplantation embryos and blastomeres. *Biol. Reprod.* **80**, 194–202 (2009).
4. Galan, A. *et al.* Functional genomics of 5- to 8-cell stage human embryos by blastomere single-cell cDNA analysis. *PLoS One* **5**, e13615 (2010).
5. Virant-Klun, I. *et al.* Expression of pluripotency and oocyte-related genes in single putative stem cells from human adult ovarian surface epithelium cultured in vitro in the presence of follicular fluid. *BioMed Res. Int.* **2013**, 1–18 (2012).
6. Danilchik, M. V. & Gerhart, J. C. Differentiation of the animal-vegetal axis in Xenopus laevis oocytes. I. Polarized intracellular translocation of platelets establishes the yolk gradient. *Dev. Biol.* **122**, 101–112 (1987).
7. King, M. L., Messitt, T. J. & Mowry, K. L. Putting RNAs in the right place at the right time: RNA localization in the frog oocyte. *Biol. Cell* **97**, 19–33 (2005).
8. Sindelka, R., Jonak, J., Hands, N., Bustin, S. A. & Kubista, M. Intracellular expression profiles measured by real-time PCR tomography in the Xenopus laevis oocyte. *Nucleic Acids Res.* **36**, 387–392 (2008).
9. Sindelka, R., Sidova, M., Svec, D. & Kubista, M. Spatial expression profiles in the Xenopus laevis oocytes measured with qPCR tomography. *Methods* **51**, 87–91 (2010).
10. Roth, S. The origin of dorsoventral polarity in Drosophila. *Philos. Trans. R. Soc. Lond. B. Biol. Sci.* **358**, 1317–1329 (2003).
11. Aanstad, P. & Whitaker, M. Predictability of dorso-ventral asymmetry in the cleavage stage zebrafish embryo: an analysis using lithium sensitivity as a dorso-ventral marker. *Mech. Dev.* **88**, 33–41 (1999).
12. Sive, L. H., Grainger, M. R. & Harland, M. R. Early development of Xenopus laevis – A laboratory manual. Cold Spring Harbor Laboratory Press 2000, chapter 2, figure 2.1.
13. Vincent, J. P. & Gerhart, J. C. Subcortical rotation in Xenopus eggs: an early step in embryonic axis specification. *Dev. Biol.* **123**, 526–539 (1987).
14. Denegre, J. M. & Danilchik, M. V. Deep cytoplasmic rearrangements in axis-respecified Xenopus embryos. *Dev. Biol.* **160**, 157–164 (1993).
15. Miller, J. R. *et al.* Establishment of the dorsal-ventral axis in Xenopus embryos coincides with dorsal enrichment of dishevelled that is dependent on cortical rotation. *J. Cell Biol.* **146**, 427–437 (1999).
16. Marikawa, Y., Li, Y. & Elinson, R. P. Dorsal determinants in the Xenopus egg are firmly associated with the vegetal cortex and behave like activators of the Wnt pathway. *Dev. Biol.* **191**, 69–79 (1997).
17. Darras, S., Maikawa, Y., Elinson, R. P. & Lemaire, P. Animal and vegetal pole cells of early Xenopus embryos respond differently to maternal dorsal determinants: implications for the patterning of the organiser. *Development* **124**, 4275–4286 (1997).
18. Hyatt, B. A., Lohr, J. L. & Yost, H. J. Initiation of vertebrate left-right axis formation by maternal Vg1. *Nature* **384**, 62–65 (1996).
19. King, M. L., Messitt, T. J. & Mowry, K. L. Putting RNAs in the right place at the right time: RNA localization in the frog oocyte. *Biol. Cell* **97**, 19–33 (2005).
20. Kofron, M. *et al.* New roles for FoxH1 in patterning the early embryo. *Development* **131**, 5065–5078 (2004).
21. Kofron, M. *et al.* Wnt11/β-catenin signaling in both oocytes and early embryos acts through LRP6-mediated regulation of axin. *Development* **134**, 503–513 (2007).
22. Cuykendall, T. N. & Houston, D. W. Identification of germ plasm-associated transcripts by microarray analysis of Xenopus vegetal cortex. *Dev. Dyn.* **239**, 1838–1848 (2010).
23. Cuykendall, T. N. & Houston, D. W. Vegetally localized Xenopus trim36 regulates cortical rotation and dorsal axis formation. *Development* **136**, 3057–3065 (2009).
24. Bergkvist, A. *et al.* Gene expression profiling – Clusters of possibilities. *Methods* **50**, 323–335 (2010).
25. Keller, R. E. Vital dye mapping of the gastrula and neurula of Xenopus laevis: I. Prospective areas and morphogenetic movements of the superficial layer. *Dev. Biol.* **42**, 222–241 (1975).
26. Keller, R. E. Vital dye mapping of the gastrula and neurula of Xenopus laevis: II. Prospective areas and morphogenetic movements of the deep layer. *Dev. Biol.* **51**, 118–137 (1976).
27. Kikkawa, M., Takano, K. & Shinagawa, A. Location and behavior of dorsal determinants during first cell cycle in Xenopus eggs. *Development* **122**, 3687–3696 (1996).
28. Weaver, C. & Kimelman, D. Move it or lose it: axis specification in Xenopus. *Development* **131**, 3491–3499 (2004).
29. Medina, A., Wendler, S. R. & Steinbeisser, H. Cortical rotation is required for the correct spatial expression of nr3, sia and gsc in Xenopus embryos. *Int. J. Dev. Biol.* **41**, 741–745 (1997).
30. Kugler, J. M. & Lasko, P. Localization, anchoring and translational control of oskar, gurken, bicoid and nanos mRNA during Drosophila oogenesis. *Fly (Austin)* **3**, 15–28 (2009).
31. Steinhauer, J. & Kalderon, D. Microtubule polarity and axis formation in the Drosophila oocyte. *Dev. Dyn.* **235**, 1455–1468 (2006).
32. Hainski, A. M. & Moody, S. A. Xenopus maternal mRNAs from dorsal animal blastomere induce a secondary axis in host embryo. *Development* **116**, 347–355 (1992).
33. Tao, Q. *et al.* Maternal Wnt11 activates the canonical Wnt signaling pathway required for axis formation in Xenopus embryos. *Cell* **120**, 857–871 (2005).
34. Schroeder, K. E., Condic, M. L., Eisenberg, L. M. & Yost, H. J. Spatially regulated translation in embryos: asymmetric expression of maternal wnt-11 along the dorso-ventral axis in Xenopus. *Dev. Biol.* **214**, 288–297 (1999).
35. Ståhlberg, A., Rusnakova, V., Forootan, A., Anderova, M. & Kubista, M. RT-qPCR work-flow for single-cell data analysis. *Methods* **59**, 80–88 (2013).

Acknowledgements

This study was supported by Grant agency of Czech Republic 301/09/1752; Ministry of Youth, Education and Sports of the Czech Republic AV0Z50520701; BIOCEV CZ.1.05/1.1.00/02.0109 from the ERDF and by the grant SVV–2013-267212.

Author contributions

M.F. performed the experiments and together with M.K. analyzed the obtained data. R.S. and M.K. conceived and designed the experiments. All authors co-wrote the manuscript and approved the final paper.

Additional information

Supplementary information accompanies this paper at http://www.nature.com/scientificreports

Competing financial interests: The authors declare no competing financial interests.

How to cite this article: Flachsova, M., Sindelka, R. & Kubista, M. Single blastomere expression profiling of *Xenopus laevis* embryos of 8 to 32-cells reveals developmental asymmetry. *Sci. Rep.* **3**, 2278; DOI:10.1038/srep02278 (2013).

Single blastomere expression profiling of *Xenopus laevis* embryos of 8 to 32-cells reveals developmental asymmetry

Monika Flachsova, Radek Sindelka and Mikael Kubista

Supplementary figure S1.

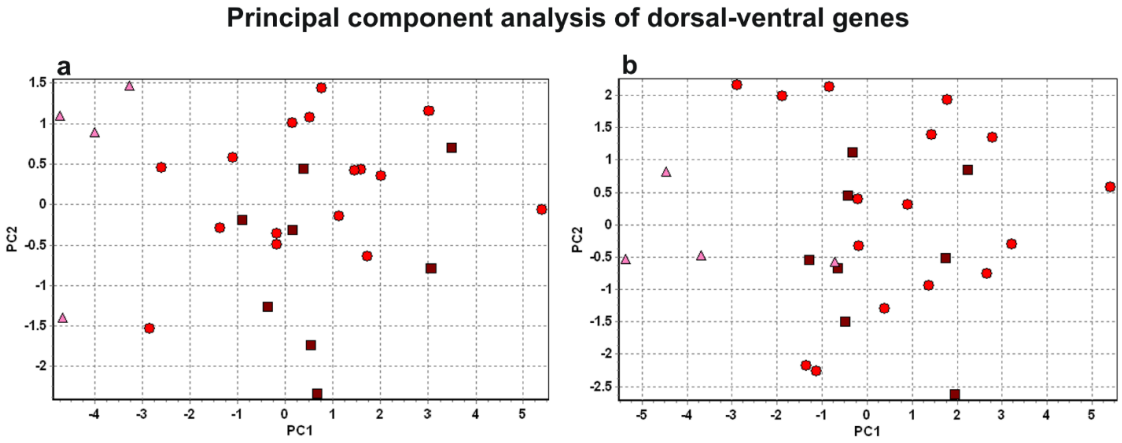

We have performed PCA with just the ten dorsal-ventral patterning genes (*dvl2, dvl3, lrp6, wnt11, tcf3, gsk3b, ctnnb1, foxh1, trim36, axin1*). The PCA was performed separatelly for animal (figure A) or vegetal blastomeres (figure B) to avoid bias introduced by animal-vegetal gradients. On the graphs triangles indicate blastomeres from the 8-cell stage; squares from the 16-cell stage, and circles from the 32-cell stage. If those genes specify dorsal and ventral blastomeres, we should see two clusters with the same number of blastomeres per stage. But this is not the case in our results. We conclude that there is no dorsal-ventral localization pattern.

4.3. Intracellular microRNA profiles form in the *Xenopus laevis* oocyte that may contribute to asymmetric cell division

Sidova M., Sindelka R., Castoldi M., Benes V. a Kubista M. *Scientific Reports* 2015 (přijat k publikaci – květen 2015). IF 5.078

Asymetrická časo-prostorová lokalizace funkčních maternálních transkriptů a proteinů není závislá pouze na jejich nerovnoměrné distribuci, ale může být ovlivněna i regulačními procesy či molekulami. Mezi tyto molekuly patří miRNA, které se zásadním způsobem podílí na posttranskripční regulaci mRNA a translaci proteinů. Z tohoto důvodu byla naše pozornost soustředěna na studium lokalizačních profilů miRNA uvnitř zralého oocytu *X. laevis*. Měření vycházelo z qPCR tomografie, kdy došlo k rozdělení oocytu na pět částí podél animálně-vegetativní osy. Vlastní kvantifikace miRNA probíhala pomocí metody RT-miQPCR (Benes *et al.*, 2015). Tato metoda využívá univerzální adaptor, tzv. miLINKER, který prodlouží 3´ konec jednovláknové RNA, což následně umožní její přepis do cDNA a posléze kvantifikaci miRNA pomocí qPCR. Tímto postupem byla určena lokalizace 12 miRNA podél animálně-vegetativní osy zralého oocytu. K přesnější charakterizaci lokalizačních profilů miRNA byly vybrány tři maternální transkripty, které zastupovali všechny typy animálně-vegetativních profilů získaných v publikaci 4.1. Jedna polovina studovaných miRNA (miR-16c, miR-18b, miR-363-3p, miR-20b, miR-93a a miR-5102-5p) vykazovala lokalizaci posunutou směrem k animální polovině, která odpovídala profilu maternálního transkriptu *maml1*. Oproti tomu druhá polovina miRNA (miR-19b, miR-221, miR-148b, miR-25, miR-22 a miR-100) projevovala vegetativní lokalizační profil podobný transkriptu *gdf1*. Žádná ze studovaných miRNA nejevila známky strmého lokalizačního profilu vegetativního pólu, který byl zastoupen transkriptem *cdx1*. Tato práce představuje první studii, která dokazuje asymetrickou lokalizací nekódujících RNA v rámci jedné buňky. Nerovnoměrná lokalizace miRNA uvnitř oocytu naznačuje, že i miRNA lze zařadit do skupiny klíčových biomolekul, které se učastní časo-prostorového určení tělního plánu v průběhu časného embryonálního vývoje.

SCIENTIFIC REPORTS

OPEN

Intracellular microRNA profiles form in the *Xenopus laevis* oocyte that may contribute to asymmetric cell division

Received: 28 October 2014
Accepted: 18 May 2015
Published: xx xx xxxx

Monika Sidova[1,2], Radek Sindelka[1], Mirco Castoldi[3], Vladimir Benes[4] & Mikael Kubista[1,5]

Asymmetric distribution of fate determinants within cells is an essential biological strategy to prepare them for asymmetric division. In this work we measure the intracellular distribution of 12 maternal microRNAs (miRNA) along the animal-vegetal axis of the *Xenopus laevis* oocyte using qPCR tomography. We find the miRNAs have distinct intracellular profiles that resemble two out of the three profiles we previously observed for mRNAs. Our results suggest that miRNAs in addition to proteins and mRNAs may have asymmetric distribution within the oocyte and may contribute to asymmetric cell division as cell fate determinants.

A central question in developmental biology is how the original fertilized oocyte gives rise to a complex organism made up of hundreds of different cell types. The key mechanism is asymmetric cell division that produces daughter cells with uneven distribution of deterministic biomolecules leading to different fates. Asymmetric cell division is induced by asymmetric cellular organization and polarization of fate determinants that are localized to distinct regions within the cell. Previously proteins and mRNA molecules have been identified as cell fate determinants [reviewed in[1]]. It has been shown that cell fate determinants are asymmetrically distributed already in the oocyte of several species, including the fruit fly (*Drosphila melanogaster*)[2], the zebrafish (Danio rerio)[3,4] and the African clawed frog (*Xenopus*)[5,6]. This asymmetry leads to the formation of unequal blastomeres within the first few cell divisions[7].

The *Xenopus* oocyte is an excellent model system to study early development. Its two distinguishable halves, referred to as the animal and vegetal hemispheres, are characterized by different pigmentation, which makes it easy to align the oocytes and study intracellular distributions of mRNAs. Most maternal mRNAs synthesized during oogenesis are evenly distributed along the animal-vegetal axis of *Xenopus* oocyte, though a small subset has been reported differentially distributed at either the animal or vegetal pole[8,9]. A more recent whole transcriptome analysis using microarrays suggest some 300 transcripts are localized in the vegetal cortex of the *Xenopus* oocytes[10], which represents 2–3% of the maternally expressed genes. Two different pathways for the localization of the vegetal RNAs have been identified[11]. The early initiated pathway called METRO (messenger transport organizer) uses specific binding elements of mRNAs to attach them to a mitochondrial cloud that is formed during early oogenesis. Cis-acting elements, such as clusters of short nucleotide repeats, thought to mediate binding to a conserved complex of RNA-binding proteins, have been identified as well as trans acting protein coding elements[12]. METRO is required for the localization of cdx1 and dazl mRNAs that are incorporated into germinal granules needed for germ cell formation[13]. The late pathway is activated during mid

[1]Laboratory of Gene Expression, Institute of Biotechnology, Academy of Sciences of the Czech Republic, Videnska 1083, Prague, 142 20 Czech Republic. [2]Charles University in Prague, Faculty of Science, Department of Cell Biology, Vinicna 7, Prague, 128 43, Czech Republic. [3]Department of Gastroenterology Hepatology and Infectiology, University Hospital of Dusseldorf, Moorenstrasse 5, Dusseldorf, 40225 Germany. [4]EMBL Genomics Core Facility, Meyerhofstr. 1, Heidelberg, D-69117 Germany. [5]TATAA Biocenter AB, Odinsgatan 28, Göteborg, 411 03 Sweden. Correspondence and requests for materials should be addressed to M.K. (email: mikael.kubista@ibt.cas.cz)

and late oogenesis and depends on the cytoskeleton and microtubule motors[14]. It localizes particular mRNAs, such as *gdf1* and *vegt*, with sequence elements UUUCU and UUCAC[15–18] in their 3' untranslated regions (3´UTRs) that code for transcription factors controlling germ layer formation[19]. Notably, localized maternal mRNAs, such as *vegt, fatvg, xlsirts*, and *gdf1* in *Xenopus* and *oscar* in *Drosophila*, are important for the organization of cytokeratin and actin networks through a mechanism that does not require their translation[20–23]. *Vegt* mRNA, for example, is integrated into the cytoskeleton and its removal causes collapse of the cytokeratin network, while removal of *fatvg* mRNA induces hyperpolymerization of cytokeratin and actin filaments[20,24]. Some mRNAs have been reported more abundant in the animal hemisphere[25]. However, no particular mechanism has been described that would give rise to a localization of some mRNAs towards the animal pole and no particular functions have been ascribed to animally localized mRNA[1,8]. In fact, as we shall argue, weak polarization towards the animal side may develop spontaneously in the absence of active mechanisms and may in fact be the normal distribution. Another mechanism inducing intracellular rearrangement in the *Xenopus* oocyte is the cortical rotation. It follows fertilization by accumulation of dorsalizing biomolecules in the future dorsal side of the embryo and creates the dorsal-ventral developmental axis.

Using real-time quantitative PCR (qPCR) tomography and single cell expression profiling we measured intracellular mRNA profiles within the *Xenopus* oocyte and their distribution among blastomeres during the early developmental stages up to 32 cells. We discovered three distinct animal-vegetal mRNA profiles[26], but found no evidence for mRNA asymmetry along the dorso-ventral or left-right axes[27]. We concluded that while the animal-vegetal asymmetry in *Xenopus* is induced by mRNA molecules the dorso-ventral asymmetry and possibly also the left-right asymmetry should be induced by uneven distribution of other biomolecules. Indeed, in several species asymmetric localization of β-catenin protein has been found critical for the formation of the dorso-ventral developmental axis[28].

In this work we investigate if miRNAs show intracellular asymmetry, which would make them candidate cell fate determinants. miRNAs are 22–24 bases short single-stranded oligoribonucleotides that primarily regulate mRNA translation by binding to target mRNAs. Targeted locus of mRNAs for miRNA binding is usually at their 3' UTR. It is well established that the 3'UTR of eukaryotic mRNAs is important for many of the mRNA functions. The 3'UTR site contains sequences that regulate the stability of the transcript, directs its localization, and may also contain other regulatory cis-acting elements. Recent studies have demonstrated that 3'UTRs can be functional independently of translation[29]. In this study we measure the intracellular profiles in mature *Xenopus* oocytes of the 12 selected miRNAs: miR-16c, miR-18b, miR-363-3p, miR-20b, miR-93a, miR-5102-5p, miR-19b, miR-221, miR-148b, miR-25, miR-22, miR-100, which have been ascribed maternal origin[30,31] using qPCR tomography[26,32].

Results

We performed expression analysis of selected miRNAs and maternal mRNAs in *Xenopus laevis* oocytes using qPCR tomography[32]. The oocytes (in total six oocytes from two females) were cryo-sectioned along the animal-vegetal axis and extracted RNA was analyzed by RT-qPCR[26,32]. The intracellular distributions of the 12 maternal miRNAs: miR-16c, miR-18b, miR-363-3p, miR-20b, miR-93a, miR-5102-5p, miR-19b, miR-221, miR-148b, miR-25, miR-22 and miR-100 were measured along the animal-vegetal axis in five consecutive segments of the *Xenopus laevis* oocyte. In addition we measured the distributions of three mRNAs with known localizations: *maml1* (animal localization), *gdf1* (vegetal localization), and *cdx1* (extreme vegetal localization); reflecting the three mRNA animal-vegetal profiles found previously[26,27]. An RNA spike was used to optimize the extraction protocol. Measuring the RT-qPCR efficiency of the spike we found a maximum of 1.25 ng of total RNA could be extracted without compromising the reactions (Supplement Fig. 1).

Our analysis revealed that the miRNAs we studied arrange in two distinct intracellular profiles that appear similar to two out of the three profiles we previously observed for mRNAs[26]. Specifically, miR-16c, miR-18b, miR-363-3p, miR-20b, miR-93a, miR-5102-5p and *maml1* mRNA are predominant in the center of the oocyte with slight asymmetry towards the animal hemisphere (Fig. 1a, Fig. 2a), while miR-19b, miR-221, miR-148b, miR-25, miR-22, miR-100 and *gdf1* mRNA are more abundant in the vegetal hemisphere (Fig. 1b, Fig. 2b). None of the studied miRNAs showed the extreme vegetal localization represented by the *cdx1* mRNA (Fig. 2b). Separation of the studied miRNAs into two groups with distinct animal-vegetal profiles was supported by the multivariate statistical analyses hierarchical clustering (presented as a dendrogram in Fig. 3a) and the Kohonen self-organizing map (SOM; Fig. 3b). Both classification methods clearly divide the miRNA and mRNA intracellular profiles into two clusters with preferential animal and vegetal distributions, respectively, and are henceforth referred to as the animal and vegetal groups.

We found no pattern within neither the animal nor the vegetal group that could be identified as a miRNA consensus sequence and ascribed to the asymmetric distribution of the miRNAs (Fig. 4). Using MicroCosm Targets Version 5 database (http://www.ebi.ac.uk/enright-srv/microcosm/htdocs/targets/v5/) we predicted target mRNAs for the studied miRNAs (Fig. 4) and were particularly interested in target mRNAs that form intracellular profiles along the animal-vegetal axis of the *Xenopus* oocyte[26,27,32]. The animal *foxh1*, *lrp6*, *eef1a1*, *bmp2*, *pax6*, *apc*, *mos* and *tcf3* mRNAs showed potential to hybridize with some of the studied miRNAs, but from both groups: animal miR-16c, miR-20b and miR-363-3p and vegetal miR-19b and miR-221. The only vegetal mRNA that was predicted to interact with asymmetrically

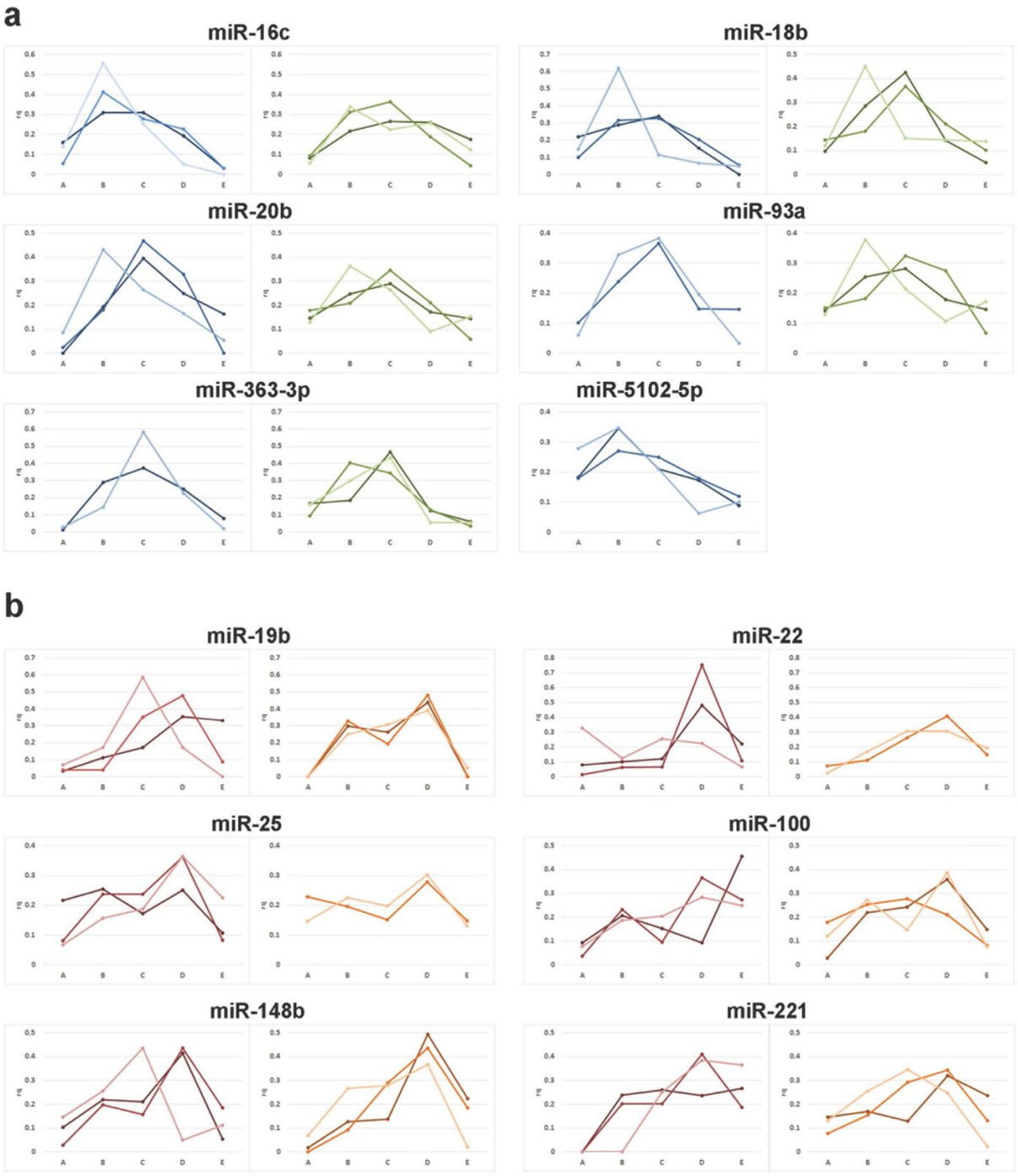

Figure 1. **a**. Individual intracellular profiles of miR-16c, miR-18b, miR-20b, miR-93a, miR-363-3p and miR-5102-5p predominantly localized in the center of the oocyte with slight asymmetry towards the animal hemisphere. Blue lines indicate oocytes from the first female and green lines indicate oocytes from the second female. **b**. Individual intracellular profiles of miR-19b, miR-22, miR-25, miR-100, miR-148b, and miR-221 localized in the vegetal hemisphere. Red lines indicate oocytes from the first female and orange lines indicate oocytes from the second female. Y-axis indicates relative quantity and x-axis indicates the section from the animal pole (section A) to vegetal pole (section E).

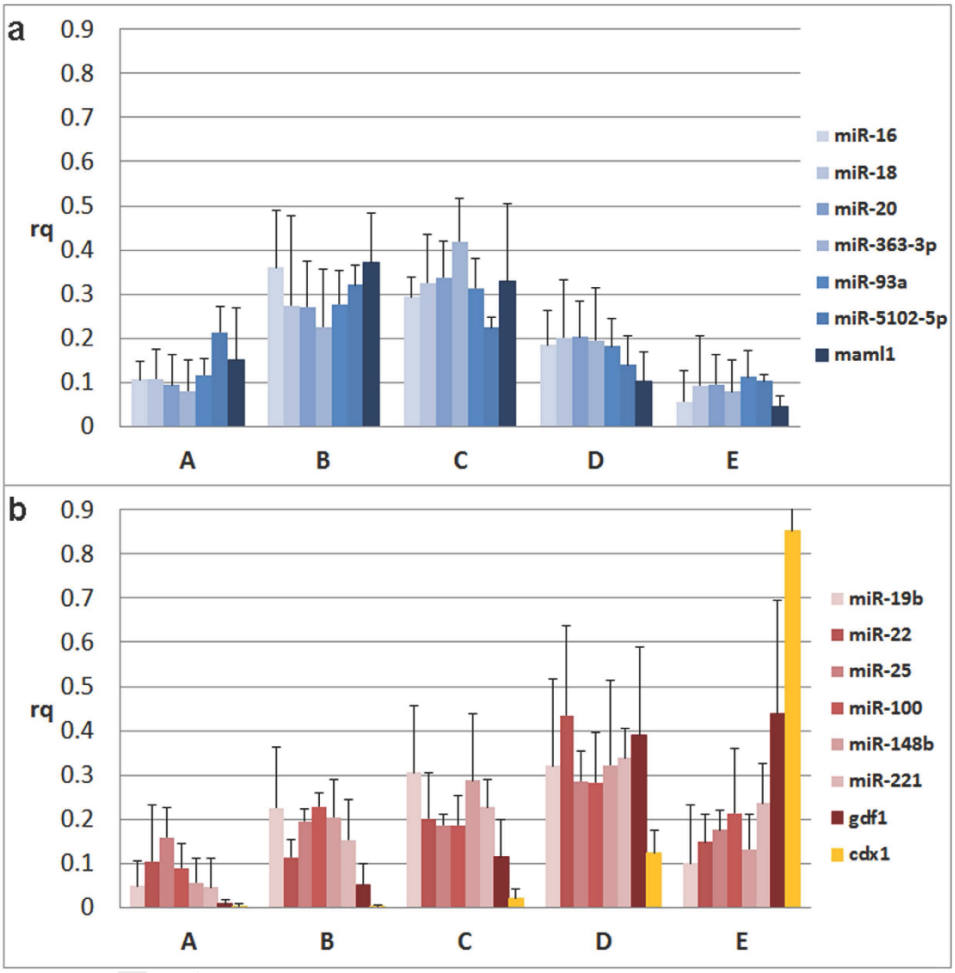

Figure 2. Intracellular profiles of the miRNAs and the selected reference mRNAs measured using qPCR tomography (*maml1*- dark blue, *gdf1* – dark red, *cdx1* - yellow). Y-axis indicates relative quantity and x-axis indicates the section from the animal pole (section A) to vegetal pole (section E). **a**. Spatial profiles of miR-16c, miR-18b, miR-20b, miR-93a, miR-363-3p and miR-5102-5p (indicated in blue scale), which are predominant in the animal hemisphere like the mRNA *maml1* (dark blue). **b**. Intracellular profiles of miR-19b, miR-22, miR-25, miR-100, miR-148b, and miR-221 (indicated in red scale), which are predominant in the vegetal hemisphere like the mRNA *gdf1* (dark red). Both graphs also show the mRNA *cdx1* (yellow), which has an extreme vegetal profile.

localized miRNAs was *ddx25*. It showed complementarity to the animal miR-20b as well as to the vegetal miR-100.

Discussion

Our results demonstrate that miRNAs, in addition to proteins and mRNAs, have asymmetric distribution in the *Xenopus* oocyte and may contribute to asymmetric cell division as cell fate determinants. Formation of intracellular profiles requires the cell offers an asymmetric environment. Indeed, the *Xenopus laevis* oocyte is asymmetric, with the animal and vegetal hemispheres having quite different compositions and the nucleus being located off center towards the animal pole[33,34]. There are also asymmetric perturbations, such as the sperm entry, that induce asymmetric distribution of cell fate determinants that leads to the dorsal-ventral asymmetry[19]. However, sperm entry does neither induce the mRNA asymmetry we reported earlier nor the miRNA asymmetry we observe here, as these profiles are present in the unfertilized oocyte.

miRNAs are transcribed in the cell nucleus and should stay close to it unless transported away. Since the nucleus in *Xenopus* oocytes is located closer to the animal hemisphere it is conceivable that passive diffusion of miRNAs secreted from the nucleus spontaneously produces the distribution with slight

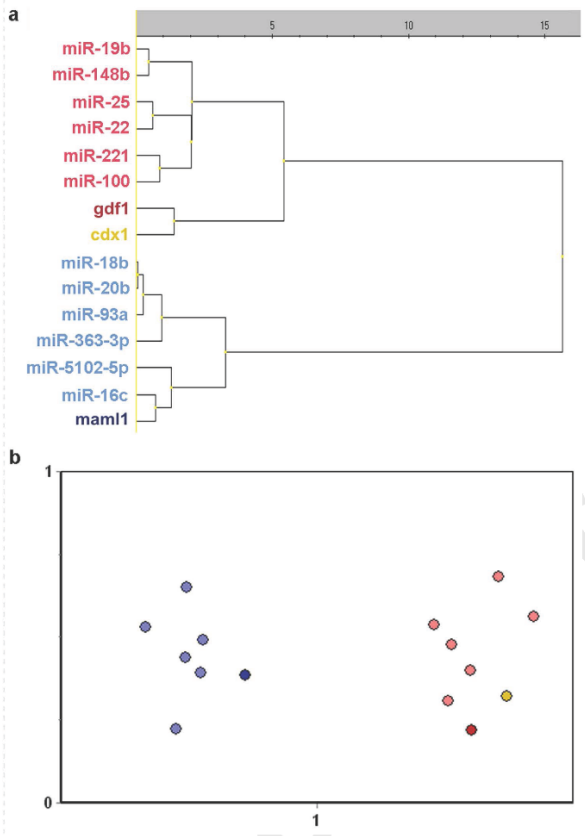

Figure 3. Hierarchical clustering (**a**) and SOM classification (**b**) of intracellular profiles along the animal-vegetal axis of the *Xenopus laevis* oocyte. The hierarchical clustering is presented in a dendrogram, where the similarity between miRNAs/mRNAs is indicated by the height at which they are joined. Both the dendrogram and the SOM clearly separate the miRNA and mRNA profiles into two clusters. miR-16c, miR-18b, miR-20b, miR-93a, miR-363-3p and miR-5102-5p (light blue) cluster with animally localized mRNA *maml1* (dark blue), while miR-19b, miR-22, miR-25, miR-100, miR-148b, and miR-221 (light red) cluster with vegetally localized *gdf1* (dark red) and *cdx1* (yellow) mRNAs.

	miRNA	sequence	predicted target
Animal	miR-16c	5′-UAGCAGCACGUAAAUACUGGAG-3′	foxh1
	miR-18b	5′-UAAGGUGCAUCUAGUGCAGUUAG-3′	
	miR-20b	5′-CAAAGUGCUCAUAGUGCAGGUAG-3′	ddx25, lrp6
	miR-93a	5′-CAAAGUGCUGUUCGUGCAGGUAG-3′	
	miR-363-3p	5′-AAUUGCACGGUAUCCAUCUGUAA-3′	eef1a1, bmp2
	miR-5102-5p	5′-GGGAGTTTGACTGGGGCG-3′	
Vegetal	miR-19b	5′-UGUGCAAAUCCAUGCAAAACUGA-3′	pax6, bmp2, apc
	miR-22	5′-AAGCUGCCAGUUGAAGAACUGU-3′	
	miR-25	5′-CAUUGCACUUGUCUCGGUCUGA-3′	
	miR-100	5′-AACCCGUAGAUCCGAACUUGUG-3′	ddx25
	miR-148b	5′-UCAGUGCAUCACAGAACUUUGU-3′	
	miR-221	5′-AGCUACAUUGUCUGCUGGGUUUC-3′	mos, tcf3, foxh1, apc

Figure 4. Sequences of the studied miRNAs and their predicted target mRNAs (animal mRNAs are shown in blue, vegetal mRNAs in red). Target prediction was performed using MicroCosm Targets Version 5 database (http://www.ebi.ac.uk/enright-srv/microcosm/htdocs/targets/v5/). The conservation is indicated by colored bases: red color indicates high evolutionary conservation, while blue color indicates low conservation. A sequence of miR-5102-5p indicated in black and two nucleotides on the 3′ end of miR-363-3p were not found in the database. Yellow boxes indicate miRNA seed sequences (from 2nd to the 8th nucleotide in the 5′ end).

animal enrichment that we observe for half of the studied miRNAs (miR-16c, miR-18b, miR-20b, miR-93a, miR-363-3p and miR-5102-5p). These miRNAs could then reflect the normal population of miRNAs. The distribution towards the vegetal hemisphere of the other miRNAs, however, must be driven by an active process. miRNAs bind their target mRNAs through hybridization requiring sequence complementarity. Although not all miRNA bases are required for sequence specific hybridization, there is hardly enough sequence flexibility to encompass a consensus binding sequence that could interact with one cellular component. We have extensively studied the sequences of the vegetally distributed miRNAs looking for patterns, but have not found motifs that could be identified as a consensus. Even though the gradient profiles along the animal-vegetal axis of miRNAs are similar to the profiles of mRNAs, we currently have no evidence that miRNA localization is induced by the binding of the miRNAs via a consensus sequence to a single localized molecular target. This raises the question how the miRNAs become asymmetrically distributed within the oocyte. Since interaction with an asymmetric environment is required, at least for the miRNAs with vegetal distribution, we find the idea that the vegetal miRNAs interact with vegetal mRNAs attractive. Despite extensive modelling with the MicroCosm Targets Version 5 database we have not been able to substantiate this hypothesis. This could be limitations in the *in silico* approach, which identifies sequences relevant for the transcriptional silencing mechanism mediated by miRNAs, which primarily is based on hybridization of complementary, consecutive bases, and does not consider more complex modes of interaction.

During our comparative analysis of miRNAs and search for consensus sequences, we also compared the seed sequences of the studied miRNAs. The seed sequence is a region from the 2nd to the 8th nucleotide at the 5′ end of the miRNA[35]. This sequence plays a critical role in the regulatory function of the miRNA through hybridization to the complementary 3′ UTR site of the target mRNA. The MicroCosm Targets Version 5 database predicts miRNA-mRNA interactions primarily based on sequence complementarity with highly rewarded seed sequence complementarity. We found that the three animally distributed miRNAs, miR-18b, miR-20b and miR-93a, have similar seed sequences: "AA$_A$\$^G$GUGC". The database predicts that miR-20b (AAAGUGC) regulates *ddx25* and *lrp6* mRNAs, but does not identify those as targets for miR-18b, which has only one mismatch in the seed sequence (AAGGUGC). A single base mismatch in the seed sequence can perhaps be discriminative. However, the targets were not identified for miR-93a, which has identical seed sequence to miR-20b (AAAGUGC). Hence, the *in silico* analysis considers features beyond simple sequence complementarity, which are relevant for miRNA-mRNA interaction in relation to gene regulation, but may not apply to interactions leading to asymmetric intracellular distribution. It is conceivable these interactions are different, perhaps even involving non-consecutive sequences and exposed bases, and are therefore not recognized by the MicroCosm Targets Version 5 database. The numbers of known vegetally distributed mRNAs and in particular miRNAs are currently too few to develop models based on interactions that go beyond contiguous hybridization. As these numbers grow more advanced modelling will be possible. An interesting suggestion by an anonymous reviewer is that the miRNAs become actively distributed as pre-miRNAs, before being processed by Dicer, through sequences either in the loop or in the passenger strand. This is an attractive hypothesis and will be possible to test when sequence information about pre-miRNAs in *Xenopus laevis* becomes available. As for now the mechanism behind the vegetal distribution of miRNAs along the animal-vegetal axis within *Xenopus laevis* oocytes remains elusive.

In our studies of intracellular distribution of miRNAs and mRNAs we find molecules that co-localize with the nuclei and are more abundant in the animal hemisphere and we find molecules that show vegetal distribution. For miRNAs there is one vegetal profile, while for mRNAs there are two distinct vegetal profiles; one of which has extreme vegetal localization. In the literature many mRNAs with vegetal, extreme vegetal and animal distributions have been reported and in addition to those majority of mRNAs are assumed to have normal distribution, with presumably should symmetric[8]. However, in our studies we have never found RNA molecules with even distribution across the oocyte. Of course, having only analyzed a rather small number of mRNAs and miRNAs those with even distribution may have escaped notice. Another possibility is there are no RNAs with even distribution across the oocyte; rather the distribution obtained in the absence of active mechanisms could have slight animal asymmetry due to the animal offset of the nuclei, where the RNAs are produced. We find this possibility attractive considering that no active mechanism behind animal distribution has ever been found and there is no evidence in the literature that the animal distribution should be different from normal. Hence, we propose mRNAs in the *Xenopus laevis* oocyte can have one out of three intracellular profiles: the spontaneous "normal" profile with slight localization towards the animal pole, vegetal localization, and extreme vegetal localization. For miRNAs we observe only the normal spontaneously formed animal profile and the vegetal localization.

In conclusion, we have discovered that certain miRNAs, including miR-16c, miR-18b, miR-363-3p, miR-20b, miR-93a and miR-5102-5p, are predominant in the animal hemisphere where the nuclei is located and possibly obtain this localization passively, while other miRNAs, including miR-19b, miR-221, miR-148b, miR-25, miR-22 and miR-100, are predominant in the vegetal hemisphere of the *Xenopus* oocyte. The latter miRNAs show similar internal profile as mRNAs oriented by the late pathway and should require active transport. None of the analyzed miRNAs displays the extreme vegetal distribution associated with the METRO oriented mRNAs. We speculate that the 3'UTR of some late pathway oriented mRNAs may contain sequences that bind the vegetally localized miRNAs or pre-miRNAs leading

to co-localization. The vegetal distribution of some miRNAs suggests they contribute to asymmetric cell division and play a role in early embryogenesis.

Methods

Ethical Statement. This study was carried out in compliance with the Act No 246/1992 Coll., on the protection of animals against cruelty. Official permission was issued to the Faculty of Science; Charles University in Prague by the Central Commission for Animal Welfare of the Ministry of Agriculture of the Czech Republic (accreditation No. 24773/2008-10001, date of expiry 10.12.2013).

***In vitro* fertilization, oocytes fixation and sectioning, RNA extraction.** Two *Xenopus laevis* females were injected with 450 U of hCG (human chorionic gonadothropin) hormone and ovulated oocytes were obtained 12 hours after stimulation by gentle manual squeezing. Three oocytes from each female were collected and immediately embedded in a drop of OCT (optimal cutting temperature) medium on a pre-cooled dissection block. The block was placed for 10 minutes in the cryostat chamber (−19 °C) to temperature equilibrate the samples. The temperature of the section knife was −18 °C. The oocytes were cut into 45 slices, each being 30 μm thick, across the animal-vegetal axis. Consecutive slices were pooled into five tubes with nine slices in each. The first tube (denoted "A" in the figures) contained slices from the endmost animal part of the oocyte, while the last tube (denoted "E") contains the endmost vegetal part. 300 μl of TRIzol reagent (Invitrogen) was added to each tube to extract total RNA. Samples were carefully homogenized by vortexing for 2 min and incubated for 5 min at room temperature to dissolve completely. Manufacturer's instructions were followed during isolation, with the addition of 7 μg of glycogen (Sigma-Aldrich) to the isopropanol to enhance the RNA precipitation yield. Precipitated RNA was redissolved in 15 μl of RNase/DNase-free water and its concentration was measured using the Nanodrop ND1000 system.

Control of inhibition. Yolk stored in the vegetal part of the oocyte is severe inhibitor of reverse transcription (RT) and quantitative PCR (qPCR). All samples were tested for inhibition using an RNA spike (TATAA Biocenter). SuperScript™ III Reverse transcriptase kit (Invitrogen) was used for cDNA synthesis. Four different input amounts of total RNA (10 ng, 5 ng, 2.5 ng and 1.25 ng) were evaluated using RT-qPCR (Supplement Fig. 1). Severe inhibition was observed when analyzing the spike in the vegetal samples prepared from 10, 5 and 2.5 ng of total RNA. Using 1.25 ng of total RNA for cDNA synthesis the recovery yields of the RNA spike approached 100%. This was the same protocol as used in Flachsova *et al.* (2013)[27]. The cDNA samples were diluted 8 times to a final volume of 80 μl and stored at −20 °C. Three mRNAs (*maml1*, *cdx1* and *gdf1*), each representing one out of the three mRNA intracellular profiles observed previously[26,27], were included for comparison. qPCR and melting curves were measured on a real-time CFX96 cycler system (BioRad). qPCR mix contained 2 μl of cDNA, 0.5 μl of forward and reverse primers (mixture 1:1, 10 μM each), 5 μl of iQ™ SYBR® Green Supermix (Bio-Rad), and deionized water in a total volume of 10 μl. The temperature profile was: activation of polymerase at 95 °C for 3 min., followed by 40 cycles of denaturation at 95 °C for 15 sec., annealing at 60 °C for 20 sec., and elongation at 72 °C for 30 sec. The formation of expected PCR products was confirmed by measuring melting curves between 65 °C and 95 °C in 0.5 °C intervals.

Quantification of miRNA by qPCR. miRNA expression profiling was performed using miQPCR[36], which is a method for global RT-qPCR profiling of miRNAs[37,38]. Briefly, the 3'ends of single-stranded RNAs are extended uniformly with a specific adaptor named miLINKER. This adapter is then used as an anchor to prime cDNA synthesis during reverse transcription and for detection of the selected amplicon during the qPCR. For each sample 1.25 ng of total RNA was treated with the miLINKER (5 μM for each extension). Elongated samples were reverse transcribed using Superscript II (Invitrogen) following the supplier's instructions. miRNA specific qPCR requires 100 pg of cDNA, 2.5 μM of the universal primer (i.e. complementary to the miLINKER) and 2.5 μM of a miRNA specific primer. qPCR of miRNAs was performed using iQ™ SYBR® Green Supermix (Bio-Rad, total reaction volume 10 μl) on an CFX384 cycler (BioRad) with the same protocol as for the mRNAs described above. Tailing, reverse transcription and qPCR reagents were prepared as mastermixes for all 30 samples (six oocytes; each 5 sections). The miRNA specific primers were designed to be complementary to the target miRNA with a G nucleotide overhang on the 3´end, which binds to the first nucleotide of the attached miLINKER. The annealing temperature was set to 60 °C and estimated using the Tm calculator provided by Applied Biosystems (http://www6.appliedbiosystems.com/support/techtools/calc/). Primer specificity was verified by blast (http://blast.ncbi.nlm.nih.gov/Blast.cgi). Primer assays were designed for 27 randomly selected maternal miRNAs. 12 assays with highest efficiency (probably the most abundant) and robustness were used for expression profiling (Supplement Tab. 1).

Data analysis. The measured Cq values of the animal-vegetal segments were converted to relative quantities using the equation (1): $Xsection = \frac{2^{-cq_i}}{\sum_{j=1}^{5} 2^{-cq_i}}$. Where Cq_i is the Cq value measured in the i^{th} section. The same amount of total RNA was analyzed per section serving as normalizer. $x_{section}$ can thus

be considered as the relative amount or fraction of the particular miRNA/mRNA in that segment[32]. The relative amounts in each segment were averaged across all oocytes from both females and are presented in bar/line charts with the x-axis representing the segment position from the animal pole along the animal-vegetal axis and the y-axis indicating the relative quantity (Fig. 1, Fig. 2). Individual profiles of all 12 miRNAs can be found in Fig. 1. The data were also analyzed with the software GenEx (MultiD) to determine correlations between the miRNAs' and maternal mRNAs' intracellular profiles. For multivariate analysis data were autoscaled along genes and profiles were analyzed for similarities using the Kohonen self-organizing map (SOM) and hierarchical clustering (Fig. 3). We used SOM with two boxes (2×1) to force the data into two groups based on the measured profiles. Using three boxes, one box ended up empty supporting the conclusion that the profiles indeed reflect only two distinct distributions (not shown). Independent SOM trainings yielded the same two groups evidencing robust classification. SOM training of only the miRNAs, leaving out the mRNAs, gave a separation into the same groups, evidencing that the separation is not induced by the mRNAs but a property of the miRNAs. The biological variability between the females was tested using unpaired, 2-tails t-test. The p-values were > 0.05 indicating higher variability among oocytes than between samples from different females.

All methods were carried out in accordance with the approved guidelines and all experimental protocols were approved by named institutions, including any relevant details in the methods section.

References

1. Houston, D. W. Regulation of cell polarity and RNA localization in vertebrate oocyte. *Int Rev Cell Mol Biol.* **306,** 127–185 (2013).
2. Ephrussi, A. & Lehmann, R. Induction of germ cell formation by oskar. *Nature* **358,** 387–392 (1992).
3. Hashimoto, Y. *et al.* Localized maternal factors are required for zebrafish germ cell formation. *Dev. Biol.* **268,** 152–161 (2004).
4. Howley, C. & Ho, R. K. mRNA localization patterns in zebrafish oocytes. *Mech. Dev.* **92,** 305–309 (2000).
5. Kloc, M. & Etkin, L. D. RNA localization mechanisms in oocytes. *J Cell Sci.* **118,** 269–282 (2005).
6. King, M. L., Zhou, Y. & Bubunenko, M. Polarizing genetic information in the egg: RNA localization in the frog oocyte. *Bioessays* **21,** 546–557 (1999).
7. Pandur, P. D., Sullivan, S. A. & Moody, S. A. Multiple maternal influences on dorsal-ventral fate of Xenopus animal blastomeres. *Dev Dyn.* **225,** 581–587 (2002).
8. King, M. L., Messitt, T. J. & Mowry, K. L. Putting RNAs in the right place at the right time: RNA localization in the frog oocyte. *Biol Cell.* **97,** 19–33 (2005).
9. Mowry, K. L. & Cote, C. A. RNA sorting in Xenopus oocytes and embryos. *FASEB J.* **13,** 435–445 (1999).
10. Cuykendall, T. N. & Houston, D. W. Identification of germ plasm-associated transcripts by microarray analysis of Xenopus vegetal cortex RNA. *Dev Dyn.* **239,** 1838–1848 (2010).
11. Kloc, M. & Etkin, L. D. Two distinct pathways for the localization of RNAs at the vegetal cortex in Xenopus oocytes. *Development* **121,** 287–297 (1995).
12. Snedden, D. D., Bertke, M. M., Vernon, D. & Huber, P. W. RNA localization in Xenopus oocytes uses a core group of trans-acting factors irrespective of destination. *RNA* **19,** 889–895 (2013).
13. Zhou, Y. & King, M. L. Sending RNAs into the future: RNA localization and germ cell fate. *IUBMB Life* **56,** 19–27 (2004).
14. Yisraeli, J. K., Sokol, S. & Melton, D. A. A two-step model for the localization of maternal mRNA in Xenopus oocytes: involvement of microtubules and microfilaments in the translocation and anchoring of Vg1 mRNA. *Development* **108,** 289–298 (1990).
15. Deshler, J. O., Highett, M. I. & Schnapp, B. J. Localization of Xenopus Vg1 mRNA by Vera protein and the endoplasmic reticulum. *Science* **276,** 1128–1131 (1997).
16. Gautreau, D., Cote, C. A. & Mowry, K. L. Two copies of a subelement from the Vg1 RNA localization sequence are sufficient to direct vegetal localization in Xenopus oocytes. *Development* **124,** 5013–5020 (1997).
17. Lewis, R. A. *et al.* Conserved and clustered RNA recognition sequences are a critical feature of signals directing RNA localization in Xenopus oocytes. *Mech Dev.* **121,** 101–109 (2004).
18. Bubunenko, M., Kress, T. L., Vempati, U. D., Mowry, K. L. & King, M. L. A consensus RNA signal that directs germ layer determinants to the vegetal cortex of Xenopus oocytes. *Dev Biol.* **248,** 82–92 (2002).
19. White, J. A. & Heasman, J. Maternal control of pattern formation in Xenopus laevis. *J Exp Zool B Mol Dev Evol.* **310,** 73–84 (2008).
20. Kloc, M., Bilinski, S. & Dougherty, M. T. Organization of cytokeratin cytoskeleton and germ plasm in the vegetal cortex of Xenopus laevis oocytes depends on coding and non-coding RNAs: three-dimensional and ultrastructural analysis. *Exp Cell Res.* **313,** 1639–1651 (2007).
21. Kloc, M. Teachings from the egg: new and unexpected functions of RNAs. *Mol Reprod Dev.* **76,** 922–932 (2009).
22. Kloc, M., Foreman, V. & Reddy, S. A. Binary function of mRNA. *Biochimie* **93,** 1955–1961 (2011).
23. Jenny, A. *et al.* A translation-independent role of oskar RNA in early Drosophila oogenesis. *Development* **133,** 2827–2833 (2006).
24. Kloc, M. *et al.* Potential structural role of non-coding and coding RNAs in the organization of the cytoskeleton at the vegetal cortex of Xenopus oocytes. *Development* **132,** 3445–3457 (2005).
25. Kloc, M. *et al.* RNA localization and germ cell determination in Xenopus. *Int Rev Cytol.* **203,** 63–91 (2001).
26. Sindelka, R., Sidova, M., Svec, D. & Kubista, M. Spatial expression profiles in the Xenopus laevis oocytes measured with qPCR tomography. *Methods* **51,** 87–91 (2010).
27. Flachsova, M., Sindelka, R. & Kubista, M. Single blastomere expression profiling of Xenopus laevis embryos of 8 to 32-cells reveals developmental asymmetry. *Sci Rep* **3,** 2278 (2013).
28. Wylie, C. *et al.* Maternal beta-catenin establishes a 'dorsal signal' in early Xenopus embryos. *Development* **122,** 2987–2996 (1996).
29. Mercer, T. R. *et al.* Expression of distinct RNAs from 3' untranslated regions. *Nucleic Acids Res.* **39,** 2393–2403 (2011).
30. Watanabe, T. *et al.* Stage-specific expression of microRNAs during Xenopus development. *FEBS Lett.* **579,** 318–324 (2005).
31. Ambady, S., Wu, Z. & Dominko, T. Identification of novel miRNAs in Xenopus laevis matephase II arrested eggs. *Genesis* **50,** 286–299 (2012).
32. Sindelka, R., Jonak, J., Hands, R., Bustin, S. A. & Kubista, M. Intracellular expression profiles measured by real-time PCR tomography in the Xenopus laevis oocyte. *Nucleic Acids Res.* **36,** 387–392 (2008).
33. Gurdon, J. B. Changes in somatic cell nuclei inserted into growing and maturing amphibian oocytes. *J Embryol Exp Morph.* **20,** 401–414 (1968).
34. Jullien, J., Pasque, V., Halley-Stott, R. P., Miyamoto, K. & Gurdon, J. B. Mechanism of nuclear reprogramming by eggs and oocytes: a deterministic process?. *Nat Rev Mol Cell Biol.* **12,** 453–459 (2011).

35. Hibio, N., Hino, K., Shimizu, E., Nagata, Y. & Ui-Tei, K. Stability of miRNA 5′terminal and seed regions in correlated with experimentally observed miRNA-mediated silencing efficacy. *Sci Rep.* **2,** 996 (2012).
36. Benes, V. *et al.* Identification of cytokines-induced modulation of microRNAs expression and secretion as measured by a novel microRNA specific qPCR assay. Accepted in *Sci Rep.* (2015).
37. Ibberson, D., Benes, V., Muckenthaler, M. U. & Castoldi, M. RNA degradation compromises the reliability of microRNA expression profiling. *BMC Biotechnol.* **9,** 102 (2009).
38. Castoldi, M. *et al.* The liver-specific microRNA miR-122 controls systemic iron homeostasis in mice. *J Clin Invest.* **121,** 1386–1396 (2011).

Acknowledgments

This study was supported by Ministry of Youth, Education and Sports of the Czech Republic RVO: 86652036 and grant LK21305; BIOCEV CZ.1.05/1.1.00/02.0109 from the ERDF and by the Charles University grant SVV 260206.

Author Contributions

All authors have seen and approved the manuscript and its content. The authors are aware of the responsibilities connected to authorship. MS prepared and processed the samples and took part in the statistical analyses. RS designed the experiments. MC and VB optimized quantification of miRNAs through the miQPCR and provided the design of miRNA specific primer. MK participated in the statistical analyses and supervised the experiments.

Additional Information

Supplementary information accompanies this paper at http://www.nature.com/srep

Competing financial interests: The authors declare no competing financial interests.

How to cite this article: Sidova, M. *et al.* Intracellular microRNA profiles form in the *Xenopus laevis* oocyte that may contribute to asymmetric cell division. *Sci. Rep.* **5**, 11157; doi: 10.1038/srep11157 (2015).

Intracellular microRNA profiles form in the *Xenopus laevis* oocyte that may contribute to asymmetric cell division

Authors

Monika Sidova, Radek Sindelka, Mirco Castoldi, Vladimir Benes and Mikael Kubista

Supplement information

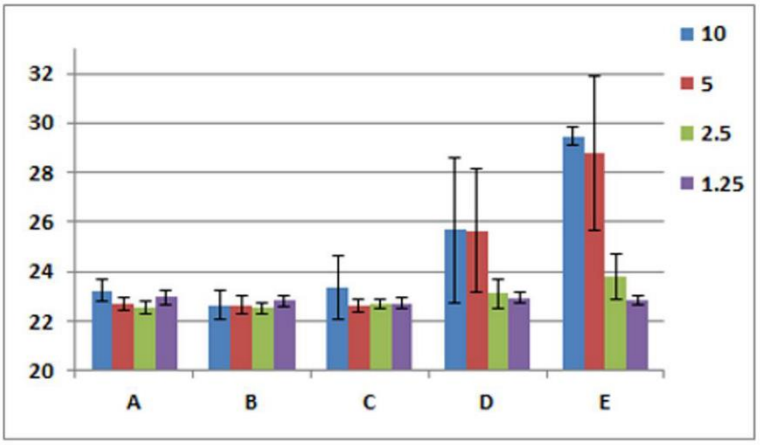

Supplement Figure 1. Optimization of experimental protocol using an RNA spike. 10 ng (blue), 5 ng (red), 2.5 ng (green), and 1.25 ng (violet) of total RNA and same amount of the RNA spike were used for reverse transcription. Spike cDNA was than quantified using qPCR. Y-axis shows Cq value and x-axis indicates section from the animal pole (section A) to vegetal pole (section E). Error bars indicate standard deviation of biological replicates.

miRNA	primer	Tm
miR-16c	TAGCAGCACGTAAATACTGGAGG	59.30
miR-18b	TAAGGTGCATCTAGTGCAGTTAGG	59.52
miR-19b	TGCAAATCCATGCAAAACTGAG	61.83
miR-20b	CAAAGTGCTCATAGTGCAGGTAGG	60.98
miR-22	AGCTGCCAGTTGAAGAACTGTG	60.44
miR-25	ATTGCACTTGTCTCGGTCTGAG	60.27
miR-93a	GTGCTGTTCGTGCAGGTAGG	60.29
miR-100	CCGTAGATCCGAACTTGTGG	58.99
miR-148b	TCAGTGCATCACAGAACTTTGTG	59.79
miR-221	GCTACATTGTCTGCTGGGTTTG	60.50
miR-363-3p	AATTGCACGGTATCCATCTGTAAG	60.08
miR-5102-5p	GAGTTTGACTGGGGCGG	58.52
miR-15a	TAGCAGCACATAATGGTTTGTGAG	60.02
miR-15c	TAGCAGCACATCATGGTTTGTAG	58.77
miR-22	AGCTGCCAGTTGAAGAACTGTG	60.44
miR-24a	GCTCAGTTCAGCAGGAACAGG	60.93
miR-27b	TCACAGTGGCTAAGTTCTGCG	60.03
miR-34a	GGCAGTGTCTTAGCTGGTTGTG	60.69
miR-34b	AGGCAGTGTAGTTAGCTGATTGG	58.47
miR-122	TGGAGTGTGACAATGGTGTTTG	60.28
miR-124	ACGCGGTGAATGCCAAG	60.20
miR-140-3p	CACAGGGTAGAACCACGGAG	59.00
miR-191	GAATCCCAAAAGCAGCTGTG	59.26
miR-210	CGTGTGACAGCGGCTGAG	61.23
miR-214	CAGGCACAGACAGGCAGTG	60.03
miR-222	ACATCTGGCTACTGGGTCTCG	60.11
miR-375	CGTTCGGCTCGCGTTAG	60.08

Supplement Table 1. Primer assays and their predicted Tm of maternal miRNAs. The primer assays were designed for 27 randomly selected maternal miRNAs. 12 assays (miR-16c, miR-18b, miR-19b, miR-20b, miR-22, miR-25, miR-93a, miR-100, miR-148b, miR-221, miR-363-3p, miR-5102-5p, shown in red) showed higher and more reproducible expression than the other 15 miRNAs (miR-15a, miR-15c, miR-22, miR-24a, miR-27b, miR-34a, miR-34b, miR-122, miR-124, miR-140-3p, miR-191, miR-210, miR-214, miR-222, miR-375, shown in blue).

4.4. Effects of *post mortem* and physical degradation on RNA integrity and quality

Sidova M., Tomankova S., Abaffy P., Kubista M. a Sindelka R. *Biomolecular Detection and Quantification* (zvaný článek, vydání srpen 2015). IF bude přidělen

Kvalita výsledků při měření genové exprese závisí především na integritě a stabilitě izolované RNA. Již částečná degradace RNA vzorku představuje zdroj technické variability a může vést k chybným závěrům. Cílem této publikace bylo objasnit vliv enzymatické a teplotní degradace na kvalitu RNA vzorků. V rámci experimentů byly použity dva systémy: zralé oocyty *X. leavis* představovaly zástupce maternální RNA a pulci *X. laevis* ve stádiu 40 zastupovali komplexní biologický vzorek (již mají vyvinuty všechny orgány). Intenzita enzymatické degradace byla studována *post mortem* v časech 0, 5, 10, 20 a 40 minut po usmrcení oocytů a pulců. Teplotní degradace byla studována na izolované celkové RNA, která byla zahřívána na teplotu 80 ^{o}C po dobu 0, 1, 2, 4 a 6 hodin. U všech vzorků byly prostřednictvím kapilární elektroforézy stanoveny tzv. hodnoty RQI (RNA Quality Indicator) a zároveň byla pomocí RT-qPCR vyhodnocena stabilita 16-ti vybraných RNA (*odc, imp3, RNA pol. II, maml1, atub, acta, eef1a1, mrp1, ubc, ant1, mdh2a, xk81a1, scaRNA11, 5S rRNA, cyc1* a *18S rRNA*). Na základě dosažených výsledků se ukázalo, že během teplotní degradace dochází ke snížení integrity RNA v rámci hodin a postiženy jsou ve stejné míře všechny typy RNA. Na druhou stranu degradace *post mortem* působí v řádech jednotek či desítek minut a k jejímu účinku je mnohem citlivější mRNA, zatímco rRNA (ribosomal RNA), scaRNA (small cajal body-specific RNA) a mtRNA (mitochondrial RNA) vykazují vysokou stabilitu. Přestože hodnoty RQI u vzorků degradovaných *post mortem* nenaznačovaly sníženou integritu RNA, analýza RT-qPCR odhalila, že mRNA byla zatížena degradací. Tento fakt se negativně odrazil ve vyhodnocení kvality RNA. Dále byla dokázána vyšší stabilita maternální RNA oproti RNA z pulců. Důvodem je, že oocyty pravděpodobně obsahují více ochraných faktorů, které zvyšují stabilitu této RNA. Poslední výsledek ukazuje, že nedochází k preferenční degradaci transkriptů od 3´ nebo 5´ konce v průběhu degradace *post mortem*.

Title

Effects of *post-mortem* and physical degradation on RNA integrity and quality

Authors

Monika Sidova[1,2] , Silvie Tomankova[1], Pavel Abaffy[1], Mikael Kubista[1,3], Radek Sindelka[1*]

1) Laboratory of Gene Expression, Institute of Biotechnology, Academy of Sciences of the Czech Republic, Videnska 1083, 142 20 Prague, Czech Republic

2) Charles University in Prague, Faculty of Science, Department of Cell Biology, Vinicna 7, 128 43, Prague, Czech Republic

3) TATAA Biocenter AB, Odinsgatan 28, 411 03 Göteborg, Sweden

*Corresponding author

sindelka@ibt.cas.cz, tel. +420-241063623, fax. +420 241 063 610

Abstract

The precision and reliability of quantitative nucleic acid analysis depends on the quality of the sample analyzed and the integrity of the nucleic acids. The integrity of RNA is currently primarily assessed by the analysis of ribosomal RNA, which is the by far dominant specie. The extrapolation of these results to mRNAs and microRNAs, which are structurally quite different, is questionable. Here we show that ribosomal and some nucleolar and mitochondrial RNAs, are highly resistant to naturally occurring *post-mortem* degradation, while mRNAs, although showing substantial internal variability, are generally much more prone to nucleolytic degradation. In contrast, all types of RNA show the same sensitivity to heat. Using qPCR assays targeting different regions of mRNA molecules, we find no support for 5' or 3' preferentiality upon *post-mortem* degradation.

Introduction

The quality of biological samples is very sensitive to the handling and treatment before the nucleic acids are extracted for analysis and degrading enzymes are inhibited or removed. Analyzing RNA is more challenging than analyzing DNA, because double-stranded DNA is more stable than single-stranded RNA, deoxyribonucleases (DNases) are readily denatured and inhibited compared to the highly stable ribonucleases (RNAses). The *post-mortem* degradation of nucleic acids in biological samples has proven useful in forensic pathology, where the time of death can be estimated [1]. In diagnostic samples *post-mortem* nucleic acid degradation is only a nuisance that shall be controlled and kept to a minimum [2-4]. Usually the confounding processing (technical) variation introduced by DNA degradation is small and can be ignored. For RNA analysis situation is quite different and several reports show expression data can be seriously biased and highly unreliable [5-11]. The main cause is poor RNA quality and integrity. This is particularly serious in medical molecular diagnostic, and has been thoroughly addressed by the SPIDIA consortium (www.spidia.eu), which ultimately led to the formulation of CEN and ISO guidelines for the preanalytical process in molecular diagnostics. The guidelines teach RNA quality/integrity shall be tested in workflows aiming to quantify RNA biomarkers.

Currently, the quality of RNA in biological samples is determined by electrophoresis that separate the dominant RNA species by size. Those are ribosomal RNAs (rRNAs), which make up about 85% of total RNA in eukaryotes. These eukaryotic ribosomal RNAs are presented in four distinct sizes, referred to as small (5S and 5.8S) and long (18S and 28S), where the size is given in Svedberg units, reflecting the sedimentation coefficient [12]. The long rRNAs are usually produced in a 1:1 ratio and because of the roughly double size of the 28S species the electropherogram of fully intact RNA shows distinct bands for the 18S and 28S rRNAs, with the 28S band having approximately twice the intensity. A ratio deviating from 2 indicates RNA degradation [13, 14]. The 28S:18S ratio shows correlation with RNA integrity [15], but can be affected by factors such as aging [16] and apoptosis [17]. Several companies have developed systems to measure RNA integrity based on the separation of the RNA molecules, such as the automated capillary electrophoresis systems such as Experion from Bio-Rad Laboratories, USA and Agilent Bioanalyzer 2100 from Agilent Technologies, USA. Those systems use chip-based technology for RNA quality and quantity measurements. The entire electropherogram is analyzed and then, using a complex algorithm trained to take into account all the features, the RNA quality/integrity is presented as a single quality indicator. The Bioanalyzer software uses RIN (RNA Integrity Number), while the Experion uses RQI (RNA Quality Indicator). Hence, the indicator is affected by several factors including the

presence of small RNA fragments from degradation, presence of molecules longer than the 28S, and overall low signals of the rRNAs [14]. Recently, alternative instruments for large scale and sensitive RNA quality and integrity determination appeared such as Fragment Analyzer™ (Advanced Analytical Technologies), QIAxcel Advanced System (Qiagen), ScreenTape (Agilent Technologies). These instruments also score RNA integrity using complex indicators such as RIS (RNA Integrity Score) for QIAxcel Advanced System and RIN^e (RNA integrity number equivalent) for ScreenTape.

The indicators produced by the different instruments are not readily comparable, because each uses its own algorithm, but they all score RNA quality as a number between 1 and 10, where 1 indicates completely degraded RNA and 10 fully intact RNA [6, 18]. In addition to the platform to platform variation, also the repeatability (repletion on the same instrument) and reproducibility (repetition on a different instrument of the same type) of the integrity index estimates has been questioned, particularly on extensively degraded samples. Furthermore the assessment of the RNA integrity is based on properties of the rRNAs and does not necessarily reflect the state of the mRNA pool.

The quality of extracted RNA depends on the source tissue [8]. Tissues such as spleen and liver that are rich in nucleases degrade RNA faster and to greater extent than in tissues with less RNase activity such as muscle and heart [19]. Common recommendation is to only analyse RNA from samples with RIN/RQI larger than five and microRNA from sample with RIN/RQI larger than seven [20]. RNA degradation is complex and three different types of mechanisms can be distinguished: enzymatic, physical and chemical. Enzymatic degradation occurs naturally in *post-mortem* tissue [21]. It initiates with either polyA tail/5' cap removal or endonucleolytic cleavage followed by exonuclease degradation [22, 23]. Physical (e.g. UV light, high temperature) and chemical (e.g. aldehydes, paraffin) degradation is by quite different mechanisms. It may induce crosslinking, oxidation and modification of RNA molecules. In this work we study the effects of the main degradation mechanisms on different RNA molecules under defined conditions.

Materials and Methods

Ethics statement

The study was carried out in accordance with the Act No 246/1992 Coll., on the protection of animals against cruelty. Official permission was issued to Biotechnology institute AS CR, v.v.i. by the Central Commission for Animal Welfare under the Ministry of Agriculture of Czech Republic.

RNA samples preparation

Xenopus laevis females were injected with 500 U of human chorionic gonadotrophin hormone (hCG, Sigma) to stimulate ovulation of oocytes. The females were kept overnight at 18 ºC and oocytes were obtained by gentle squeezing. The oocytes were *in vitro* fertilized by sperm suspension prepared in L-15 Leibowitzs medium with 15% of fetal bovine serum. Fertilized oocytes were covered with 0.1x MBS medium (Modified Barth´s Saline; 88 mM NaCl, 1 mM KCl, 0.7 mM CaCl2, 1 mM MgSO4, 5 mM HEPES, 2.5 mM NaHCO3, pH 7.7) for 20 min. Jelly coats were removed by 2% cysteine treatment (pH 7.7) followed by repeated washes with 0.1x MBS. The oocytes and tadpoles at stage 40 (3 biological replicates per condition) were collected and deep frozen at -80ºC, which cause their death. After thawing, the samples were incubated at room temperature for 0, 5, 10, 20 and 40 minutes. The total RNA was extracted using RNeasy Micro Kit (Qiagen). Manufacturer´s instructions were followed during the extraction and elution was performed using 15 µl of water. Concentration of extracted total RNA was measured using the Nanodrop® ND1000 quantification system. Heat degradation was performed with total RNA extracted from tadpoles at stage 40. Purified RNA was divided into separate tubes and heat treated for 0, 1, 2, 4 and 6 hours at 80ºC. The RNA quality was evaluated using Experion capillary electrophoresis system (Bio-Rad) and RNA StdSens chip (manufacture´s instructions were followed).

cDNA preparation

Isolated RNA from each sample was reverse transcribed into cDNA using SuperScript™ III Reverse transcriptase kit (Invitrogen). 50 ng and 300 ng of total RNA were reverse transcribed from oocytes and tadpoles (stage 40) samples, respectively. The RNA was mixed with 0.5 µl of oligo-dT and random hexamers (mixture 1:1, 50 µM each), 0.5 µl of dNTPs (10 mM each), 0.5 µl of spike (*in vitro* transcribed artificial RNA, TATAA Biocenter) and DNase/RNase free water to a total volume of 6.5 µl. The spike was included to test for any unspecific bias in the processing of the degraded samples. The mixture was incubated for 5 min at 75ºC, 20 s at 25ºC followed by cooling to 4ºC for 1 min. 100 U of enzyme, 20 U of RNaseOUT™ (recombinant ribonuclease inhibitor, Invitrogen), 0.5 µl of 0.1 M DTT and 2 µl of 5x first strand synthesis buffer were added to a final volume of 10 µl. The mixture was then incubated at 25ºC for 5 min, 50ºC for 60 min, 55ºC for 15 min and 75ºC for 15 min. 50 µl of water was added to the cDNA and the samples were stored at -20ºC. qPCR assays for 16 transcripts (*odc, imp3, RNA pol. II, maml1, atub, acta, eef1a1, mrp1, ubc, ant1, mdh2a, xk81a1, scaRNA11, 5S rRNA, cyc1* and *18S rRNA*) were designed using NCBI Primer-Blast (http://www.ncbi.nlm.nih.gov/tools/primer-blast/). Amplicon length was set to between 90 bp – 200 bp and Tm 60ºC. Specificity of all assays was confirmed by melting curve analysis measured from 65ºC to 95ºC

in 0.5ºC intervals. qPCR mix contained 5 µl of JumpStart mastermix (Sigma), 0.5 µl of forward and reverse primers mix (mixture 1:1, 10 µM each), 2 µl of cDNA and water to final volume of 10 µl. qPCR was performed on a CFX384 cycler system from Bio-Rad. PCR conditions were: initial denaturation at 95ºC for 2 min, 40 repeats of denaturation at 95ºC for 15 sec, annealing at 60ºC for 20 sec and elongation at 72ºC for 20 sec.

Data analysis

Cq values of biological replicates were averaged and standard deviations were calculated (data not shown, SD < 0.6). Measured transcripts levels in figures 2, 4 and 5B are shown relative to those measured at time 0 as $2^{Cqo-Cqi}$; where Cq_0 is the Cq value measured at time 0 and Cq_i is the Cq at the time *i* of degradation. In figures 2 and 5B the ratios are expressed in logarithmic scale. The data were analysed with GenEx (MultiD, version 6). Briefly, data were pre-processed using a cut-off at 36 cycles and missing data were substituted by the average of valid Cq values at that stage and time. All data were converted to relative quantities (relative to the highest Cq for each gene, artificially assigning an expression of 1 to the least expressed sample) and transformed to log2 scale. The data were mean centred (for each gene, subtracting the average expression across all samples) and two tests were applied to classify the profiles: the Kohonen self-organizing map (SOM, with two boxes) and hierarchical clustering presented as a dendrogram (Fig. 3). The SOM classification was repeated using independent seeds to validate the result.

Results

RNA degradation is faster in tadpole samples compared to oocytes

Total RNA was extracted from *Xenopus* oocytes and tadpoles at stage 40. The oocytes were selected because of their simple nature being a single cell, while the tadpoles at stage 40 were selected to represent a complex biological sample. The tadpoles have already most of the body tissues, such as internal and sensory organs, differentiated. Samples were collected at 0, 5, 10, 20 and 40 minutes *post-mortem*. Total RNA was extracted and integrity was assessed by gel electrophoresis using Experion capillary electrophoresis system (Fig. 1). Oocyte RNA samples showed first signs of degradation, reflected by the presence of short fragments and the disappearing of the 28S rRNA band, 10 minutes *post-mortem*. The RNA quality was still quite high with RQI of 8 at 40 minutes *post-mortem* (Fig. 1A). In contrast, tadpole samples showed significant RNA degradation already 5 minutes *post-mortem* with RQI of 6.5 and after 40 minutes RQI was 3.4 (Fig. 1B).

Different rates of rRNA and mRNA post-mortem degradation

Next we tested if *post-mortem* RNA degradation depends on the type of RNA. As control for technical variation an RNA spike was added to all samples before the reverse transcription. The average standard deviation of the spike across all biological replicates was 0.37 cycles for the oocyte samples and 0.46 cycles for the tadpole at stage 40 samples. These low SDs reflect high reproducibility of the reverse transcription and the qPCR step.

We designed qPCR assays for the 5S and 18S rRNA, the small nucleolar *scaRNA11*, the mitochondrial transcript *cyc1,* and for 12 mRNAs. Temporal degradation profiles were measured *post-mortem* (Fig. 2). Two distinct degradation profiles appeared, which we refer to as unstable and stable RNAs. The unstable RNAs include the genes: *odc, imp3, RNA pol. II, maml1, atub, acta, eef1a1, mrp1, ubc, ant1, mdh2a, xa81a1*. Several of these are so called housekeepers and often used as reference genes in expression studies. The degradation of unstable RNAs in the tadpole samples showed more than two orders of magnitude faster degradation than for the same RNAs prepared from the oocytes. In the oocyte samples, the fraction of unstable RNAs dropped from ~77% at 10 minutes to ~27 % at 40 minutes *post-mortem*. For the tadpole samples the fraction of unstable RNAs dropped from about 16 % at 10 minutes to 0.4 % at 40 minutes *post-mortem*. These results are in concordance with the overall RNA degradation measured using gel electrophoresis (Fig. 1).

The stable RNAs include *5S rRNA, 18S rRNA, scaRNA11* and *cyc1,* and exhibit minimal degradation. Their levels showed minimal changes during 40 minutes *post-mortem* in the oocyte samples (Fig. 2C) and only limited degradation (to 50-70%) with the tadpole samples. Notably, none of these RNAs is a cellular mRNA. The distinct difference in stability of stable and unstable RNAs was further supported by multiway analysis. Both SOM and hierarchical clustering clustered the stable RNAs with the RNA spike separately from the unstable RNAs (Fig. 3). The RNA spike was added after RNA extraction and was not degraded. Similarity of degradation pattern with spike RNA was used as a representation of stable RNA.

Differential sensitivity of RNA 5' and 3' ends to degradation

Three major pathways of enzymatic mRNA degradation have been described. Degradation is initiated by the removal of the 5' cap, deadenylation at the 3' end, or by endonucleolytic cleavage within the mRNA [23, 24]. The deprotected mRNA is then rapidly degraded by exonucleases [25, 26]. To test if degradation of mRNAs is preferential at either end we designed 5 separate qPCR assays covering essentially the entire length of *xk81a1* (cytokeratin) and *atub (*alpha tubulin*)* mRNAs. All qPCR assays were designed with similar amplicon length (80-110 bp) and their efficiencies

were higher than 90%. Uniformity of assay efficiencies, minimal biological variability of oocyte samples (standard deviation of biological replicates from one female is ~ 0.3 of Cq) and possibility to use samples at time 0 as a reference allow us precise normalization and comparison of all assays. All five qPCR assays per transcript showed similar decrease of mRNA content to ~60% at 10 minutes and to 20% at 20 minutes. Our data show no indications of statistically significant degradation preference for 5' or 3' ends for neither of studied genes (Fig. 4). The relationship among the assays was tested using Pearson correlation. The *xk81a1* assays showed r-coeficients > 0.96 and the *atub* assays showed r-coeficients > 0.97 indicating high correlation among all five qPCR assays. In all cases the p-values were < 0.05.

Physical degradation has the same effect on ribosomal and messenger RNA

Physical degradation was induced by heat treatment of purified tadpole at stage 40 RNA, because this RNA showed higher sensitivity to degradation and has higher complexity compared to oocyte. The tadpole RNA samples were incubated at 80^{o}C for 0, 1, 2, 4, and 6 hours to induce degradation. Overall integrity of the RNA was assessed by gel electrophoresis (Fig. 5A) and degradation of the same transcripts as in the study of natural *post-mortem* degradation in Fig. 2 was measured with RT-qPCR (Fig. 5B).

Under the conditions used, the heat-induced degradation had much lower impact on the measured transcript levels compared to the natural *post-mortem* degradation. Heat induced degradation could be noticed first after one hour (Fig. 5A). The RQI values decreased to about 4.8 after one hour of heat treatment and continued slowly decreasing for up to six hours. At earlier time points degradation was hardly noticed (5, 10, 20 and 30 minutes, Supplement Fig. 1). Neither did we see any significant degradation when using the lower temperature of 70^{o}C for up to even 6 hours (Supplement Fig. 2). Notably, we found that also the impact of heat on the different RNA molecules varies, but differently from the effect of *post-mortem* degradation. The only RNA that showed resistance to the heat treatment was *scaRNA11;* its level remained close to 100 % during the entire degradation. All the other RNAs, were degraded at roughly the same rate.

Discussion

Accurate quantification of gene expression with methods such as RT-qPCR, microarray profiling and next-generation sequencing requires integral RNA of high quality. It is well established that the pre-analytical steps in molecular analysis, comprising sample collection, transportation, storage, and extraction, may have profound effect on the RNA and, via reverse transcription, the cDNA quality and introduce substantial technical bias [2-4]. It is therefore critical to use highly

optimized and validated pre-analytics, but also to test the quality and integrity of the extracted RNA. This is included in most workflows and also requested in the recent guidelines from the European Committee for Standardization. Our results presented here, suggests that testing of relevant RNA quality and integrity may be complicated.

We selected oocytes and tadpoles at stage 40 of frogs as model for our study of RNA degradation, because they are easily accessible, contain several micrograms of total RNA and, most importantly, sibling oocytes and tadpoles at stage 40 are synchronous and have nearly identical transcript levels, which makes the impact of individual variation that confounds the study negligible. Hence, we are neither limited by material nor biological reproducibility in those experiments. Routine assessment of RNA integrity and quality is based on the analysis of 18S and 28S rRNA, which are the far most abundant RNA molecules in most biological samples. Traditionally this was done by classical electrophoresis comparing their abundance, and is today done with more sensitive techniques, such as capillary electrophoresis, that analyze the entire electropherogram with advanced multivariate algorithms in commercial software and calculate integrity indexes. Hence, ribosomal RNA molecules are used as prime indicator of RNA integrity.

Our main goal was to determine whether rRNA degradation reflects accurately mRNA degradation. The main conclusion of our manuscript is, that rRNA degradation is useful for artificial degradation, but it is the poor prediction tool for natural *post-mortem* degradation of mRNA fraction. While eletrophoresis report indicated slight or even no degradation of rRNAs (Fig. 1), quantification of RNA levels using RT-qPCR revealed majority of mRNA molecules to be degraded to several percent of their original concentrations. We can speculate that ribosomal RNA is more protected against enzymatic degradation than mRNA, because of its structure lacking cap and polyA tail. Localization of rRNA into ribosomes and covering of rRNA molecules with other proteins can also increase its protection against intercellular RNAses. Physical and chemical degradation mechanism is independent on RNA structure, so rRNA fraction should degrade at the same rate as mRNA. Similar conclusion can be predicted for *scaRNA11* and mitochondrial *cyc1*. Those transcripts are located in nucleolus and mitochondia and this covering increases their protection during enzymatic *post-mortem* degradation. Several classes of small noncoding RNAs including *scaRNA11* has modified cap [27], which can increase their stability. High stability of *scaRNA11* to physical degradation can be explained by its short size, which prevents breaks and degradation during heat treatment.

Degradation rate is directly dependent on sample complexity. We compared oocyte samples as simple model versus tadpole at stage 40 samples as complex model. Oocyte showed minimal *post-mortem* degradation of rRNA pool and just slow degradation of mRNA pool. In contrast, tadpole samples showed gradual rRNA

degradation on a gel electrophoreogram, but quantification using RT-qPCR showed minimal decrease of rRNA molecules. We suggest that rRNAs are cleaved in complex samples faster than in simple samples, but the cleavage is not complete and short qPCR amplicons can still detect those fragments. Messenger RNA in tadpole samples were degraded two orders of magnitude faster than in oocyte samples. This can be explained by lack of protection factors in the tadpole samples. Oocyte as a single cell is full of material (RNA, protein, lipids etc.) and this matrix can surround and protect RNA molecules from *post-mortem* degradation. Further, oocyte mRNA fraction is not fully polyadenylated at 3' ends, and that could increase their stability too. On the other hand, tadpole mRNAs are mature with polyA tails and mRNAs are actively translated, so there would be minimal protection from surrounding molecules. In addition, tadpole samples probably content much higher concentration of RNAses. All these factors are probably behind the observed differences in degradation rates in our samples.

RNA molecules inside the cells are very sensitive to natural *post-mortem* degradation, but purified RNA samples (without RNAses) can be degraded by other factors such as temperature, UV light, various chemicals etc. The mechanisms of physical and chemical degradation is assumed to differ from natural *post-mortem* degradation. In theory, physical and chemical degradation is not dependent on RNA structure including presence of cap and polyA tail. We used physical RNA degradation induced by heat treatment to demonstrate different mechanism. Overall the physical degradation using 80 degrees incubation showed much slower degradation rate compared to *post-mortem* degradation. As expected, the ribosomal RNAs showed the same trend of degradation as mRNAs during physical degradation. The only exception in our hypothesis was small nucleolar RNA and we hypothesize that its short length makes it more stable to physical degradation than longer mRNA and rRNA molecules.

In conclusion, we performed several experiments to demonstrate problematic side of RNA integrity/quality estimation. We can summarize our finding: 1) ribosomal RNA is not useful indicator for natural degradation of mRNA in the *post-mortem* samples, but could be valuable indicator of physical and chemical degradation studies; 2) comparison of gene expression in samples with different degradation is problematic and could be overcome using proper references; and 3) *post-mortem* degradation of mRNA is not 5' or 3' end sensitive.

Acknowledgements

This study was supported by Ministry of Youth, Education and Sports of the Czech Republic AV0Z50520701 and grant LK21305; BIOCEV CZ.1.05/1.1.00/02.0109 from the ERDF and by the Charles University grant SVV 260206.

References

1. Sampaio-Silva F, Magalhaes T, Carvalho F, Dinis-Oliveira RJ and Silvestre R. Profiling of RNA degradation for estimation of post mortem interval. PLoS One 2013, 8:e56507.
2. Malentacchi F, Pazzagli M, Simi L, Orlando C, Wyrich R, Hartmann CC, Verderio P, Pizzamiglio S, Ciniselli CM, Tichopad A, Kubista M, Gelmini S. SPIDIA-DNA: an external quality assessment for the pre-analytical phase of blood samples used for DNA-based analyses. Clin Chim Acta 2013, 424: 274–286.
3. Malentacchi F, Pazzagli M, Simi L, Orlando C, Wyrich R, Günther K, Verderio P, Pizzamiglio S, Ciniselli CHM, Zhang H, Korenkova V, Rainen L, Bar T, Kubista M and Gelmini S. Second external quality assessment for the pre-analytical phase of blood samples used for RNA based analyses. PlosOne 2014, 9(11):e112293.
4. Zhang H, Korenkova V, Sjöback R, Svec D, Björkman J, Kruhøffer M, Verderio P, Pizzamiglio S, Ciniselli CHM, Wyrich R, Oelmueller U, Kubista M, Lindahl T, Lönneborg A, Rian E. Biomarkers for monitoring pre-analytical quality variation of mRNA in blood samples. PlosOne 2014, 9(11): e111644.
5. Raeymarkers L. Quantitative PCR: theoretical consideration with practical implication. Anal Biochem. 1993, 214:582-585.
6. Imbeaud S, Graudens E, Boulanger V, Barlet X, Zaborski P, Eveno E, Mueller O, Schroeder A and Auffray C. Towards standardization of RNA quality assessment using user-independent classifiers of microcapillary electrophoresis traces. Nucleic Acids Res. 2005, 33:e56.
7. Fleige S and Pfaffl MW. RNA integrity and the effect on the real-time qRT-PCR performance. Mol Aspects Med. 2006, 27:126-139.
8. Fleige S, Walf V, Hunch S, Prgomet C, Sehm J and Pfaffl MW. Comparison of relative mRNA quantification models and the impact of RNA integrity in quantitative real-time RT-PCR. Biotechnol. Lett. 2006, 28:1601-1613.
9. Strand C, Enell J, Hedenfalk I and Ferno M. RNA quality in frozen breast cancer samples and the influence on gene expression analysis – a comparison of three evaluation methods using microcapillary electrophoresis traces. BMC Mol Biol. 2007, 8:38.

10. Takano EA, Mikeska T, Dobrovic A, Byrne DJ and Fox SB. A multiplex endpoint RT-PCR assay for quality assessment of RNA extracted from formalin-fixed paraffin-embedded tissues. BMC Biotechnol 2010, 10:89.
11. Gallego Romero I, Pai AA, Tung J and Gilad Y. RNA-seq: impact of RNA degradation on transcript quantification. BMC Biol. 2014, 12:42.
12. Larson DE, Zahradka P and Sells BH. Control points in eukaryotic ribosome biogenesis. Biochem Cell Biol. 1991, 69:5-22.
13. Sambrook J, Fritsch EF, Maniatis T. Molecular Cloning: A Laboratory Manual. NY: Cold Spring Harbor Laboratory Press 1989, 2nd edn.
14. Mueller O, Lightfoot S and Schroeder A. RNA Integrity Number (RIN) – Standardization of RNA quality control application. Agilent Application Note 2004, Publication 5989-1165EN:1-8.
15. Miller CL, Diglisic S, Leister F, Webster M and Zolken RH Evaluatung. RNA status for RT-PCR in extracts of postmortem human brain tissue. Biotechniques 2004, 36:628-633.
16. Mori N, Mizuno D and Goto S. Increase in the ratio of 18S RNA to 28S RNA in the cytoplasm of mouse tissues during aging. Mech Ageing Dev. 1978, 8:285-297.
17. Houge G, Robaye B, Eikhom TS, Golstein J, Mellgren G, Gjertsen BT, Lanotte M and Doskeland SO. Fine mapping of 28S rRNA sites specifically cleaved in cells undergoing apoptosis. Mol Cell Biol. 1995, 15:2051-2062.
18. Schroeder A, Mueller O, Stocker S, Salowsky R, Leiber M, Gassmann M, Lightfoot S, Menzel W, Granzow M, Ragg T. The RIN: an RNA integrity number for assigning integrity values to RNA measurements. BMC Mol Biol. 2006, 7:3.
19. Bauer M. RNA in forensic science. Forensic Sci Int Genet. 2007, 1:69-74.
20. Ibberson D, Benes V, Muckenthaler M and Castoldi M. RNA degradation compromises the reliability of microRNA expression profiling. BMC Biotechnology 2009, 9:102.
21. Fordyce SL, Kampmann ML, van Doorn NL and Gilbert MT. Long-term RNA persistence in postmortem contexts. Investig Genet. 2013, 4:7.
22. Yamashita A, Chang TC, Yamashita Y, Zhu W, Zhong Z, Chen CY and Shyu AB. Concerted action of poly(A) nuclaeses and decapping enzymes in mammalian mRNA turnover. Nat Struct Mol Biol. 2005, 12:1054-1063.
23. Schoenberg DR. Mechanisms of endonuclease-mediated mRNA decay. Wiley Interdiscip Rev RNA 2011, 2:582-600.
24. Garneau NL, Wilusz J and Wilusz CJ. The highways and byways of mRNA decay. Nat Rev Mol Cell Biol. 2007, 8(2):113-126.
25. Beelman CA and Parker R. Degradation of mRNA in eukaryotes. Cell 1995, 81(2):179-183.

26. Lubas M, Damgaard CK, Tomecki R, Cysewski D, Jensen TH and Dziembowski A. Exonuclease hDIS3L2 specifies an exosome-independent 3´-5´ degradation pathway of human cytoplasmic mRNA. EMBO J. 2013, 32(13):1855-1868.
27. Matera AG, Terns RM, Terns MP. Non-coding RNAs: lessons from the small nuclear and small nucleolar RNAs. Nat Rev Mol Cell Biol. 2007, 8(3):209-20.

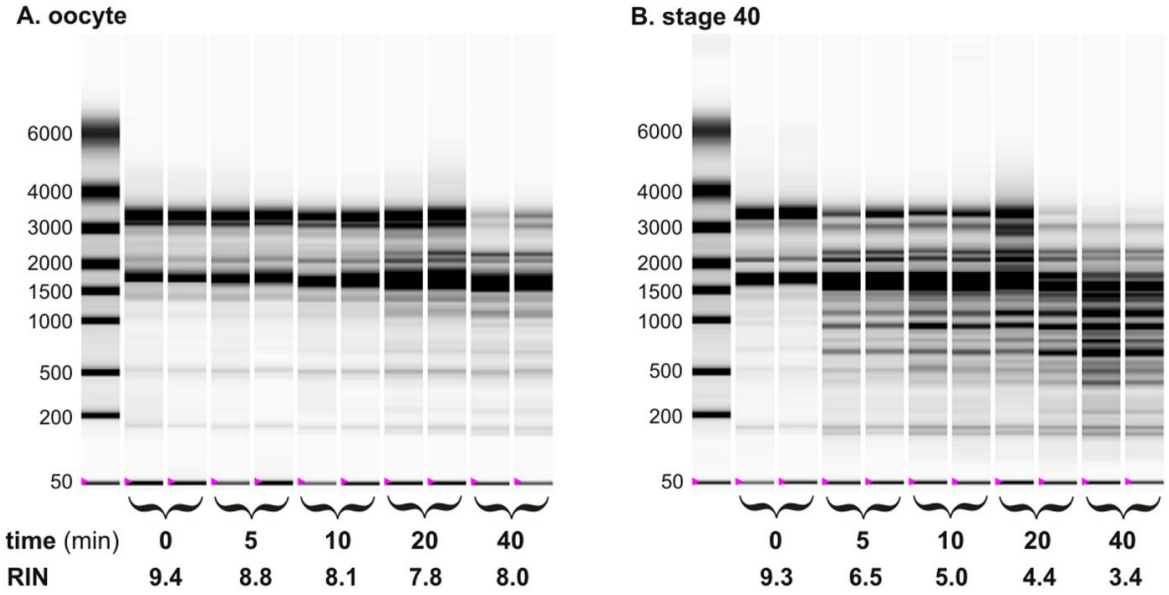

Fig. 1. Experion electropherograms of total RNAs and determined RQI values for *post-mortem* degraded (**A.**) oocytes and (**B.**) tadpole embryos at stage 40 measured at intervals 0, 5, 10, 20 and 40 minutes *post-mortem*.

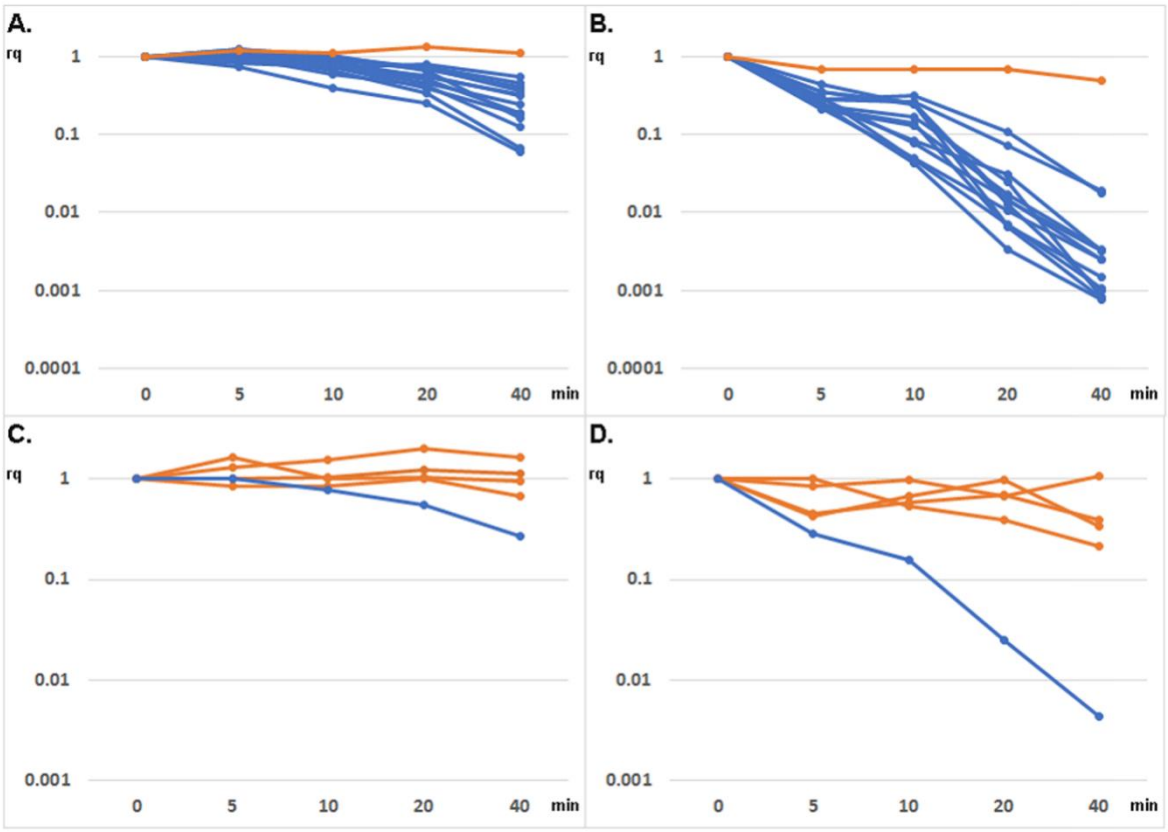

Fig. 2. Temporal degradation profiles of unstable genes (in blue - *odc*, *imp3*, *RNA pol. II*, *maml1*, *atub*, *acta*, *eef1a1*, *mrpl1*, *ubc*, *ant1*, *mdh2a*, *xk81a1*) - shown in **A.** oocyte and **B.** tadpole at stage 40. Degradation profiles of stable genes (in orange - *scaRNA11*, *5S rRNA*, *cyc1* and *18S rRNA*) - **C.** oocyte and **D.** tadpole at stage 40. Axes x in all graphs indicate intervals of *post-mortem* samples in minutes and axes y indicate relative quantity transferred to log scale. Profiles for stable genes were averaged in panels A., B. and profiles for unstable genes were averaged in panels C., D. to simplify comparison.

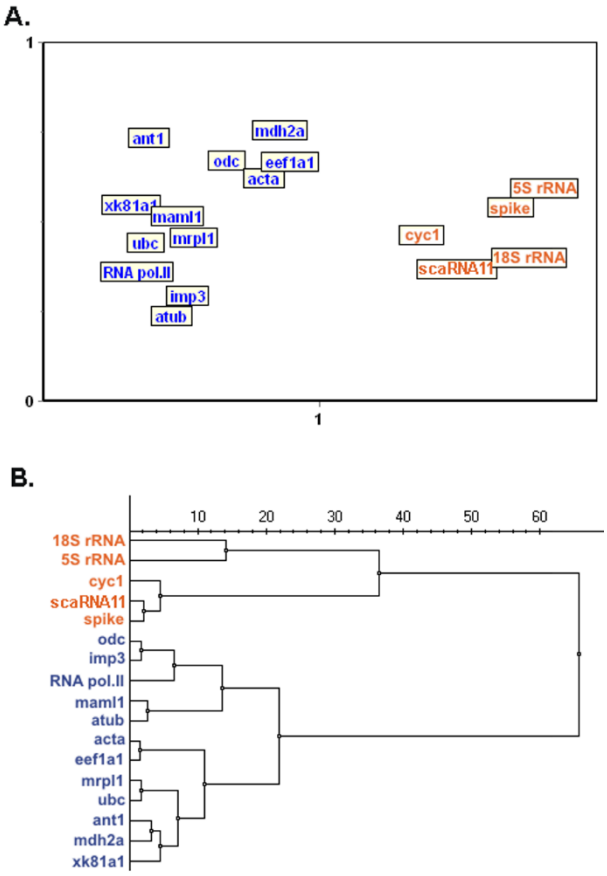

Fig. 3. Statistical analysis of degradation profiles. (**A.**) SOM analysis and (**B.**) hierarchical clustering for stable (orange) and degraded (blue) transcripts in *post-mortem* samples. RNA spike, which was added before reverse transcription, is included in analysis to indicate stable RNA level.

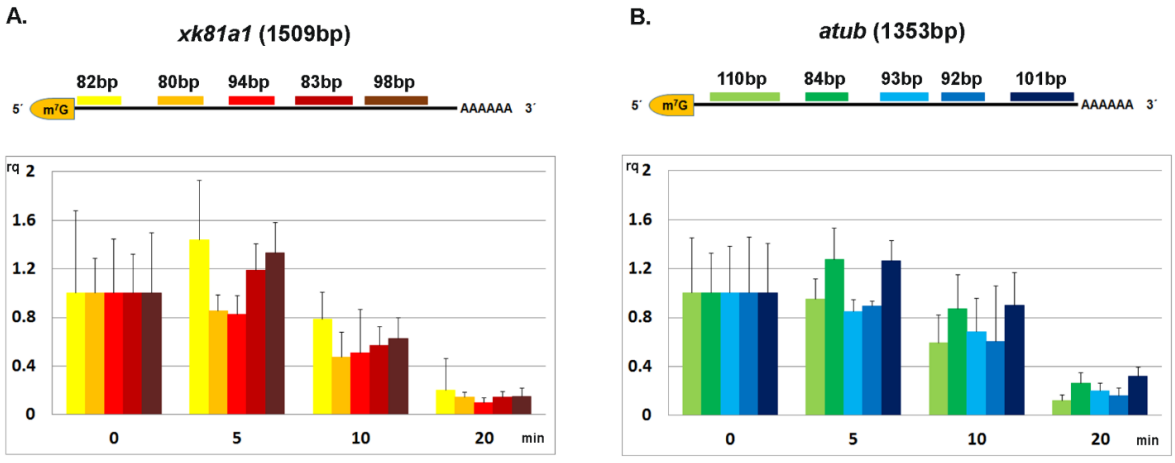

Fig. 4. Five different qPCR assays covering the whole molecules of (**A.**) *xk81a1* and (**B.**) *atub* were designed and quantified to determine 5' and 3' specific degradation. Axis x indicates *post-mortem* intervals in minutes and axis y indicates relative quantity.

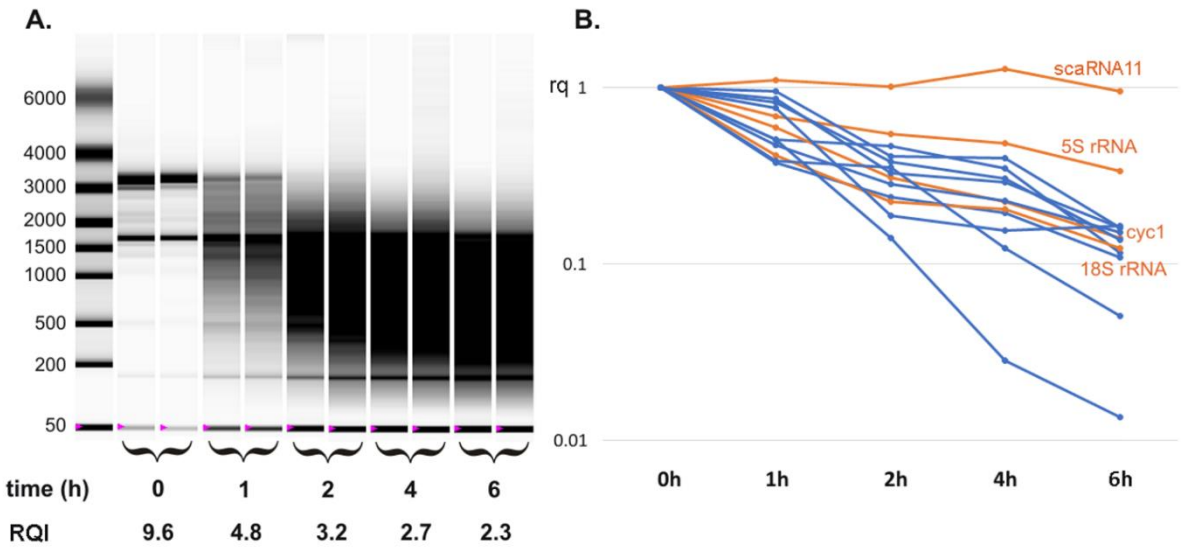

Fig. 5. Heat degradation. Extracted RNAs from embryos were heated for 0, 1, 2, 4 and 6 hours (axis x) at 80ºC. (**A.**) Total RNA quality and RQI was tested by Experion system. (**B.**) Temporal degradation profiles of 16 transcripts measured using RT-qPCR. *Post-mortem* unstable genes are shown in blue (*odc*, *imp3*, *RNA pol. II*, *maml1*, *atub*, *acta*, *eef1a1*, *mrpl1*, *ubc*, *ant1*, *mdh2a*, *xk81a1*) and stable genes are shown in orange (*scaRNA11*, *5S rRNA*, *cyc1* and *18S rRNA*).

Supplement information

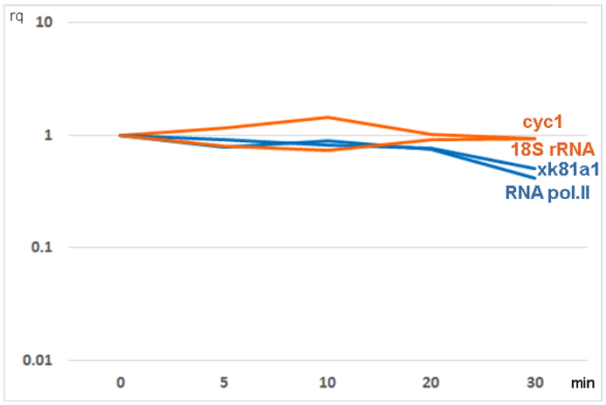

SFig. 1. Heat degradation at 80ºC. Extracted RNAs from embryos were heated for 0, 5, 10, 20 and 30 minutes (axis x). Temporal degradation profiles of *cyc1*, *18S rRNA*, *RNA pol. II*, *xk81a1* transcripts measured using RT-qPCR. Unstable genes are shown in blue and stable genes are shown in orange.

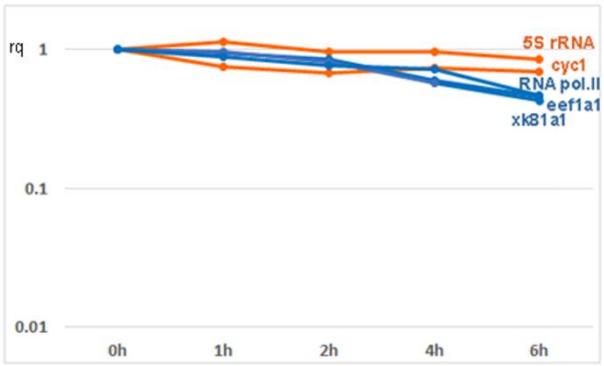

SFig. 2. Heat degradation at 70ºC. Extracted RNAs from embryos were heated for 0, 1, 2, 4 and 6 hours (axis x). Temporal degradation profiles of *RNA pol. II*, *eef1a1*, *5S rRNA*, *xk81a1*, *cyc1* transcripts measured using RT-qPCR. Unstable genes are shown in blue and stable genes are shown in orange.

4.5. Pre-amplification in the context of high-throughput qPCR gene expression experiment

Korenkova V., Scott J., Novosadova V., Jindrichova M., Langerova L., Svec D., **Sidova M.** a Sjoback R. *BMC Molecular Biology* 2015, 16:5. IF 2.057

Vysokokapacitní qPCR systém BioMark™ (Fluidigm) představuje revoluční přístup v možnostech studia genové exprese. Jeho kvantifikační kapacita umožňuje analyzovat 48 vzorků dohromady s 48 geny a dokonce i 96 vzorků proti 96 genům. V součtu dochází ke kvantifikaci 2304 nebo 9216 reakcí najednou v rámci jediného čipu. Objem každé reakce činí pouhých 6,7 nl a předpoklad uspěšné kvantifikace vyžaduje vysoce koncentrovaný templát. Z tohoto důvodu byl do protokolu kvantifikace přídán pre-amplifikační krok, který exponenciálně navyšuje množství měřených templátových molekul. Předmětem této práce bylo vyhodnocení základních faktorů, které ovlivňují pre-amplifikační reakci, a tím pozorovat jejich vliv na výsledek kvantifikace měřené pomocí vysokokapacitního BioMark™ systému. Byly kombinovány tři následující faktory: 1) počet pre-amplifikačních cyklů (15, 18, 21 a 24), 2) množství celkové RNA použité do reverzní transkripce (0,078 ng, 0,32 ng, 1,25 ng, 5 ng a 20 ng) a 3) míra exprese studovaného genu (5 genů pokrývající rozsah od nízké exprese po vysokou). Výsledky ukazují, že nejefektivnější pre-amplifikace vyžaduje kombinaci vyšší koncentrace vzorku s menším počtem pre-amplifikačních cyklů. Naměřená efektivita dosahovala hodnoty 95% v případě použití 5 ng templátu a 18 cyklů pre-amplifikace a dokonce 100% účinnost byla pozorována u kombinace 20 ng templátu s 15 nebo 18 cykly. Ve všech těchto případech docházelo k pre-amplifikaci všech typů genů se stejnou účinností. Zvyšování počtu pre-amplifikačních cyklů (21 a 24 cyklů) mělo za následek výrazné snížení pre-amplifikační efektivity a zároveň byla zaznamenána zvýšená variabilata vysoce exprimovaných genů. V neposlední řadě tyto výsledky ukazují, že variabilita pre-amplifikačního kroku dosahuje nižších hodnot než variabilita způsobená reverzní transkripcí.

Korenková et al. BMC Molecular Biology (2015) 16:5
DOI 10.1186/s12867-015-0033-9

BMC Molecular Biology

METHODOLOGY ARTICLE Open Access

Pre-amplification in the context of high-throughput qPCR gene expression experiment

Vlasta Korenková[1*], Justin Scott[2], Vendula Novosadová[1], Marie Jindřichová[1], Lucie Langerová[1], David Švec[1], Monika Šídová[1] and Robert Sjöback[3]

Abstract

Background: With the introduction of the first high-throughput qPCR instrument on the market it became possible to perform thousands of reactions in a single run compared to the previous hundreds. In the high-throughput reaction, only limited volumes of highly concentrated cDNA or DNA samples can be added. This necessity can be solved by pre-amplification, which became a part of the high-throughput experimental workflow. Here, we focused our attention on the limits of the specific target pre-amplification reaction and propose the optimal, general setup for gene expression experiment using BioMark instrument (Fluidigm).

Results: For evaluating different pre-amplification factors following conditions were combined: four human blood samples from healthy donors and five transcripts having high to low expression levels; each cDNA sample was pre-amplified at four cycles (15, 18, 21, and 24) and five concentrations (equivalent to 0.078 ng, 0.32 ng, 1.25 ng, 5 ng, and 20 ng of total RNA). Factors identified as critical for a success of cDNA pre-amplification were cycle of pre-amplification, total RNA concentration, and type of gene. The selected pre-amplification reactions were further tested for optimal Cq distribution in a BioMark Array. The following concentrations combined with pre-amplification cycles were optimal for good quality samples: 20 ng of total RNA with 15 cycles of pre-amplification, 20x and 40x diluted; and 5 ng and 20 ng of total RNA with 18 cycles of pre-amplification, both 20x and 40x diluted.

Conclusions: We set up upper limits for the bulk gene expression experiment using gene expression Dynamic Array and provided an easy-to-obtain tool for measuring of pre-amplification success. We also showed that variability of the pre-amplification, introduced into the experimental workflow of reverse transcription-qPCR, is lower than variability caused by the reverse transcription step.

Keywords: High-throughput qPCR, Exponential pre-amplification, Microfluidics, Gene expression, Fluidigm, BioMark, Degraded samples, FFPE

Background

The popularity of real time PCR steadily increases as well as the number of platforms, detection chemistries and multiple choices of analytical methods. Several years ago, the boom in high-throughput instruments changed the way of studying gene expression and enabled researchers to perform large scale studies based on the most sensitive and specific quantitative PCR method. The first commercially available high-throughput qPCR instrument was the BioMark™ System from Fluidigm that was launched in 2006. Microfluidic Dynamic Arrays provided by Fluidigm are able to combine either 48 samples with 48 assays or 96 samples with 96 assays in a combinatorial manner inside the integrated fluidic circuit (IFC) [1]. The BioMark System is able to process a high number of reactions (9,216) in a single run, each reaction taking place in volume of 6.7 nl [2]. With this number of reactions in a single run and its versatility and the freedom of the custom designed assays, BioMark System outperforms other high-throughput qPCR systems. There

* Correspondence: vlasta.korenkova@ibt.cas.cz
[1]Laboratory of Gene Expression, Institute of Biotechnology, Academy of Sciences of the Czech Republic, Prague, Czech Republic
Full list of author information is available at the end of the article

are only a few high-throughput qPCR instruments on the market that can be compared with BioMark System: OpenArray using a chip with 3,072 reactions, each for 33-nanolitre reaction volumes (Life Technologies) [3] and SmartChip with 5,184 reactions, each for 100-nanolitre reaction volumes (Wafergen) [4]. All these systems are designed to significantly simplify experimental workflow, increase throughput and reduce costs, while providing excellent data quality. Even though these instruments are built on different platforms, one attribute is common for all of them and that is a need for highly concentrated starting sample material.

The problem with an insufficient number of copies of the target in the reaction can be overcome with the help of pre-amplification. For the purposes of BioMark System a specific target amplification (also known as STA) is used, which is a multiplex PCR run with cDNA template and with a limited number of cycles, which is an exponential type of pre-amplification enabling simultaneous gene expression measuring of multiple targets in a single sample [5-7]. This kind of pre-amplification increases the amount of the initial cDNA or DNA template molecules several-fold, quantitatively amplifies just the target genes to be measured, and preserves the relationships between the transcripts. Even though pre-amplification has been used for many years [8,9] and it has been incorporated in high-throughput qPCR instruments workflows [10-13], it is still the least studied part of qPCR workflow that might introduce an additional bias if it is used without caution and appropriate controls.

In last few years, we witnessed that along with new techniques and new bioinformatic approaches come praiseworthy effort for proper standardization and control of the whole experimental process to eliminate widespread publication of poor data, resulting in inappropriate conclusions [14]. Because of the initiator of the whole process, MIQE guidelines [15], the quality and transparency of the laboratory results has been improved considerably. Pre-amplification process should not be omitted from this effort and it should be thoroughly validated and correctly reported as well as other parts of reverse transcription-qPCR workflow. It means that controls of pre-amplification should include at least paired non-preamplified and pre-amplified samples and each assay should be tested independently before the main experiment as described by Rusnakova [16]. For unbiased pre-amplification, the same difference between Cq values of non-preamplified and pre-amplified cDNA samples is expected for all assays; only reproducible small deviations are acceptable. Reproducibility is critical. Other controls as pre-amplified no template control (NTC) and pre-amplified control of reverse transcription without reverse transcriptase (RT-) should also be included. The reason is to ensure that quantification will not be influenced by eventual primer-dimer formation or by assays that would amplify gDNA. RT- control could be successfully replaced by a valid prime assay, which accurately corrects all reactions in BioMark Array for signals derived from gDNA using only one extra valid prime assay and pre-amplified genomic DNA (gDNA) [17]. As the pre-amplification reaction is a highly complex multiplex system (it is possible to pre-amplify almost limitless number of measured genes), simultaneous amplifications of the large number of targets may interfere; therefore it is necessary to use highly optimized qPCR assays with high efficiency and high precision and to run only a limited number of cycles and avoiding high-abundant targets if possible [18]. Even though it is possible to use fewer cycles of pre-amplification (10–14) for qPCR experiments with conventional qPCR instruments, high-throughput qPCR experiments require more than 14 pre-amplification cycles. Fluidigm advanced protocols recommend 14 cycles for conventional profiling [19] and 18 cycles for single-cell profiling [20]. These numbers of pre-amplification cycles are calculated for highly optimized assays but in practice pre-amplification PCR efficiencies are not close to 100% that is why these numbers are minimal and often suboptimal [18].

Here, we focus on identifying factors which influence the pre-amplification reaction and the pre-amplification limits, especially a limiting higher number of cycles for pre-amplification, which has not been studied systematically yet. Our aim is to find out the optimal conditions for BioMark Array that would give us an optimal distribution of quantifiable Cq values across the Array by using the proper amount of mRNA transferred into a reverse transcription reaction; the proper fraction of the cDNA used for pre-amplification and the proper fraction of the pre-amplified and correctly diluted cDNA, transferred into each sample well in BioMark Array.

Results and discussion

Evaluating variables in pre-amplification reaction using regular qPCR instrument

The primary purpose of pre-amplification is to enhance amount of input material, which can be, in some instances, very low even for conventional qPCR: single cell analysis [16,21], microRNA analysis [22], analysis of formalin-fixed, paraffine embedded tissues [23] or to enhance initial amount of material to be sufficient for high-throughput instrument [1]. The amount of pre-amplified transcripts correlates with the initial cDNA target copy numbers as has been shown previously for both good quality samples [24] and bad quality samples, e.g. formalin-fixed paraffin-embedded samples [23]. The exponential pre-amplification should not be affected by the quality of original RNA because the product of reverse transcription, cDNA molecule, is pre-amplified. That is

why the quality of RNA will influence only the reverse transcription step.

Even though the pre-amplification reaction itself is quite simple, there are several factors that can influence the final result. To identify and evaluate these factors we performed pre-amplification experiment combining different conditions. We evaluated four donors and five genes having high, medium and low expression levels. The genes were FKBP, STK10, EIF3M, CD83, and RND1 and were selected as representative from 24 well-characterized assays (Additional file 1) that were used later on for the summarizing BioMark experiment. Their mean Cq values for four non-pre-amplified samples were 18.7, 21.5, 23.7, 26.7, 34.0, respectively, which expression is spanning four orders of magnitude of dynamic range. Each sample was pre-amplified using four different cycles (15, 18, 21, and 24) and at five different concentrations (equivalent to 0.078 ng, 0.32 ng, 1.25 ng, 5 ng, and 20 ng of total RNA). The copy number of each transcript and sample was estimated for each assay. The estimated copy number for the low expressed gene RND1 was confirmed by dPCR. The limit of detection (LOD), the limit of quantification (LOQ) and the efficiency were determined for all 5 assays (Additional file 1).

Obtained non-pre-amplified Cq data and pre-amplified Cq data were subtracted to calculate an 'experimental difference' of pre-amplification: $\Delta Cq_{experimental} = Cq_{non\text{-}preamp} - Cq_{preamp}$. A 'theoretical difference' of pre-amplification was calculated as: $\Delta Cq_{theoretical}$ = number of pre-amplification cycles – $\log_2$ (all dilutions during the processing of the sample). The final formula was $\Delta\Delta Cq = \Delta Cq_{theoretical} - \Delta Cq_{experimental}$. An obtained ΔΔCq value, 'expression differential', close to zero indicates pre-amplification uniformity (example of calculation in Additional file 2). We set $\Delta\Delta Cq = 1.5$ as a quality threshold for an acceptable pre-amplification. This threshold value is in agreement with the threshold value recommended by Applied Biosystems in TaqMan PreAmp Master Mix Kit guide [11]. The values lower than the quality threshold ($\leq \pm 1.5$) were named a 'success'. The values higher than a quality threshold and the missing values, caused by missing copies in the reaction, were categorized as a 'failure' (16 or 4% of cases) (Additional file 2).

In order to evaluate which factors affect the 'success' of pre-amplification, we tested these data variables: Cycles (number of pre-amplification cycles), Log_copy ($\log_2$ copy number of cDNA used for pre-amplification), Log_concentn ($\log_2$ concentration of cDNA, presented as total RNA equivalent, used for pre-amplification), Donor, GeneNo (gene number = different transcripts) that were used in explanatory binomial candidate model. The optimal model was then derived in SPSS using the backward stepwise method to eliminate non-significant terms, which were Donor and Log_copy. Because all terms are known beforehand and controllable, the model could serve also as a predictive model with sensitivity of 81% and specifity 67% (Additional file 3).

Individual statistical tests uncovered important details of the pre-amplification process. Concentration of cDNA sample used for pre-amplification had significant effect on the overall likelihood of 'success' when tested for all Genes and Cycles together ($p = 0.012$); the higher Concentration, the higher 'success' (Additional file 4A). When individual Genes were taken in account and all Cycles were together, Concentration had significant effect only on low copy genes, RND1 ($p < 0.001$) and CD83 ($p = 0.001$) (Additional file 4B). Both genes show high failure rates in the low concentrated pre-amplification reactions (up to 5 ng) because the low template concentration corresponds to the low number of copies in pre-amplification (<10 copies of cDNA). These findings are in agreement with Bengtsson [25], who claims that when amplifying less than 20 cDNA copies the level of technical noise of PCR amplification increases dramatically, technical reproducibility decreases, thus the accurate quantification is reached if >20 target molecules per PCR are amplified.

Copy number of cDNA used for pre-amplification was not significant in the predictive model because Copy number (Log_copy) did not have a significant effect on the overall likelihood of 'success' when all Genes and all Cycles were combined together ($p = 0.322$) (Additional file 5A). However, if each Gene was tested independently with all Cycles together, the same results as for variable Concentration were obtained. Copy number had significant effect on low copy genes RND1 ($p = 0.0001$) and CD83 ($p = 0.0004$) (Additional file 5B). Additional information was derived if Copy number was compared for all Genes and each Cycle independently. Whereas the likelihood of 'success' increased with increasing Copy number for cycles 15 ($p = 0.0006$) and 18 ($p = 0.0002$), it decreases for cycle 24 ($p = 0.0007$). The contradictory directions for individual Cycles can explain why there was no overall significant effect above (Additional file 5C). The increasing 'success'of pre-amplification with higher Copy numbers has been described before, for example, using different copy numbers of ERCC RNA-42 standard with 14 cycles of pre-amplification [26]. However, the effect of high copy number transcripts combined with higher pre-amplification cycles (>18 cycles) has not been systematically investigated for bulk experiments before.

Finally, effect of number of Cycles on pre-amplification 'success' was tested. We show that the number of Cycles had a highly significant effect on overall likelihood of 'success' ($p < 0.001$) if tested for all Genes and Concentration together. Increasing Cycle numbers decreased the likelihood of 'success' (Additional file 6A). If both Genes and Cycles were tested independently, Cycle number had significant effect only on high copy genes EIF3M ($p = 0.001$), STK10 ($p < 0.001$) and FKBP ($p < 0.001$). Increasing Cycle

numbers drastically decreased the likelihood of 'success' (Additional file 6B). The presence of highly abundant transcripts has also effect on pre-amplification process, this effect was combined with number of Cycles. While pre-amplifiying 21 and 24 cycles, the quality of pre-amplification steeply dropped, which is shown in summary figure (Figure 1). The percentage of affected genes displayed in this figure can be found in Additional file 7. This would probably be caused by getting under optimal concentration of primers in the multiplex pre-amplification reaction. The possibility of exhausting reagents during qPCR reaction was ruled out by testing limiting dilutions of PCR product of FKBP (data not shown).

Applying the results, we can speculate why 18 s rRNA, which is often used as a reference gene using conventional qPCR would not be suitable transcript for pre-amplification as was also suggested by Stahlberg [18]. The previously published data demonstrated that the highest correlation observed for samples pre-amplified with 18 s rRNA measured with microfluidic BioMark Array and non-preamplified samples measured by conventional qPCR cycler was 0.801 [27]. The expression of 18 s rRNA is so abundant that we recommend to exclude it from pre-amplification reaction completely. 18 s rRNA would not be detected reliably because of the very high concentration of transcripts present after pre-amplification. This reason would cause the inability of any instrument to set the correct baseline. On the other hand, for the same reason, it is possible to quantify 18 s rRNA in BioMark array without pre-amplification (Additional file 8). The simple clue for identifying possible unsuitable targets for pre-amplification is their measured Cq value. The Cq value of the non-preamplified high-abundant transcript should not be lower than the number of cycles being used for its pre-amplification.

After summarizing all results together, combination of significant variables Cycle and Concentration reveals that a cycle 15 or 18 combined with a concentration of 20 ng is the best pre-amplification option using good quality samples, although any concentration higher than 1.25 ng is likely to be sufficient if the cycle is 18 or 15 (Table 1). In other words, the solution is to minimize number of Cycles and maximize Concentration of the sample. Presented model (Table 1) can also be applied for degraded samples, e.g. formalin-fixed paraffin-embedded samples. If RNA samples are degraded, less cDNA could be formed during reverse transcription, thus less target copies of cDNA can be pre-amplified. Using our outcomes (recommended combinations of concentrations and cycles), the highly expressed transcripts will never be over-preamplificated.

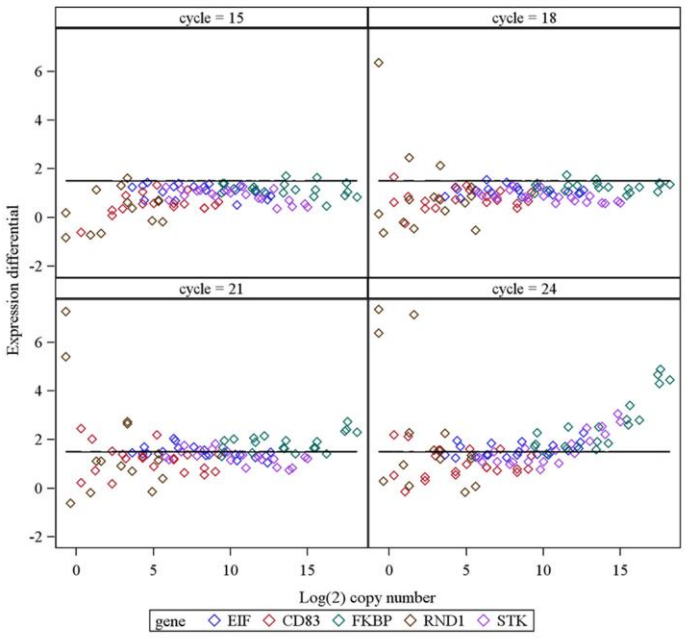

Figure 1 A plot showing the quality of pre-amplification. Successfully pre-amplified samples lie bellow the quality threshold, which corresponds to $\Delta\Delta Cq = 1.5$ (expression differential). The quality of pre-amplification gets worse with increasing number of pre-amplification cycles. During cycles 15 and 18 only small number of samples amplified with low copy gene RND1 (lowest concentrations) and high copy gene FKBP are affected. At cycles 21 and 24, the quality of pre-amplification is affected in all genes to some extent. The least affected gene is CD83, the most affected are high copy genes.

Table 1 A pivot table showing the success rate as a percentage for the possible combinations of Cycles (pre-amplification cycles) and concentrations for all five genes

Average of success	Concentration (equivalent of total RNA in ng used in pre-amplification)					
Cycles	0.078	0.32	1.25	5	20	Grand total
15	75%	90%	90%	90%	100%	89%
18	80%	80%	90%	95%	100%	89%
21	40%	30%	60%	75%	80%	57%
24	45%	50%	55%	40%	40%	46%
Grand total	60%	63%	74%	75%	80%	70%

Cycle 18 combined with a Concentration of 5 and 20 ng, and Cycle 15 combined with a concentration of 20 ng is optimal for successful BioMark experiment.

However, the right concentration and dilution of samples need to be tested for the low expressed genes.

Optimal dilution for BioMark system

The regular BioMark high-throughput gene expression experiment consists of high number of assays (up to 48 or up to 96) [1] that are amplified at the same time, resulting in the big spread of Cq values from highly expressed to lowly expressed genes. If either the concentration of the sample, the number of pre-amplification cycles or dilution after pre-amplification are not set correctly, the final result will not be optimal. Some transcripts could be under-amplified, which can result in a loss of detection sensitivity and generation of missing values. We should also avoid over-cycling of highly expressed transcripts. If the concentration of copies for a certain assay is too high in the sample, the instrument might not be able to distinguish the background of the reaction and set the baseline properly. The obtained Cq values will not be reliable.

For a successful BioMark experiment, it is desirable for the majority of the data to fall in the range about Cq = 6 to Cq = 23 [28,29]. In contrast to the regular qPCR cyclers, the optimal range of quantifiable Cq values in BioMark instrument is approximately 10 cycles lower [26]. This is caused by the fundamental difference between the size of the surface that comes into contact with the sample mix during the qPCR reaction in the Dynamic Array and in the conventional micro-titer plate. In contrast to the polypropylene surface in conventional micro-titer plates, the percentage of surface of polydimethylsiloxane nanochamber [30] that is connected with the reaction volume is much larger. It leads to a higher sensitivity of the microfluidic system, earlier detection of the fluorescence signal and thus shorter cycling time.

In order to identify the best concentration and dilution of pre-amplified samples that would be suitable for the BioMark experiment, we performed an experiment with 48.48 GE Dynamic Array using already pre-amplified samples from previous experiment with cycles 15, 18 and 21 respectively and with the concentrations 1.25 ng, 5 ng and 20 ng, respectively. The samples were diluted 20 and 40 fold, respectively to determine the best conditions for BioMark instrument. All obtained Cq data (from 21 assays excluding 3 reference genes) was normalized with GAPDH, PPIB and GUSB reference genes, which should cancel out the differences among the different concentrations and different amplification cycles but not the natural variability among donors. We set these criteria: missing data were not acceptable, the lowest Cq in Dynamic Array should be 6 and three samples should be distinguished and fall into respective groups. That is why, the two lowest concentrations (1.25 ng and 5 ng) for 15 cycle pre-amplification were removed from the analysis immediately. These criteria helped us to set up the principal component analysis that was used to reduce the dimensionality of a data set, which consisted of the 21 normalized gene assays, 3 pre-amplification cycles, 2 dilutions and 3 concentrations of 3 samples. PCA data was auto-scaled to reduce the effect of variation in the overall expression levels of the different genes. Only samples that created three separated compact groups were selected for further analysis. After removal of all samples pre-amplified 21 cycles and samples pre-amplified 18 cycles of concentration 1.25 ng, the data set was reanalyzed and the first 3 components of PCA explained 78.4% variability of auto-scaled data set. The right choice of selected samples from PCA was validated with another method, Kohonen's self-organizing feature map (SOM) that confirmed separation of samples into 3 distinct groups (Figure 2).

As a result, the highest concentration, 20 ng, for 15 cycles pre-amplification, both 20x and 40x diluted; and 5 ng and 20 ng concentrations for 18 cycles of pre-amplification, both 20x and 40x diluted fulfilled our criteria for successful and reliable pre-amplification and would give the best unbiased result with maximum detectable data for BioMark gene expression experiment.

Pre-amplification variability

In order to demonstrate how the combination of optimal conditions for success of pre-amplification would affect variability, the yield and standard deviations (SD) of pre-amplified FKBP, STK10, EIF3M, CD83, and RND1 were measured by qPCR. Pre-amplification reactions were performed in replicates of four on one cDNA that was synthetized from the same RNA pool. SD_{PRE} of combined pre-amplification and qPCR (Table 2) was calculated as weighted sum of the SDs of the qPCR (SD_{qPCR}) and SD of the pre-amplification reaction (SD_{pre}). SD_{PRE} was in the range of 0.14 – 0.24, which corresponds to variability 10% - 17% in estimated number of cDNA molecules (averaged variability for all genes is 13%). Variability increases towards the low expressed genes with higher Cq

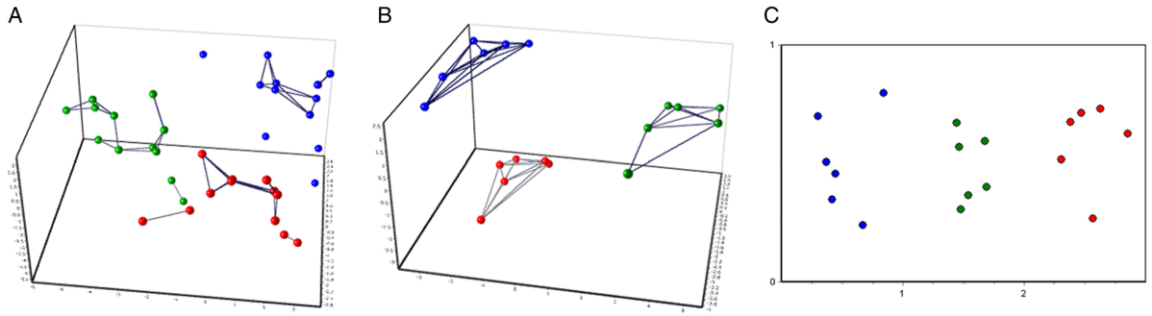

Figure 2 Identification of the best concentration and dilution of pre-amplified samples for the BioMark experiment. A. 3-D principal component analysis. PCA is based on 21 differentially expressed, auto-scaled genes, which classified pre-amplified samples into three groups according to donors (blue = donor 1, red = donor 2, green = donor 3). Samples pre-amplified 15, 18 and 21 cycles are shown, diluted both 20x and 40x. It is difficult to distinguish clearly 3 groups. **B**. Only acceptable pre-amplifications useful for BioMark GE Dynamic Array are selected: 15 cycles - 20 ng, dilution 20x and 40x, respectively; 18 cycles – 5 and 20 ng, dilution 20x and 40x, respectively. **C**. SOM with samples selected for Figure 2B, confirms 3 distinct groups.

values (Table 2), which is caused by well described statistical effects [31].

Previously, it has been described that experimental variation in the reverse transcription-qPCR (without pre-amplification) is mainly attributable to the reverse transcription step [32]. To confirm this statement also for reverse transcription–qPCR with the additional pre-amplification step, we performed the experiment where the yield and standard deviations of cDNA synthesis of the FKBP, STK10, EIF3M, CD83, and RND1 were measured by qPCR. This time reverse transcription reactions were performed in replicates of four on material from the same RNA pool as in previous pre-amplification experiment (Table 2). SD_{RT} of combined reverse transcription and qPCR (Table 2) was calculated as weighted sum of the SDs of the qPCR (SD_{qPCR}) and SD of the RT reaction (SD_{rt}). SD_{RT} was in the range of 0.24 – 0.41, which corresponds to variability 17% - 33% in estimated number of cDNA molecules (averaged variability for all genes is 23.6%). After comparison, the pre-amplification variability within the reverse transcription-qPCR experiment is significantly lower ($p = 0.015$) than variability caused by cDNA synthesis step.

Conclusion

In order to perform a valid experiment that would lead to reliable results, it is necessary to know both the capabilities and limitations of the used method and instrument. Even though BioMark instrument performs the regular qPCR reaction, we need to take some special properties into account when setting high-throughput qPCR experiment. The most distinct deviation from the regular qPCR experiment workflow is the necessity of pre-amplification.

As has been demonstrated, pre-amplification success is based on several variables, the most important ones are number of pre-amplification cycles, concentration of the sample used for pre-amplification, and the gene itself.

Table 2 Comparison of reverse transcription (RT) and pre-amplification (PRE) variability

	RND1	*CD83*	*EIF3M*	*STK10*	*FKBP*	AVG var.
Efficiency (E)	91%	100%	97%	94%	100%	
Cq RT	31.7	25.6	24.6	22.1	20.2	
$SD_{RT} = \sqrt{SD(rt)^2 + SD(qPCR)^2}$	0.38	0.41	0.24	0.40	0.29	
Variability RT = $(1 + E)^{SD_{RT}}$	28%	33%	18%	17%	22%	23.6%
Cq PRE*	23.6	17.1	16.2	13.4	12.1	
$SD_{PRE} = \sqrt{SD(pre)^2 + SD(qPCR)^2}$	0.24	0.18	0.18	0.14	0.16	
Variability PRE = $(1 + E)^{SD_{PRE}}$	17%	13%	13%	10%	12%	13%
Expression Differential	1.2	0.7	1.0	0.7	1.3	

*Equivalent of 5 ng of total RNA was used in 18 cycle pre-amplification, pre-amplified cDNA diluted 40x.

After testing possible combinations of these variables, we came to the conclusion that pre-amplification for the BioMark System using good quality samples is optimal between 15–18 pre-amplification cycles and higher concentrations of cDNA samples (5–20 ng of transcribed total RNA per pre-amplification reaction) diluted either 20x or 40x after pre-amplification. Use of higher amplification cycles (21 or 24) in bulk experiments (not in single cell experiments) is very limited because high abundant targets will cause an exhaustion of primers and reagents from pre-amplification reaction, thus they will cause lowering of pre-amplification success.

The success of the pre-amplification can be tested by our improved, easy-to-obtain, universal formula called "expression differential". The algorithm, which is presented here, evaluates the "expression differential" based on a ΔΔCq value obtained subtracting ΔCq experimental - ΔCq expected or "theoretical". Formula can be used universally, for pre-testing of the quality of pre-amplification assays in high-throughput gene expression experiment as well as in RT-qPCR experiments with FFPE-RNA.

And finally, we show that variability of the pre-amplification, introduced into the experimental workflow of reverse transcription-qPCR, is lower than variability caused by the reverse transcription step.

Methods

Sample collection and preparation

Blood was collected in BD K_2EDTA tubes (BD, cat. no. 367525), 10 ml draw volume, from healthy volunteers. After approval by Norwegian south east regional committee for medical and health research ethics (REC South East), all participants signed a written informed consent before participating in the study in accordance with the Helsinki declaration. As soon as possible after the first blood tube collection, EDTA blood from each volunteer was transferred to and PAXgene® Blood RNA Tubes (PAXgene) (PreAnalytiX) to maintain gene expression, incubated at room temperature for 2 hours, and then stored at −80°C.

Isolation of RNA, quality control and reverse transcription

RNA from blood collected in the PAXgene tubes was extracted according to the standard protocol: PAXgene Blood RNA Kit (Qiagen) and stored at −80°C.

RNA quantity and purity was measured using NanoDropTM 1000 Spectrophotometer (Thermo Scientific). $OD_{260/280}$ ratios for all samples were between 1.8 and 2.0. RNA integrity number (RIN) was checked using capillary electrophoresis performed on Agilent Bioanalyzer 2100, with RNA 6000 Nano Assay (Agilent Technologies). Sample 1 RIN = 8, sample 2 RIN = 7.3, sample 3 RIN = 7.7, sample 4 RIN = 7.6. Pooled sample 5 for variability modeling had RIN = 7.5.

cDNA synthesis was performed using High Capacity cDNA Reverse Transcription Kit (Life Technology) according to the manufacturer's protocol with random hexamers in the final volume of 50 μl containing 500 ng total RNA using a cycler C1000 (Bio-Rad). cDNA samples were stored at −20°C and diluted just before use. For dilution of samples GenElute-LPA (Sigma Aldrich) diluted in 1xTE according to the manufacturer instructions was used.

Primer and probe design

qPCR assays and a RND1 probe were designed by TATAA Biocenter, Sweden (Additional file 1). To avoid the amplification of genomic DNA all assays were placed to span and/or have one primer covering an intron/exon boundary. Criteria for the assays were: good linearity (5 log dynamic range at LC480 error < 0.2), efficiency (≥80%, ≤105%), specificity (no amplification of gDNA or at least 5 cycle's difference between target and genomic Cq-value) and clear NTCs. All assays were initially evaluated with SYBR green chemistry to test the primers. After approval of the primers a hydrolysis probe for RND1 was designed and evaluated in the same way as described for the primers. PCR products were analyzed for specificity (single product) on a pre-made 2.2% agarose gel (Flash Gel system, Lonza). All primer designs were performed with Primer BLAST [33] followed by probe design with Beacon Designer® (PREMIER Biosoft International). Primers and the probe were ordered from Eurofins. Primers were HPSF purified. Probe was labelled with FAM as reporter and BHQ1 as quencher and HPLC purified.

Real time PCR, copy number estimation, efficiency and limit of detection

10 μl qPCR reactions using SYBR green were prepared from 5 μl 2x TATAA SYBR GrandMaster Mix (TATAA Biocenter), 0.4 μl primers (final concentration 400 nM), 2.6 μl MB water, 2 μl cDNA (or pre-amplified cDNA diluted 20x). The qPCR was run in CFX384 (Bio-Rad) using the standard program 95°C for 1 min followed by 40 cycles 95°C for 3 s, 60°C for 60 s, and 72°C for 10s plus melting curve. At least triplicate qPCR reactions were performed for each qPCR experiment. Cq data were obtained by regression using Bio-Rad CFX Manager Software 3.0 (Bio-Rad).

For determination of the number of copies, PCR products were purified using QIAquick PCR Purification Kit (Oiagen) according to the manufacturer instructions, concentration was measured using Quibit® 2.0 Fluorometer (Life Technologies) and number of copies were calculated. Standard curves using PCR product of known copy numbers were generated and the copy numbers of tested samples were interpolated. The cDNA RND1 copy number for four donors was confirmed also by dPCR using a probe.

Limit of detections (LOD) was determined from standard curves with 6 replicates for each dilution, 8 dilutions 1:3 for assays: EIF3M, CD83, FKBP, RND1, STK10. (Additional file 1). Dilutions were made with carrier TE-LPA (Sigma Aldrich). The efficiency of remaining assays was determined from the standard curves generated from PCR product diluted 1:10 000 in TE-LPA with 3 replicates and 5 dilution 1:9 (Additional file 1). All standard curve experiments were run in CFX384 (Bio-Rad) with TATAA SYBR GrandMaster Mix (TATAA Biocenter).

Gene specific pre-amplification for experiments using intercalating dye

A single aliquot of each cDNA sample (diluted in carrier TE-LPA), equivalent to 20 ng RNA, 5 ng RNA, 1.25 ng RNA, 0.32 ng RNA, 0.078 ng RNA, respectively, was used for pre-amplification with TATAA PreAmp GrandMaster® mix (TATAA Biocenter) at either 15 cycles, 18 cycles, 21 cycles or 24 cycles, respectively. The total volume of pre-amplification was 10 μl for each sample. The reaction contained 5 μl of pre-amplification mastermix, 2 μl of cDNA, 1 μl of pooled primers with a final concentration of each primer of 25 nM and 2 μl of MB water. The cDNA samples were subjected to pre-amplification. The following temperature protocol was used: 95°C for 30 s, followed by 15, 18, 21, 24 cycles, respectively at 95°C for 15 s and 60°C for 4 min. 24 assays were pre-amplified as multiplex and only 5 selected assays (see above) were tested in the experiment. A list of 24 assays used for pre-amplification is described in Additional file 1. As a control, water (NTC) was included in the pre-amplification reaction. The pre-amplified cDNA was immediately used or placed in freezer at −20°C. The pre-amplified cDNA was diluted prior to use at either 20x or 40x with MB water.

High-throughput real time PCR with Eva green

qPCR was performed using the high-throughput platform BioMark™ HD System and the 48.48 GE Dynamic Arrays (Fluidigm) in duplicates in assays. 5 μL of Fluidigm sample premix consisted of 1 μL of either 20x or 40x diluted pre-amplified cDNA, 0.25 μL of 20x SG loading reagent (Fluidigm), 2.5 μL of Sso Fast Eva green mastermix (Bio-Rad), 0.1 μL of 4x diluted ROX (Invitrogen) and 1.15 μL of RNase/DNase-free water. Each 5 μL assay premix consisted of 2 μL of 10 μM primers (final concentration 400 nM primers), 2.5 μL 2x Assay loading reagent (Fluidigm) and 0.5 μL of RNase/DNase-free water. The samples and assays were mixed inside the chip using Nanoflex IFC controller (Fluidigm). Thermal conditions for qPCR were: 98°C for 40 s, 35 cycles of 95°C for 10 s, and 60°C for 40 s plus melting curve analysis. Data was processed by automatic threshold for each assay, with derivative baseline correction using BioMark Real-Time PCR Analysis Software 3.1.2 (Fluidigm). The quality threshold was set at the default setting of 0.65.

qPCR data pre-processing and statistical analysis

The Cq data obtained from conventional qPCR cycler CFX384 was analyzed using IBM SPSS Statistics (Version 21) and an Excel (Version 14.3.4) pivot table. Tested variables were: Cycles (number of pre-amplification cycles), Log_copy ($\log_2$ copy number of cDNA used for pre-amplification), Log_concentn ($\log_2$ concentration of cDNA, presented as total RNA equivalent, used for pre-amplification), Donor, GeneNo (gene number = different transcripts). Copy number was analyzed as both a categorical and continuous variable. As the distribution of Copy number and Concentration were not normally distributed these were also log transformed (base 2). Each experiment was classified as a'success' or'failure'. An experiment was classified as a'success' if the'expression differential' was less than ± 1.5 (Additional file 2). An experiment was classified as a'failure' if the'expression differential' was greater than 1.5 or missing.'Expression differential' consisted of the'theoretical expression' minus the'experimental expression' (detailed description in results).

Measures of experiment behavior and outcome were compared against the likelihood of success to detect any statistical relationships. Univariate categorical measures were compared against experimental 'success' under specified conditions using the Chi-squared test (expected values were so high that the Fisher's Exact test was not used). Univariate continuous measures were compared against experimental 'success' using Box plots and group summary tables. A full variable logistic regression model was pared back to an optimal model using the backward stepwise method by eliminating non-significant terms. A classification (or confusion) table was produced and the sensitivity and specificity calculated. A pivot table was produced showing the success rate as a percentage for the possible combinations of Cycles and Concentrations.

All BioMark data were pre-processed in the software GenEx Enterprise 5.4.0.520 (MultiD Analyses AB). PPIB, GAPDH and GUSB were selected for normalization using Normfinder software. Principal component analysis (PCA) [34] and Kohonen self-organizing maps (SOM) [35] was performed using 21 original independent variables (21 normalized genes). PCA and SOM were performed with data that were normalized, the lowest expression was recalculated to 1, log2 transformed and auto-scaled using GenEx Enterprise software. All expression values were auto-scaled in order to remove the influence of both the expression level and the magnitudes of the changes and gave rise to classification based on the relative changes in expression. The SOM of size 3 x 1 dividing the samples into 3 groups was trained using GenEx with the following parameters: 0.1 learning rate, 3 neighbors and 5,000

iterations. The SOM analysis was repeated five times with identical classification.

Difference between variability of reverse transcription step and pre-amplification step was tested by paired, two tailed *t* test using GenEx Enterprise 5.4.0.520 (MultiD Analyses AB).

Additional files

Additional file 1: The Excel sheet with information on 24 assays used for pre-amplification. Five assays highlighted in gray were used for experiment 3.1. Additional information are added for these assays: LOD, LOQ.

Additional file 2: Table of all samples and their Cq and calculated characteristics as Concentration, Copy numbers, Cycle, Success and the example of the pre-amplification algorithm (expression differential) application.

Additional file 3: Construction and results of explanatory binomial candidate model explaining which combination of factors will influence the 'success'.

Additional file 4: Tables showing how Concentration of RNA (an equivalent of mRNA transferred into pre-amplification reaction) influences 'success'. A. Tested for all Genes and all Cycles together. B. Tested for each Gene independently and all Cycles together.

Additional file 5: Figures showing how Copy number (copy number of cDNA used for pre-amplification) influences 'success'. A. Tested for all Genes and all Cycles together. B. Tested for each Gene independently and all Cycles together. C. Tested for all Genes and each Cycle independently.

Additional file 6: Tables showing how number of Cycles (number of pre-amplification cycles) influences 'success'. A. Tested for all Genes and Concentrations together. B. Tested for each Gene independently.

Additional file 7: A pivot table showing the success rate as a percentage for the possible combinations of Cycles and Concentrations for individual genes. The additional information for Figure 1.

Additional file 8: A standard curve of non-preamplified sample detected by 18S rRNA used in GE Dynamic Array 48.48.

Abbreviations

Cq: Cycle of quantification; EDTA: Ethylenediaminetetraacetic acid; gDNA: Genomic DNA; GeneNo: Gene number = different transcript; IFC: Integrated fluidic circuit; LOD: Limit of detection; Log_concentn: Log_2 concentration of cDNA, presented as total RNA equivalent, used for pre-amplification; Log_copy: Log_2 copy number of cDNA used for pre-amplification; LOQ: Limit of quantification; MB water: Molecular biology grade water; NTC: No template control; PCA: Principal component analysis; qPCR: Quantitative polymerase chain reaction; RIN: RNA integrity number; RT-: Negative control in reverse transcription, without reverse transcriptase; SOM: Kohonen self-organising map; SD: Standard deviation; STA: Specific target amplification; TE-LPA: Linear polyacrylamide carrier in TE buffer.

Competing interests

All authors have read and understood BMC Molecular Biology policy on declaration of interests and declare that we have no competing interests, only Robert Sjöback is employed by TATAA Biocenter, which is a producer of TATAA PreAmp GrandMaster Mix and TATAA SYBR GrandMaster Mix.

Authors' contributions

VK wrote the manuscript, elaborated design of the study and evaluated results. JS provided main part of statistical analysis. VN participated in statistical analysis. MJ carried out the pre-amplification experiments. LL carried out the BioMark experiments. DS and MS designed and validated primers and a probe. RS participated in coordination of the study and helped to draft the manuscript. All authors read and approved the final manuscript.

Acknowledgements

The authors are thankful to volunteers who participated in the study and DiaGenic ASA that provided us with the isolated samples and cooperated with us within the scope of SPIDIA project. We thank Prof. Mikael Kubista for valuable comments. This project was funded by BIOCEV CZ.1.05/1.1.00/02.0109 from ERDF, Go8 Fellowship Australia, CZ: GACR: P304/12/1585, CZ: GACR:GA15-08239S and CZ: GACR: P303/13/02154S.

Author details

[1]Laboratory of Gene Expression, Institute of Biotechnology, Academy of Sciences of the Czech Republic, Prague, Czech Republic. [2]QFAB Bioinformatics, University of Queensland - St Lucia QLD, Brisbane, Australia. [3]TATAA Biocenter, Göthenburg, Sweden.

Received: 25 July 2014 Accepted: 12 February 2015
Published online: 11 March 2015

References

1. Spurgeon SL, Jones RC, Ramakrishnan R. High throughput gene expression measurement with real time PCR in a microfluidic dynamic array. PLoS One. 2008;3:e1662.
2. BioMark™ HD System. [http://www.fluidigm.com/biomark-hd-system.html]
3. Real-Time PCR Using OpenArray® Technology. [http://www.lifetechnologies.com/au/en/home/life-science/pcr/real-time-pcr/real-time-openarray.html?icid=fr-openarray-main%20http://www.lifetechnologies.com/au/en/home/life-science/pcr/real-time-pcr/real-time-openarray.html?icid=fr-openarray-main]
4. SmartChip Real-Time PCR System. [http://www.wafergen.com/products/smartchip-realtime-pcr-system]
5. Mengual L, Burset M, Marin-Aguilera M, Ribal MJ, Alcaraz A. Multiplex preamplification of specific cDNA targets prior to gene expression analysis by TaqMan Arrays. BMC Res notes. 2008;1:21.
6. Blow N. PCR's next frontier. Nat Meth. 2007;4:869–75.
7. Iscove NN, Barbara M, Gu M, Gibson M, Modi C, Winegarden N. Representation is faithfully preserved in global cDNA amplified exponentially from sub-picogram quantities of mRNA. Nat Biotechnol. 2002;20:940–3.
8. Noutsias M, Rohde M, Block A, Klippert K, Lettau O, Blunert K, et al. Preamplification techniques for real-time RT-PCR analyses of endomyocardial biopsies. BMC Mol Biol. 2008;9:3.
9. Sindelka R, Sidova M, Svec D, Kubista M. Spatial expression profiles in the Xenopus laevis oocytes measured with qPCR tomography. Methods (San Diego, Calif). 2010;51:87–91.
10. Fluidigm. Real-Time PCR Analysis, Appendix B: Fast Gene Expression Analysis Using EvaGreen on the BioMark of BioMark HD System, part No. 68000088. [https://www.fluidigm.com/documents]
11. TaqMan PreAmp Master Mix Kit, Protocol. [http://tools.lifetechnologies.com/content/sfs/manuals/cms_039316.pdf]
12. Targeted Enrichment of Limited RNA Samples via Pre-Amplification Prior to Analysis in the WaferGen SmartChip Real-Time PCR System. [http://www.wafergen.com/wp-content/uploads/2013/01/TargetEnrchmnt_RNA_TNf.pdf]
13. OpenArray Plates for microRNA expression analysis. [http://tools.lifetechnologies.com/content/sfs/manuals/cms_092509.pdf]
14. Johnson G, Nour AA, Nolan T, Huggett J, Bustin S. Minimum information necessary for quantitative real-time PCR experiments. Methods Mol Biol (Clifton, NJ). 2014;1160:5–17.
15. Bustin SA, Benes V, Garson JA, Hellemans J, Huggett J, Kubista M, et al. The MIQE guidelines: minimum information for publication of quantitative real-time PCR experiments. Clin Chem. 2009;55:611–22.
16. Rusnakova V, Honsa P, Dzamba D, Stahlberg A, Kubista M, Anderova M. Heterogeneity of astrocytes: from development to injury - single cell gene expression. PLoS One. 2013;8:e69734.
17. Laurell H, Iacovoni JS, Abot A, Svec D, Maoret JJ, Arnal JF, et al. Correction of RT-qPCR data for genomic DNA-derived signals with ValidPrime. Nucleic Acids Res. 2012;40:e51.
18. Stahlberg A, Kubista M. The workflow of single-cell expression profiling using quantitative real-time PCR. Expert Rev Mol Diagn. 2014;14:323–31.
19. Fluidigm. Fluidigm Gene Expression Specific Target Amplification Quick Reference, part No. 68000133. [https://www.fluidigm.com/documents]

20. Fluidigm. BioMark Advanced Development Protocol Number 5: Single-Cell Gene Expression Protocol for the BioMark 48.48 Dynamic Array–Real-Time PCR, part No. 68000107. [https://www.fluidigm.com/documents]
21. Stahlberg A, Bengtsson M. Single-cell gene expression profiling using reverse transcription quantitative real-time PCR. Methods (San Diego, Calif). 2010;50:282–8.
22. Chen Y, Gelfond JA, McManus LM, Shireman PK. Reproducibility of quantitative RT-PCR array in miRNA expression profiling and comparison with microarray analysis. BMC Genomics. 2009;10:407.
23. Li J, Smyth P, Cahill S, Denning K, Flavin R, Aherne S, et al. Improved RNA quality and TaqMan Pre-amplification method (PreAmp) to enhance expression analysis from formalin fixed paraffin embedded (FFPE) materials. BMC Biotechnol. 2008;8:10.
24. Fox BC, Devonshire AS, Baradez MO, Marshall D, Foy CA. Comparison of reverse transcription-quantitative polymerase chain reaction methods and platforms for single cell gene expression analysis. Anal Biochem. 2012;427:178–86.
25. Bengtsson M, Hemberg M, Rorsman P, Stahlberg A. Quantification of mRNA in single cells and modelling of RT-qPCR induced noise. BMC Mol Biol. 2008;9:63.
26. Devonshire AS, Elaswarapu R, Foy CA. Applicability of RNA standards for evaluating RT-qPCR assays and platforms. BMC Genomics. 2011;12:118.
27. Jang JS, Kolbert C, Jen J. High throughput quantitative PCR using low-input samples for mRNA and MicroRNA gene expression analyses [abstract]. J Biomol Tech. 2013;24:S56.
28. Svec D, Rusnakova V, Korenkova V, Kubista M. Dye-Based High-Throughput qPCR in Microfluidic Platform BioMark™. In: Nolan T, Bustin SA, editors. PCR Technology: Current Innovations. 3rd ed. Boca Raton: CRC Press; 2013. p. 323–36.
29. Sorg D, Danowski K, Korenkova V, Rusnakova V, Kuffner R, Zimmer R, et al. Microfluidic high-throughput RT-qPCR measurements of the immune response of primary bovine mammary epithelial cells cultured from milk to mastitis pathogens. Animal. 2013;7:799–805.
30. Perkel JM. Microfluidics, macro-impacts. Biotechniques. 2012;52:131–4.
31. Morrison TB, Weis JJ, Wittwer CT. Quantification of low-copy transcripts by continuous SYBR Green I monitoring during amplification. Biotechniques. 1998;24:954–8. 960, 962.
32. Stahlberg A, Hakansson J, Xian X, Semb H, Kubista M. Properties of the reverse transcription reaction in mRNA quantification. Clin Chem. 2004;50:509–15.
33. Primer-BLAST. [http://www.ncbi.nlm.nih.gov/tools/primer-blast/index.cgi?LINK_LOC=BlastHome]
34. Jolliffe IT. Principal Component Analysis. 2nd ed. Springer-Verlag New York: Springer; 2002.
35. Kohonen Teuvo. Self-Organizing Maps. 3rd ed. Springer-Verlag Berlin Heidelberg: Springer; 2001.

Example for calculation of Success

Source data

number	gene	donor	Cp non-preamp	Cq preamp	dCq experimental	copy	log2 copy	cycle	concentrat	teor_diff	exp_diff	success
1	*RND1 S*	1	34.2	33.7	0.54	0.2	-2.4	15	0.08	1.36	0.82	1

Experimental difference of pre-amplification: ΔCqexperimental = Cqnon-preamp – Cqpreamp = **0.5**

Theoretical difference of pre-amplification was calculated as: ΔCqtheoretical = number of pre-amplification cycles – log2(all dilutions during the processing of the sample

Dilutions during our experiment:
non-preamplified sample: for amplification diluted after RT diluted 4x (2.5 ng RNA eqvivalent/ul), in qPCR 2 ul cDNA in 10 ul of total volume = 5x dilution. Together 20x dilutior
pre-amplified sample: for pre-amplification sample diluted 256x (0.39 ng RNA equivalent/ul),in pre-amp reaction 2 ul of cDNA in 10 ul reaction were used= 5x dilution
after pre-amplification reaction diluted 40x, in qPCR 2 ul cDNA in 10 ul of total volume = 5x dilution. Together 256000x dilutior
TOTAL dilution for the experiment: 256000/20=**12800x**
All theoretical differences calculated for our experiment

Theoretical difference	15 cycles	18 cycles	21 cycles	24 cycles	
0.078 ng RNA	**1.36**	4.36	7.36	10.36	dilution of sample causes shift of 8 cycles
0.32 ng RNA	3.36	6.36	9.36	12.36	dilution of sample causes shift of 6 cycles
1.25 ng RNA	5.36	8.36	11.36	14.36	dilution of sample causes shift of 4 cycles
5 ng RNA	7.36	10.36	13.36	16.36	dilution of sample causes shift of 2 cycles
20 ng RNA	9.36	12.36	15.36	18.36	no shift

Theoretical difference: Example 15 cycles for 0.078 ng RNA
15 cycles - 5.64 cycle (50x dilution in reaction)- 8 cycles (20 ng diluted 256x) = **1.36**
or 15 cycles -log2(12800)= 15 - 13.64 = **1.36**

Expression differential ΔΔCq = ΔCqtheoretical - Δcqexperimental
ΔΔCq = 1.36 - 0.54 = **0.82**

An experiment was classified as a Success because the Expression differential was less than ± 1.5

Additional File 3

WHAT COMBINATION OF FACTORS WILL INFLUENCE SUCCESS?

An *explanatory* (using all possible terms) binomial candidate model was constructed:

Success ~ geneNo + donor + cycle + log_concentration + log_copy

An optimal model was then derived in SPSS using the backward stepwise method to eliminate 'non-significant' terms. Deriving an optimal model:

Success ~ geneNo + cycle + log_concentration

As donor and log_copy were eliminated, this is also a *predictive* model (all terms are known beforehand and controllable).

Variables	B	S.E.	Wald	df	Sig.	Exp(B)	95% C.I.for EXP(B)	
geneNo			37.893	4	0.000			
geneNo(1)	0.358	0.38	0.891	1	0.345	1.431	0.68	3.012
geneNo(2)	2.111	0.441	22.953	1	0.000	8.257	3.481	19.584
geneNo(3)	1.708	0.418	16.704	1	0.000	5.518	2.432	12.516
geneNo(4)	1.803	0.423	18.197	1	0.000	6.067	2.65	13.892
cycle			64.653	3	0.000			
cycle(15)	2.672	0.42	40.513	1	0.000	14.464	6.353	32.929
cycle(18)	2.672	0.42	40.513	1	0.000	14.464	6.353	32.929
cycle(21)	0.543	0.316	2.942	1	0.086	1.721	0.925	3.199
log_concn	0.259	0.069	13.948	1	0.000	1.296	1.131	1.485
Constant	-1.468	0.352	17.397	1	0.000	0.23		

a Variable(s) entered on step 1: geneNo, donor, log_copy, cycle, log_concn.

Classification Table(a)

		Predicted		
		Success		Percentage Correct
Observed		Failure	Success	
Success	Failure	62	57	52.1
	Success	30	251	89.3
Overall Percentage		0.67	0.81	78.3

a The cut value is .500

The model has a sensitivity of 81% and a specificity of 67%.

Additional File 4

WILL CONCENTRATION OF RNA INFLUENCE SUCCESS?

A. For all genes and all cycles together

Concentration had a significant effect on the overall likelihood of success. Concentration was tested as a category (p=0.023), a variable (p=0.012), and a log transformed variable (p=0.001). In all cases was it significant for success. The categorical test results are displayed. The likelihood of success increases with the concentration.

concentration * Success Crosstabulation

			Success		Total
			Failure	Success	
concentn	.078	Count	32	48	80
		% within concentration	40.0%	60.0%	100.0%
	.320	Count	30	50	80
		% within concentration	37.5%	62.5%	100.0%
	1.250	Count	21	59	80
		% within concentration	26.3%	73.8%	100.0%
	5.000	Count	20	60	80
		% within concentration	25.0%	75.0%	100.0%
	20.000	Count	16	64	80
		% within concentration	20.0%	80.0%	100.0%
Total		Count	119	281	400
		% within concentration	29.8%	70.3%	100.0%

B. For each gene independently and all cycles together

Concentration had a significant effect on genes *RND1* ($p < 0.001$) and *CD83* ($p = 0.001$). Here increasing concentrations increased the likelihood of success. Gene *CD83* was still significant using the more conservative Fisher's Exact test.

concentration * Success * Gene Number Crosstabulation

Gene Number				Success	
				Failure	Success
RND1	concentration	.078	Count	12	4
			% within concentration	75.0%	25.0%
		.320	Count	10	6
			% within concentration	62.5%	37.5%
		1.250	Count	5	11
			% within concentration	31.3%	68.8%
		5.000	Count	7	9
			% within concentration	43.8%	56.3%
		20.000	Count	0	16
			% within concentration	0.0%	100.0%
	Total		Count	34	46
			% within concentration	42.5%	57.5%
CD83	concentration	.078	Count	8	8
			% within concentration	50.0%	50.0%
		.320	Count	2	14
			% within concentration	12.5%	87.5%
		1.250	Count	2	14
			% within concentration	12.5%	87.5%
		5.000	Count	1	15
			% within concentration	6.3%	93.8%
		20.000	Count	0	16
			% within concentration	0.0%	100.0%
	Total		Count	13	67
			% within concentration	16.3%	83.8%

Additional File 5

WILL COPY NUMBER INFLUENCE SUCCESS?

A. For all genes and all cycles together

Copy number (log of copy number) did not have a significant effect on the overall likelihood of success (p = 0.3218).

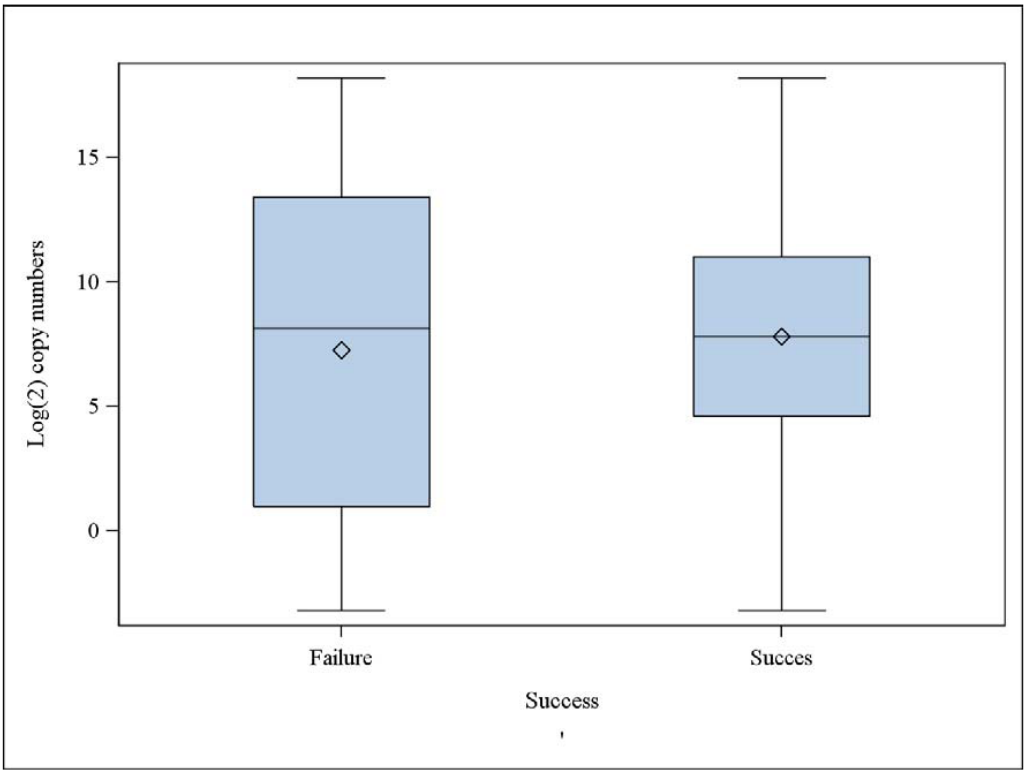

B. For each gene independently and all cycles together

Copy number only had a significant effect on genes *RND1* (p = 0.0001) and *CD83* (p = 0.0004). Here increased copy number increased the likelihood of success.

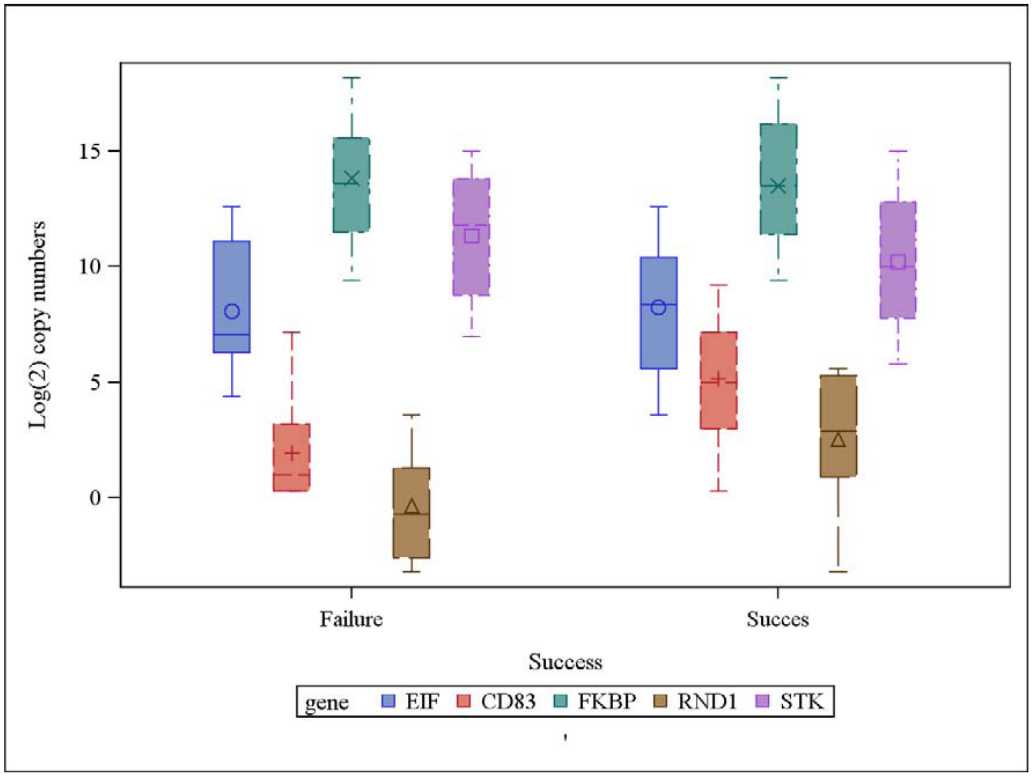

C. For all genes and each cycle independently

Copy number (log copy number) was significant for cycles 15 (p = 0.0006), 18 (p = 0.0002), and 24 (p = 0.0007). Whereas the likelihood of success increases with increasing copy number for cycles 15 and 18, it decreases for cycle 24. The contradictory directions for individual cycles means there is no overall significant effect above. Rings are outliers.

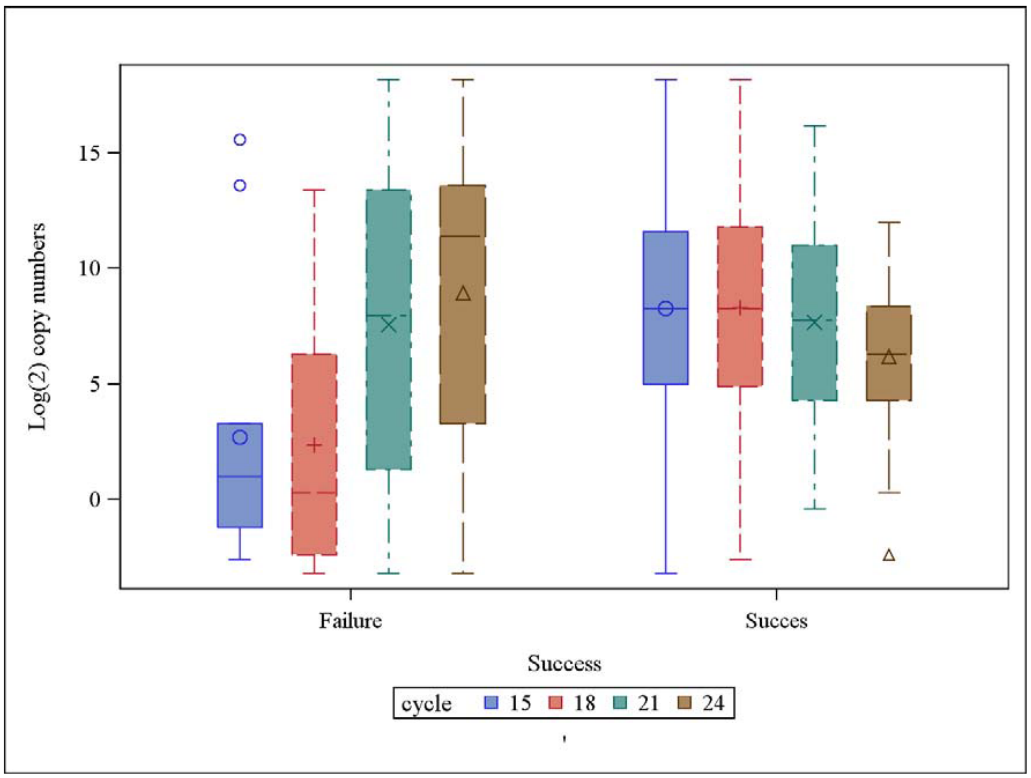

Additional File 6

WILL NUMBER OF CYCLES INFLUENCE SUCCESS?

A. *For all genes and concentrations together*

The number of cycles had a highly significant effect on the overall likelihood of success ($p < 0.001$). Increasing cycle numbers decreased the likelihood of success.

cycle * Success Crosstabulation

			Success		Total
			Failure	Success	
cycle	15	Count	11	89	100
		% within cycle	11.0%	89.0%	100.0%
	18	Count	11	89	100
		% within cycle	11.0%	89.0%	100.0%
	21	Count	43	57	100
		% within cycle	43.0%	57.0%	100.0%
	24	Count	54	46	100
		% within cycle	54.0%	46.0%	100.0%
Total		Count	119	281	400
		% within cycle	29.8%	70.3%	100.0%

B. *For each genes independently.*

Cycle number had a significant effect on genes *EIF3M* ($p = 0.001$), *STK10* ($p < 0.001$), and *FKBP* ($p < 0.001$). Increasing cycle numbers drastically decreased the likelihood of success (as above).

cycle * Success * Gene Number Crosstabulation

Gene Number				Success		Total
				Failure	Success	
EIF3M	cycle	15	Count	0	20	20
			% within cycle	0.0%	100.0%	100.0%
		18	Count	1	19	20
			% within cycle	5.0%	95.0%	100.0%
		21	Count	7	13	20
			% within cycle	35.0%	65.0%	100.0%
		24	Count	9	11	20
			% within cycle	45.0%	55.0%	100.0%
	Total		Count	17	63	80
			% within cycle	21.3%	78.8%	100.0%
STK10	cycle	15	Count	0	20	20
			% within cycle	0.0%	100.0%	100.0%
		18	Count	0	20	20
			% within cycle	0.0%	100.0%	100.0%
		21	Count	6	14	20
			% within cycle	30.0%	70.0%	100.0%
		24	Count	10	10	20
			% within cycle	50.0%	50.0%	100.0%
	Total		Count	16	64	80
			% within cycle	20.0%	80.0%	100.0%
FKBP	cycle	15	Count	2	18	20
			% within cycle	10.0%	90.0%	100.0%
		18	Count	2	18	20
			% within cycle	10.0%	90.0%	100.0%
		21	Count	16	4	20
			% within cycle	80.0%	20.0%	100.0%
		24	Count	19	1	20
			% within cycle	95.0%	5.0%	100.0%
	Total		Count	39	41	80
			% within cycle	48.8%	51.3%	100.0%

Additional File 7

DETAILED TABLE FOR FIGURE 1

A pivot table showing the success rate as a percentage for the possible combinations of Cycles and Concentrations for individual genes. The additional information for Figure 1.

Proportion of success	Concentration					
Cycle	0.078	0.32	1.25	5	20	Grand Total
RND1 S						
15	0.50	0.50	0.75	0.75	1.00	0.70
18	0.25	0.50	0.75	0.75	1.00	0.65
21	0.00	0.25	0.75	0.50	1.00	0.50
24	0.25	0.25	0.50	0.25	1.00	0.45
CD83 S						
15	0.25	1.00	1.00	1.00	1.00	0.85
18	0.75	1.00	1.00	1.00	1.00	0.95
21	0.50	0.75	0.75	1.00	1.00	0.80
24	0.50	0.75	0.75	0.75	1.00	0.75
EIF3M S						
15	1.00	1.00	1.00	1.00	1.00	1.00
18	1.00	0.75	1.00	1.00	1.00	0.95
21	0.75	0.00	0.50	1.00	1.00	0.65
24	0.50	0.75	0.75	0.75	0.00	0.55
STK10 S						
15	1.00	1.00	1.00	1.00	1.00	1.00
18	1.00	1.00	1.00	1.00	1.00	1.00
21	0.50	0.25	0.75	1.00	1.00	0.70
24	0.75	0.75	0.75	0.25	0.00	0.50
FKBP S						
15	1.00	1.00	0.75	0.75	1.00	0.90
18	1.00	0.75	0.75	1.00	1.00	0.90
21	0.25	0.25	0.25	0.25	0.00	0.20
24	0.25	0.00	0.00	0.00	0.00	0.05
Grand Total	0.60	0.63	0.74	0.75	0.80	0.70

Serial dilution (1:7) of unpreamplified blood sample, tested with *18s rRNA* in GE Dynamic Array 48.48 (Fluidigm).

	18s rRNA	#dilution
1x	14.36912	4096
8X	16.74177	512
64X	18.98181	64
512X	24.52693	8
4096X	26.7615	1
1x	14.48254	4096
8X	17.01745	512
64X	19.62085	64
512X	22.04723	8
4096X	25.9467	1
1x	13.8641	4096
8X	16.80505	512
64X	20.05284	64
512X	21.7296	8
4096X	26.41708	1

No. of samples:	15				
Slope:	-3.66867	<	-3.34254	<	-3.01642
Intercept:	28.03668	<	29.01349	<	29.99031
Efficiency:	0.85762	<	0.99147	<	1.12532
Residual variance:	0.55757				
SE(intercept):	0.45215				
SE(slope):	0.15096				
SE(Efficiency):	0.06196				
Confidence:	95%				
Critical t-value:	2.16037				
r2:	0.97417				

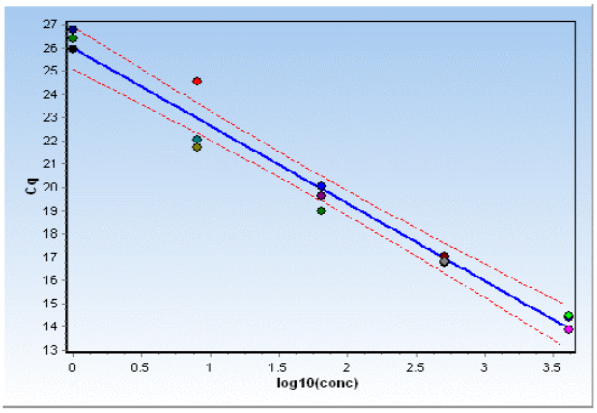

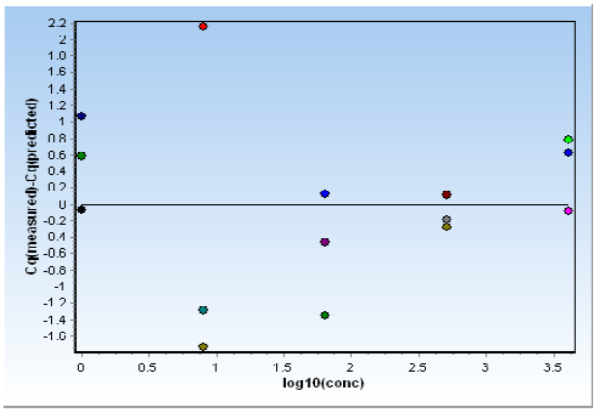

5. Diskuze

Počáteční determinace a diferenciace buněk v časném embryonálním vývoji *X. laevis* závisí na lokalizaci a distribuci maternálních faktorů. Z tohoto důvodu byl tento výzkum zaměřen zejména na lokalizaci maternální mRNA uvnitř zralého oocytu. Obecně se předpokládá, že převážná část maternální mRNA je rovnoměrně distribuována podél animálně-vegetativní osy oocytu a pouze její menší část vykazuje lokalizaci buď v animální nebo vegetativní hemisféře (Mowry and Cote, 1999; King *et al.*, 2005). Nicméně na základě našich výsledků nebyl objeven ani jeden maternální transkript, který by byl rovnoměrně distribuován. Sindelka *et al.* (2008) zavedl metodu qPCR tomografie, která umožňuje stanovit lokalizaci transkriptů uvnitř biologického vzorku. V rámci experimentů byl oocyt *X. laevis* rozdělen na 5 částí podél animálně-vegetativní osy pro určení lokalizace 15 maternálních mRNA. Součástí předkládané disertační práce jsou výsledky pokusů, u kterých byl zvýšen počet řezů z původních 5 na 15 a zároveň byl i zdvojnásoben počet kvantifikovaných genů. Cílem vyššího rozlišení bylo podrobnější popsání lokalizačních gradientů maternální mRNA a možnost identifikovat případné další lokalizační profily podél animálně-vegetativní osy zralého oocytu *X. laevis*. Analýza dat potvrdila rozdělení maternálních transkriptů do dvou hlavních skupin v závislosti na lokalizačním profilu. První a zároveň i početnější skupina transkriptů se vyskytuje v animální hemisféře. Maximum gradientu spočívá zhruba ve třetině oocytu (3. – 6. vzorek), což pravděpodobně souvisí s umístěním jádra uvnitř oocytu a pasivním transportem těchto transkriptů z místa jejich syntézy. Animální skupina maternální mRNA překvapivě zahrnuje i referenční transkripty, které se běžně používají k normalizaci genové exprese u žab rodu *Xenopus*. Tento fakt dokazuje, že ve studiích na vnitrobuněčné úrovni není vhodné používat k normalizaci referenční geny, ale spíše aplikovat normalizaci na celou buňku. Druhá skupina maternálních mRNA vykazuje lokalizaci ve vegetativní hemisféře. Vysoké rozlišení řezů oocytem umožnilo rozlišit dvě podskupiny těchto transkriptů, které se liší profilem vegetativního gradientu. Determinanty zárodečné plazmy vykazují strmý gradient, což svědčí o jejich spojení s kortexem. Ostatní vegetativně lokalizované mRNA se vyznačují pozvolným profilem směrem k vegetativnímu pólu. Tento výsledek dvou

vegetativních lokalizačních profilů zároveň souvisí s odlišným typem transportních drah, které lokalizují maternální transkripty do vegetativní hemisféry oocytu *X. laevis*.

Následující krok v průběhu výzkumu potvrdil přenos animálně-vegetativní asymetrie maternální mRNA z oocytu do dceřiných buněk v průběhu časného rýhování. Počínaje třetím buněčným dělením (vývojové stádium 8 buněk) lze na embryích pozorovat oddělení animálních blastomer od vegetativních. Z tohoto důvodu byla ke stanovení lokalizace maternálních transkriptů v jednotlivých blastomerách použita embrya ve vývojovém stádiu 8 buněk, 16 buněk a 32 buněk. Výsledek RT-qPCR analýzy dokázal, že animální blastomery obsahují jiné maternální transkripty než vegetativní blastomery.

Dalším cílem bylo nalezení molekulárních gradientů maternální mRNA s důrazem na určení dorzo-ventrální a pravo-levé tělní osy u embryí ve vývojovém stádiu 8 buněk, 16 buněk a 32 buněk. Vymezení ventrální části embrya nastává již v okamžiku průniku spermie do oocytu a následně, v průběhu procesu kortikální rotace, dochází k nahromadění dorzálních determinantů v budoucí dorzální oblasti embrya. I přestože byly v naší studii měřeny všechny známé transkripty genů z Wnt signální dráhy a jiných signálních drah specifikující dorzo-ventrální asymetrii (*dvl2, dvl3, lrp6, wnt11, tcf3, gsk3b, ctnnb1, foxh1, trim36* a *axin1*), žádný nevykazoval nerovnoměrnou distribuci podél této osy. Z tohoto vyplývá, že ačkoliv animálně-vegetativní asymetrie vzniká důsledkem nerovnoměrné distribuce maternální mRNA, vytvoření dorzo-ventrální tělní osy bude výsledek asymetrické distribuce a/nebo lokalizace jiných biomolekul, pravděpodobně proteinů. Nerovnoměrná distribuce maternálních mRNA nebyla pozorována ani ve směru pravo-levé tělní osy. Rozdělení embrya na pravou a levou část je definováno první embryonální rýhou, ale projev této osy nastupuje až po gastrulaci. Z molekulárního hlediska byl popsán gen *vg1* (*gdf1)*, který se podílí na specifikaci pravo-levé asymetrie v průběhu časného embryonálního vývoje *X. laevis* (Hyatt *et al.*, 1996). Nicméně naše výsledky neprokazují asymetrickou distribuci *vg1* transkriptu podél této osy až do vývojového stádia 32 buněk. Model iontového toku dokonce vymezuje pravo-levou tělní osu již v embryu

ve stádiu 2-4 buněk, kde se předpokládá nerovnoměrná lokalizace ATPázových pump v jednotlivých blastomerách (Blum *et al.,* 2014). Gen *atp4* představuje nezbytnou podjednotku H+/K+-ATPázové pumpy. Naše výsledky měření jeho distribuce v jednotlivých blastomerách od vývojového stádia 8 buněk až po stádium 32 buněk neprokázaly asymetrickou lokalizaci transkriptu *atp4* podél pravo-levé tělní osy (tato data nejsou zahrnuta v publikaci 4.2.). Z tohoto vyplývá, že ani pravo-levá tělní osa není určena asymetrickou distribucí maternální mRNA v průběhu časného rýhování. Za specifikaci pravo-levé tělní osy mohou být opět zodpovědné jiné biomolekuly a nebo projev této asymetrie může nastupovat až v pozdějších vývojových stádiích *X. laevis*.

Předcházející publikace vedla k závěru, že určení tělních os a tělního plánu v časném embryonálním vývoji *X. laevis* nelze vyvodit pouze na základě lokalizace maternálních transkriptů, ale je nutné znát i přesnou lokalizaci proteinů. Tento bod však zahrnuje i časo-prostorovou regulaci translace maternální mRNA. Názorný příklad představuje porovnání načasování translace *gdf1* a *vegt*. I když tyto transkripty sdílejí stejnou transportní dráhu do vegetativní hemisféry, liší se v translační aktivitě. V průběhu celé oogeneze dochází k translaci proteinu Gdf1, ale přepis *vegt* transkriptu je inhibován. Protein Vegt lze pomocí protilátek detekovat až ve zralém oocytu a jeho výskyt přetrvává až do gastrulace (Stennard *et al.,* 1999). Regulace translace maternální mRNA očividně zaujímá významnou roli v determinaci a diferenciaci buněk v průběhu časné embryogeneze. Z tohoto důvodu bylo dalším cílem stanovit lokalizační profily miRNA uvnitř zralého oocytu *X. laevis*. Ukázali jsme, že miRNA je asymetricky distribuovaná podél animálně-vegetativní osy oocytu a její lokalizační profily odpovídají dvěma ze tří lokalizačních profilů, které byly identifikovány pro maternální mRNA. Animální gradient miRNA a mRNA pravděpodobně vzniká pasivní difúzí těchto molekul z buněčného jádra, které je lokalizováno v animální hemisféře oocytu. Na druhé straně vytvoření vegetativního gradientu je způsobeno aktivním transportem, který vyžaduje konzervovanou lokalizační sekvenci. Nicméně celá nebo převážná část miRNA sekvence je nutná k interakci s cílovou mRNA, a proto tato sekvence pravděpodobně nemůže obsahovat úsek, který by umožnil další vazbu s buněčnými komponenty. Z tohoto důvodu

usuzujeme, že miRNA mohou být aktivně transportovány do vegetativní hemisféry prostřednictvím mRNA molekul, anebo k transportu dochází ještě ve formě pre-miRNA, která disponuje 70 nukleotidovou sekvencí.

Tato studie představuje výsledky, které poprvé dokazují asymetrickou lokalizací nekódujících RNA v rámci jedné buňky. Nerovnoměrná lokalizace miRNA uvnitř oocytu naznačuje jejich úlohu v časo-prostorové regulaci translace během časného embryonálního vývoje *X. laevis*. Jinými slovy lze tyto krátké regulační molekuly, společně s maternální mRNA a proteiny, zahrnout do skupiny významných buněčných determinantů, které se podílejí na diferenciaci jednotlivých buněk a na utváření tělního plánu embrya. Tuto teorii podporuje i studie, kde bylo ukázáno, že miR-18 se podílí na vymezení a formování zárodečných listů během časného embryonálního vývoje. Exprese miR-18 byla detekovaná v ektodermu a mezodermu a jeho funkce spočívá v potlačení endodermálního fenotypu (Colas *et al.*, 2012). Zároveň tato skutečnost koreluje s výsledkem pokusů provedených v Laboratoři genové exprese, kde byla miR-18 lokalizována do animální poloviny zralého oocytu, což představuje oblast presumptivního ektodermu a částečně i presumptivního mezodermu.

Na základě dosažených výsledků byly popsány lokalizační profily maternální mRNA a miRNA podél animálně-vegetativní osy zralého oocytu *X. laevis*. Ukazuje se, že nerovnoměrná lokalizace představuje klíčový mechanismus asymetrického dělení buněk během časného embryonálního vývoje. Již třínásobný rozdíl v koncentraci buněčného determinantu může vést ke kompletně odlišnému buněčnému osudu (Smith and Gurdon, 2004). Tato nerovnoměrná lokalizace se však nevztahuje pouze na maternální biomolekuly. Bylo dokázáno, že dochází i k asymetrické distribuci anorganických iontů a kovů, jako je měď, zinek a železo, uvnitř oocytu *X. laevis* (Popescu *et al.*, 2007).

Všechny výše předkládané výsledky byly stanoveny pomocí kvantitativní metody RT-qPCR. Tato metoda klade vysoké nároky na kvalitu a stabilitu použité RNA. Již částečná degradace RNA vede ke zvýšení technické variability a snižuje tak přesnost získaných výsledků. Z tohoto důvodu byla další fáze práce zaměřena

na objasnění vlivu enzymatické a teplotní degradace na integritu RNA molekul. Enzymatická degradace zastupuje přirozenou degradaci, taktéž označovanou jako degradaci *post mortem*. Vzhledem k získaným výsledkům je zřejmé, že různé typy RNA vykazují odlišnou citlivost k účinku degradace *post mortem*. Přestože u rRNA nedocházelo k degradaci ani po několika desítkách minut, mRNA podléhala degradaci v řádech jednotek minut. Pravděpodobnou příčinou se zdá být vyšší odolnost rRNA proti RNázám, které přednostně degradují molekuly s polyA koncem a methylguanosinovou čepičkou. Nízký stupeň degradace rRNA se však může promítnout do chybného vyhodnocení kvality RNA. Některé kapilární elektroforézy vyhodnocují intergitu RNA pouze na základě poměru 18S/28S rRNA. I přesto, že je analyzovaná RNA vyhodnocena jako vysoce kvalitní, může být většina mRNA molekul ve vzorku degradována. Dalším cílem výzkumu bylo porovnání vlivu enzymatické degradace *post mortem* na maternální a zygotickou RNA. Jako modelové systémy sloužili zralé oocyty *X. laevis* a pulci ve vývojovém stádiu 40. Vzhledem k výsledkům této analýzy bylo prokázáno, že maternální mRNA vykazuje o dva řády vyšší odolnost než zygotická mRNA. Tento rozdíl může být způsoben tím, že maternální mRNA je více chráněná před působením RNáz než transkriptom běžné buňky, který má nedostatek těchto ochranných faktorů.

Jako druhý byl testován mechanismus fyzikální degradace, která byla zastoupena teplotní degradací. Na základě dosažených výsledků se ukázalo, že zahříváním izolovaných vzorků RNA na teplotu 80 ^{o}C se snižuje integrita všech typů RNA se stejnou účinností a působení této degradace lze pozorovat až v řádech hodin.

Poslední cíl disertační práce souvisel s kvantifikací genové exprese prostřednictvím qPCR přístroje BioMark^{TM}. Tento vysokokapacitní systém byl použit ke stanovení lokalizace maternální mRNA podél animálně-vegetativní osy zralého oocytu *X. laevis*. Hlavní podmínkou úspěšné kvantifikace pomocí BioMark^{TM} přístroje je vysoká koncentrace templátových molekul. Dostatečné množství templátu je zajišťováno pre-amplifikační reakcí. Efektivita této reakce je však ovlivňována jak počtem zvolených cyklů, tak množstvím vstupní RNA nebo mírou exprese studovaného genu. Dle dosažených výsledků je zřejmé, že nejúčinnější pre-

amplifikační reakce probíhá při použití řádově desítek ng templátu (testováno bylo 5 a 20 ng celkové RNA) společně s 15 nebo 18 pre-amplifikačními cykly. Stejně tak je nutné, aby v průběhu pre-amplifikace nedocházelo ke zvyšení variability získaných dat. Tato podmínka byla ověřena při studiu lokalizace maternální mRNA uvnitř oocytu. Porovnání lokalizačních profilů transkriptů *maml* (animální gradient) a *vg1* (vegetativní gradient) před pre-amplifikací a po pre-amplifikaci potvrdilo, že tento krok nepředstavuje zvýšené riziko vnesení chyby do naměřených dat.

6. Závěry

1. Podařilo se identifikovat dvě hlavní skupiny maternálních mRNA, které se projevují odlišným lokalizačním gradientem podél animálně-vegetativní osy uvnitř zralého oocytu *X. laevis*. Animální gradient vzniká spontánně pasivní difúzí transkriptů z jádra, zatímco vegetativní gradient je tvořen aktivním transportem.

2. Patnáct řezů připravených z oocytu pomocí vysokorozlišovací metody umožnilo rozlišit dvě vegetativní podskupiny mRNA, které se liší profilem lokalizačního gradientu. Determinanty zárodečné plazmy jsou strmě lokalizované ve vegetativním pólu, zatímco gradient ostatních vegetativně lokalizovaných mRNA vykazuje pozvolný a kontinuální nárůst směrem k vegetativnímu pólu.

3. Byla potvrzena nerovnoměrná distribuce maternálních mRNA, které jsou asymetricky lokalizované podél animálně-vegetativní osy zralého oocytu, do jednotlivých dceřiných buněk během rýhování *X. laevis*. Animální blastomery z vývojových stádií 8 buněk, 16 buněk a 32 buněk obsahují jiné maternální transkripty než vegetativní blastomery.

4. Všechny studované maternální mRNA vykazovaly rovnoměrnou distribuci podél dorzo-ventrální a pravo-levé tělní osy u embryí z vývojových stádií 8 buněk, 16 buněk a 32 buněk. Z čehož vyplývá, že animálně-vegetativní asymetrie vzniká důsledkem gradientů mRNA, ale specifikace dorzo-ventrální a pravo-levé tělní osy vzniká nerovnoměrnou distribucí jiných biomolekul, například proteinů.

5. Byly popsány dva základní profily asymetrické lokalizace miRNA podél animálně-vegetativní osy zralého oocytu *X. laevis*. Tato nerovnoměrná lokalizace naznačuje, že miRNA společně s maternální mRNA a proteiny lze

zahrnout do skupiny významných buněčných determinantů, které se podílejí na časo-prostorové diferenciaci jednotlivých buněk a na utváření tělního plánu embrya.

6. Byl popsán vliv enzymatické degradace *post mortem* a teplotní degradace na různé typy molekul RNA. Na působení degradace *post mortem* je mnohem citlivější mRNA, zatímco rRNA vykazuje vysokou stabilitu. Z tohoto výsledku vyplývá, že při přirozené degradaci *post mortem* není žádoucí vyhodnocovat integritu celkové RNA pouze na základě integrity rRNA.

7. Bylo zjištěno, že RNA z pulců vykazuje nižší stabilitu ve srovnání s maternální RNA, která je pravděpodobně více chráněná před působením RNáz v průběhu enzymatického typu degradace *post mortem*.

8. Bylo dokázáno, že pre-amplifikační reakce nezvyšuje variabilitu naměřených dat a zároveň byly vyhodnoceny optimální podmínky počtu pre-amplifikačních cyklů, množství celkové RNA a míry exprese studovaného genu, které ovlivňují efektivitu této reakce.

7. Seznam použité literatury

Adams DS, Robinson KR, Fukumoto T, Yuan S, Albertson RC, Yelick P, Kuo L, McSweeney M and Levin M (2006) Early, H+-V+ATPase-dependent proton flux is necessary for consistent left-right patterning of non-mammalian vertebrates. *Development,* **133**:1657-1671.

Amaya E, Offield MF and Grainger RM (1998) Frog genetics: *Xenopus tropicalis* jumps into the future. *Trends Genet,* **14**:253-255.

Bartel DP (2004) MicroRNAs: genomics, biogenesis, mechanism and function. *Cell,* **116**:281-297.

Beck CW and Slack JM (2001) An amphibian with ambition: a new role for *Xenopus* in the 21st century. *Genome Biol,* **2**: reviews1029.

Bellerby CW (1934) A rapid test for the diagnostic of pregnancy. *Nature,* **133**:494-495.

Benes V, Collier P, Kordes C, Stolte J, Rausch T, Muckentaler MU, Häussinger D and Castoldi M (2015) Identification of cytokines-induced modulation of microRNAs expression and secretion as measured by a novel microRNA specific qPCR assay. Accepted in *Sci Rep*.

Bisbee CA, Baker MA, Wilson AC, Haji-Azimi I and Fischberg M (1977) Albumin phylogeny for clawed frogs (*Xenopus*). *Science,* **195**:785-787.

Blanpain C, Lowry WE, Geoghegan A, Polak L and Fuchs E (2004) Self-renewal, multipotency, and the existence of two cell populations within an epithelial stem cell niche. *Cell,* **118**:635-648.

Blum M, Schweickert A, Vick P, Wright CV and Danilchik MV (2014) Symmetry breakage in the vertebrate embryo: when does it happen and how does it work? *Dev Biol,* **393**:109-123.

Boettger T, Knoetgen H, Wittler L and Kessel M (2001) The avian organizer. *Int J Dev Biol,* **45**:281-287.

Bohnsack MT, Czaplinski K and Gorlich D (2004) Exportin 5 is a RanGTP-dependent dsRNA-binding protein that mediates nuclear export of pre-miRNAs. *RNA,* **10**:185-191.

Brengues M, Teixeira D and Parker R (2005) Movement of eucaryotic mRNAs between polysomes and cytoplasmic processing bodies. *Science,* **310**:486-489.

Bubunenko M, Kress TL, Vempati UD, Mowry KL and King ML (2002) A consensus RNA signal that directs germ layer determinants to the vegetal cortex of *Xenopus* oocytes. *Dev Biol,* **248**:82-92.

Bunney TD, De Boer AH and Levin M (2003) Fusicoccin signaling reveals 14-3-3 protein function as a novel step in left-right patterning during amphibian embryogenesis. *Development,* **130**:4847-4858.

Cai X, Hagedorn CH and Cullen BR (2004) Human microRNAs are processed from capped, polyadenylated transcripts that can also function as mRNAs. *RNA,* **10**:1957-1966.

Colas AR, McKeithan WL, Cunningham TJ, Bushway PJ, Garmire LX, Duester G, Subramaniam S and Mercola M (2012) Whole-genome microRNA screening identifies let-7 and mir-18 as regulators of germ layer formation during early embryogenesis. *Genes Dev,* **26**:2567-2579.

Cooke J (1985) The system specifying body position in the early development of *Xenopus*, and its response to early pertubations. *J Embryol Exp Morphol,* **89**:69-87.

Cuykendall TN and Houston DW (2010) Identification of germ plasm-associated transcripts by microarray analysis of *Xenopus* vegetal cortex RNA. *Dev Dyn,* **239**:1838-1848.

Dale L and Slack JM (1987) Fate map for the 32-cell stage of *Xenopus laevis*. *Development,* **99**:527-551.

Danilchik MV and Gerhadt JC (1987) Differentiation of the animal-vegetal axis in *Xenopus laevis* oocytes. I. Polarized intracellular translocation of platelets establishes the yolk gradient. *Dev Biol,* **122**:101-112.

Darras S, Marikawa Y, Elinson RP and Lemaire P (1997) Animal and vegetal pole cells of early *Xenopus* embryos respond differently to maternal dorsal determinants: implications for the patterning of the organiser. *Development,* **124**:4275-4286.

Denegre JM and Danilchik MV (1993) Deep cytoplasmic rearrangements in axis-respecified *Xenopus* embryos. *Dev Biol,* **160**:157-164.

Deshler JO, Highett J and Schnapp (1997) Localization of *Xenopus* Vg1 mRNA by vera protein and the endoplasmatic reticulum. *Science,* **276**:1128-1131.

Dumont JN (1972) Oogenesis in *Xenopus laevis* (Daudin) I. Stages of oocyte development in laboratory maintained animals. *J Morphol,* **136**:153-179.

Elinson RP and Pasceri P (1989) Two UV-sensitive targets in dorsoanterior specification of frog embryos. *Development,* **106**:511-518.

Etkin LD (1997) A new face fro the endoplasmic reticulum: RNA localization. *Science,* **276**:1092-1093.

Etkin LD and Balcells S (1985) Transformed *Xenopus* embryos as a transient expression system to analyze gene expression at the midblastula transition. *Dev Biol,* **108**:173-178.

Evans BJ, Kelley DB, Tinsley RC, Melnick DJ and Cannatella DC (2004) A mitochondrial DNA phylogeny of African clawed frogs: phylogeography and implications for polyploid evolution. *Mol Phylogenet Evol,* **33**:197-213.

Esquela-Kerscher A and Slack FJ (2006) Oncomirs – microRNAs with a role in cancer. *Nat Rev Cancer,* **6**:259-269.

Fujisue M, Kobayakawa Y and Yamana K (1993) Occurrence of dorsal axis-inducing activity around the vegetal pole of an uncleaved *Xenopus* egg and displacement to the equatirial region by cortical rotation. *Development,* **118**:163-170.

Fukumoto T, Kema IP and Levin M (2005a) Serotonin signaling is a very early step in patterning of the left-right axis in chick and frog embryos. *Curr Biol,* **15**:794-803.

Fukumoto T, Blakely R and Levin M (2005b) Serotonin transporter function is an early step in left-right patterning in chick and frog embryos. *Dev Neurosci,* **27**:349-363.

Gautreau D, Cote CA and Mowry KL (1997) Two copies of a subelement from the Vg1 RNA localization sequence are sufficient to direct vegetal localization in *Xenopus* oocytes. *Development,* **124**:5013-5020.

Gerhart J, Danilchik M, Doniach T, Roberts S, Rowning B and Stewart R (1989) Cortical rotation of the *Xenopus* egg: consequences for the anteroposterior pattern of embryonic dorsal development. *Development,* **107**:37-51.

Goda T, Abu-Daya A, Carruthers S, Clark MD, Stemple DL and Zimmerman LB (2006) Genetic screens for mutations affecting development of *Xenopus tropicalis*. *PLoS Genet,* **2**:e91.

Gurdon JB (1962) The developmental capacity of nuclei taken from intestinal epithelium cells of feeding tadpoles. *J Embryol Exp Morphol,* **10**:622-640.

Gurdon JB (1968) Changes in somatic cell nuclei inserted into growing and maturing amphibian oocytes. *J Embryol Exp Morph,* **20**:401-414.

Gurdon JB (1975) Attmepts to analyse the biochemical basis of regional defferences in animal eggs. *Ciba Found Symp,* **0**:223-239.

Gurdon JB, Elsdale TR and Fishberg M (1958) Sexually mature individuals of *Xenopus laevis* from the transplantation of single somatic nuclei. *Nature,* **182**:64-65.

Gurdon JB and Hopwood N (2000) The introduction of *Xenopus laevis* into developmental biology: of empire, pregnancy testing and ribosomal genes. *Int J Dev Biol,* **44**:43-50.

Gurdon JB, Lane CD, Woodland HR and Marbaix G (1971) Use of frog eggs and oocytes for the study of messenger RNA and its translation in living cells. *Nature,* **233**:177-182.

Hammell CM (2008) The microRNA-argonaute complex:a platform for mRNA modulation. *RNA Biol,* **5**:123-127.

Hatayama M, Mikoshiba K and Aruga J (2011) IP3 signaling is required for cilia formation and left-right body axis determination in *Xenopus* embryos. *Biochem Biophys Res Commun,* **410**:520-524.

Heasman J (2002) Morpholino oligos: making sense of antisense? *Dev Biol,* **243**:209-214.

Heasman J (2006) Maternal determinants of embryonic cell fate. *Semin Cell Dev Biol,* **17**:93-98.

Heasman J, Kofron M and Wylie (2000) Beta-catenin signaling activity dissected in the early *Xenopus* embryo: a novel antisense approach. *Dev Biol,* **222**:124-134.

Heasman J, Quarmby J and Wylie CC (1984) The mitochondrial cloud of *Xenopus* ocytes:the source of germinal granule material. *Dev Biol,* **105**:458-469.

Hibio N, Hino K, Shimizu E, Nagata Y and Ui-Tei K (2012) Stability of miRNA 5´terminal and seed regions in correlated with experimentally observed miRNA-mediated silencing efficacy. *Sci Rep,* **2**: 996.

Hirsch N, Zimmerman LB and Grainger RM (2002) *Xenopus*, the next generation: *X. tropicalis* genetics and genomics. *Dev Dyn,* **225**:422-433.

Houston DW (2013) Regulation of cell polarity and RNA localization in vertebrate oocyte. *Int Rev Cell Mol Biol,* **306**:127-185.

Hyatt BA, Lohr JL and Yost HJ (1996) Initiation of vertebrate left-right axis formation by maternal Vg1. *Nature,* **384**:62-65.

Iwasaki S and Tomari Y (2009) Argonaute-mediated translational repression (and activation). *Fly (Austin),* **3**:204-206.

Jullien J, Pasque V, Halley-Stott RP, Miyamoto K and Gurdon JB (2011) Mechanism of nuclear reprogramming by eggs and oocytes: a deterministic process? *Nat Rev Mol Cell Biol*, **12**:453-459.

King ML, Messitt TJ and Mowry KL (2005) Putting RNAs in the right place at the right time: RNA localization in the frog oocyte. *Biol Cell,* **97**:19-33.

Kloc M, Bilinski S, Chan AP, Allen LH, Zearfoss NR and Etkin LD (2001) RNA localization and germ cell determination in *Xenopus*. *Int Rev Cytol,* **203**:63-91.

Kloc M, Dougherty MT, Bilinski S, Chan AP, Brey E, King ML, Patrick CW Jr and Etkin LD (2002) Three-dimensional ultrastructural analysis of RNA distribution within germinal granules of *Xenopus*. *Dev Biol,* **241**:79-93.

Kloc M and Etkin LD (1994) Delocalization of Vg1 mRNA from the vegetal cortex in *Xenopus* oocytes after destruction of Xlsirt RNA. *Science,* **265**:1101-1103.

Kloc M and Etkin LD (1995) Two distinct pathways for the localization of RNAs at the vegetal cortex in *Xenopus* oocytes. *Development,* **121**:287-297.

Kloc M, Larabell C, Chan AP and Etkin LD (1998) Contribution of METRO pathway localized molecules to the organization of the germ cell lineage. *Mech Dev,* **75**:81-93.

Kloc M, Larabell C and Etkin LD (1996) Elaboration of the messenger transport organizer pathway for lacalization of RNA to the vegetal cortex of *Xenopus* oocytes. *Dev Biol,* **180**:119-130.

Kloc M, Spohr G and Etkin LD (1993) Translocation of repetitive RNA sequences with the germ plasm in *Xenopus* oocytes. *Science,* **262**:1712-1714.

Knoblich JA (2010) Asymmetric cell division: recent developments and their implications for tumour biology. *Nat Rev Mol Cell Biol,* **11**:849-597.

Knoblich JA (2008) Mechanisms of asymmetric stem cell division. *Cell,* **132**:583-597.

Kroll KL and Amaya E (1996) Transgenic *Xenopus* embryos from sperm nuclear transplantations reveal FGF signaling requirements during gastrulation. *Development,* **122**:3173-3183.

Kwon S, Abramson T, Munro TP, John Cm, Kohrmann and Schnapp BJ (2002) UUCAC- and vera-dependent localization of VegT TNA in *Xenopus* oocytes. *Curr Biol,* **12**:558-564.

Langley AR, Smith JC, Stemple DL and Harvey SA (2014) New insights into the maternal to zygotic transition. *Development,* **141**:3834-3841.

Legagneux V, Omilli F and Osborne HB (1995) Substrate-specific regulation of RNA deadenylation in *Xenopus* embryo and activated egg extracts. *RNA,* **1**:1001-1008.

Lee Y, Ahn C, Han J, Choi H, Kim J, Yim J, Lee J, Provost P, Radmark O, Kim S and Kim VN (2003) The nuclear RNase III Drosha initiates microRNA processing. *Nature,* **425**:415-419.

Lee Y, Kim M, Han J, Yeom KH, Lee S, Baek SH and Kim VN (2004) MicroRNA genes are transcribed by RNA polymerase II. *EMBO J,* **23**:4051-4060.

Levin M, Thorlin T, Robinson KR, Nogi T and Mercola M (2002) Asymmetries in H+/K+-ATPase and cell membrane potentials comprise a very early step in left-right patterning. *Cell,* **111**:77-89.

Lewis RA, Kress TL, Cote CA, Gautreau D, Rokop ME and Mowry KL (2004) Conserved and clustered RNA recognition sequences are a critical feature of signals directing RNA localization in *Xenopus* oocytes. *Mech Dev,* **121**:101-109.

Liu J, Valencia-Sanchez MA, Hannon GJ and Parker R (2005) MicroRNA-dependent localization of targeted mRNAs to mammalian P-bodies. *Nat Cell Biol,* **7**:719-723.

Marikawa Y, Li Y and Elinson RP (1997) Dorsal determinants in the *Xenopus* egg are firmly associated with the vegetal cortex and behave like activators of the Wnt pathway. *Dev Biol,* **191**:69-79.

Meric F, Searfoss AM, Wormington M and Wolffe AP (1996) Masking and unmasking maternal mRNA. The role of polyadenylation, transcription, splicing, and nuclear history. *J Biol Chem,* **271**:30804-30810.

Messitt TJ, Gagnon JA, Kreiling JA, Pratt CA, Yoon YJ and Mowry KL (2008) Multiple kinesin motors coordinate cytoplasmic RNA transport on a subpopulation of microtubules in *Xenopus* oocytes. *Dev Cell,* **15**:426-436.

Miller JR, Rowning BA, Larabell CA, Yang-Snyder JA, Bates RL and Moon RT (1999) Establishment of the dorsal-ventral axis in *Xenopus* embryos coincides with dorsal enrichment of dishevelled that is dependent on cortical rotation. *J Cell Biol,* **146**:427-437.

Moon RT and Kimelman D (1998) From cortical rotation to organizer gene expression: toward a molecular explanation of axis specification on *Xenopus*. *Bioessays,* **20**:536-545.

de Moor CH and Richter JD (1997) The Mos pathway regulates cytoplasmic polyadenylation in *Xenopus* oocytes. *Mol Cell Biol,* **17**:6419-6426.

de Moor CH and Richter JD (1999) Cytoplasmic polyadenylation elements mediate masking and unmasking of cyclin B1 mRNA. *EMBO J,* **18**:2294-2303.

Mowry KL and Cote CA (1999) RNA sorting in *Xenopus* oocytes and embryos. *FASEB J,* **13**: 435-445.

Newport J and Kirschner M (1982) A major developmental transition in early *Xenopus* embryos: I. characterization and timing of cellular changes at the midblastula stage. *Cell,* **30**:675-686.

Nieuwkoop PD (1969) The formation of the mesoderm in the urodelean amphibians. I. Introduction by the endoderm. *Wil Roux Arch Entw Mech Org,* **162**:341-373.

Nieuwkoop PD (1973) The „Organisation Center" of the amphibian embryo: its origin, spatial organisation and morphogenetic action. *Adv Morph,* **10**:1-39.

Pandur PD, Sullivan SA and Moody SA (2002) Multiple maternal influences on dorsal-ventral fate of *Xenopus* animal blastomeres. *Dev Dyn,* **225**:581-587.

Paris J and Philippe M (1990) Poly(A) metabolism and polysomal recruitment of maternal mRNAs during early *Xenopus* development. *Dev Biol,* **140**:221-224.

Parker R and Sheth U (2007) P bodies and the control of mRNA translation and degradation. *Mol Cell,* **25**:635-646.

Pereira G and Yamashita YM (2011) Fly meets yeast: Checking the correct orientation of cell division. *Trends Cell Biol,* **21**:526-533.

Pfeiffer DC and Gard DL (1999) Microtubules in *Xenopus* oocytes are oriented with their minus-ends towards the cortex. *Cell Motil Cytoskeleton,* **44**:34-43.

Popescu BF, Belak ZR, Ignatyey K, Ovsenek N and Nichol H (2007) Asymetric distribution of metals in the *Xenopus laevis* oocyte: a synchrotron X-ray fluorescence microprobe study. *Biochem Cell Biol,* **85**:537-542.

Preiss T, Muckenthaler M and Hentze MW (1998) Poly(A)-tail-promoted translation in yeast: implication for translational control. *RNA,* **4**:1321-1331.

Rowning BA, Wells J, Wu M, Gerhart JC, Moon RT and Larabell CA (1997) Microtubule-mediated transport of organelles and localization of beta-catenin to the future dorsal side of *Xenopus* eggs. *Proc Natl Acad Sci USA,* **94**:1224-1229.

Sander K and Faessler PE (2001) Introducing the Spemann-Mangold organizer: experiments and insights that generated a key concept in developmental biology. *Int J Dev Biol,* **45**:1-11.

Schatten H and Sun QY (2010) The role of centrosomes in fertilization, cell division and establishment of asymmetry during embryo development. *Semin Cell Dev Biol,* **21**:174-84.

Schier AF (2007) The maternal-zygotic transition: death and birth of RNAs. *Science,* **316**:406-407.

Schroeder KE, Condic ML, Eisenberg LM and Yost HJ (1999) Spatially regulated translation in embryos: asymmetric expression of maternal wnt-11 along the dorso-ventral axis in *Xenopus*. *Dev Biol,* **214**: 288-297.

Schroeder MM and Gard DL (1992) Organization and regulation of cortical microtubules during the first cell cycle of *Xenopus* eggs. *Development,* **114**:699-709.

Schweickert A, Vick P, Getwan M, Weber T, Schneider I, Eberhardt M, Beyer T, Pachur A and Blum M (2010) The nodal inhibitor Coco is a critical target of leftwards flow in *Xenopus*. *Curr Biol,* **20**:738-743.

Shahriyari L and Komarova NL (2013) Symmetric vs. asymmetric stem cell divisions: an adaptation against cancer? *PLoS One,* **8**:e76195.

Shapiro HA and Zwarenstein H (1934) A rapid test for pregnancy on *Xenopus laevis*. *Nature,* **133**:762.

Shav-Tal Y and Singer RH (2005) RNA localization. *J Cell Sci,* **118**:4077-4081.

Sindelka R, Jonak J, Hands R, Bustin SA and Kubista M (2008) Intracellular expression profiles measured by real-time PCR tomography in the *Xenopus laevis* oocyte. *Nucleic Acids Res,* **36**:387-392.

Smith JC and Gurdon JB (2004) Many ways to make a gradient. *Bioessays,* **26**:705-706.

Smits AH, Lindeboom RG, Perino M, van Heeringen Sj, Veenstra GJ and Vermeulen M (2014) Global absolute quantification reveals tight regulation of protein expression in single *Xenopus* eggs. *Nucleic Acids Res,* **42**:9880-9891.

Snedden DD, Bertke MM, Vernon D and Huber PW (2013) RNA localization in *Xenopus* oocytes uses a core group of trans-acting factors irrespective of destination. *RNA,* **19**:889-895.

Stennard F, Zorn AM, Ryan K, Garrett N and Gurdon JB (1999) Differential expression of VegT and Antipodean protein isoforms in *Xenopus*. *Mech Dev,* **86**:87-98.

Sive HL (1993) The frog prince-ss: a molecular formula for dorsoventral patterning in *Xenopus*. *Genes Dev,* **7**:1-12.

Sive HL, Grainger MR and Harland MR (2000) Early development of *Xenopus laevis* – A laboratory manual. *Cold Spring Harbor Laboratory Press*, chapter 2, figure 2.1.

Sudarwati S and Nieuwkoop PD (1971) Mesoderm induction in the anuran *Xenopus laevis*. *Roux´Arch Dev Biol,* **175**:199-204.

Sun L, Bertke MM, Champion MM, Zhu G, Huber PW and Dovichi NJ (2014) Quantitative proteomics of *Xenopus laevis* embryos: expression kinetics of nearly 4000 proteins during early development. *Sci Rep,* **4**:4365.

Tang GQ and Maxwell ES (2008) *Xenopus* miRNAs genes are predominantly located within introns and are differentially expressed in adult frog tissues via post-transcriptional regulation. *Genome Res,* **18**:104-112.

Thiebaud CH and Fischberg M (1977) DNA content in the genus *Xenopus*. *Chromosoma,* **59**:253-257.

Thomsen GH and Melton DA (1993) Processed Vg1 protein is an axial mesoderm inducer in *Xenopus*. *Cell,* **74**:433-441.

Toyoizumi R, Ogasawara T, Takeuchi S and Mogi K (2005) *Xenopus* nodal related-1 is indispensable only for left-right axis determination. *Int J Dev Biol*, **49**:923-938.

Tymowska J (1973) Karyotype analysis of *Xenopus tropicalis* Gray, *Pipidae*. *Cytogenet Cell Genet,* **12**:297-304.

Tymowska J and Fischberg M (1973) Chromosome complements of the genus *Xenopus*. *Chromosoma*, **44**:335-342.

Vandenberg LN and Levin M (2010) Far from solved: a perspective on what we know about early machanisms of left-right asymmetry. *Dev Dyn,* **239**:3131-3146.

Varnum SM and Wormington WM (1990) Deadenylation of maternal mRNAs during *Xenopus* oocyte maturation does not require specific cis-sequences: a default mechanism for translational control. *Genes Dev,* **4**:2278-2286.

Viebahn C (2001) Hensen´s node. *Genesis* **29**:96-103.

Vincent JP and Gerhart JC (1987) Subcortical rotation in *Xenopus* eggs: an early step in embryonic axis specification. *Dev Biol,* **123**:526-539.

Vincent JP, Scharf SR and Gerhart JC (1987) Subcortical rotation in *Xenopus* eggs: a preliminary study of its mechanochemical basis. *Cell Motil Cytoskeleton,* **8**:143-154.

Wang X, Xu X, Ma Z, Huo Y, Xiao Z, Li Y and Wang Y (2011) Dynamic mechanisms for pre-miRNA biding and export by Exportin-5. *RNA,* **17**:1511-1528.

Weaver C and Kimelman D (2004) Move it or lose it: axis specification in *Xenopus*. *Development,* **131**:3491-3499.

Werdien D, Peiler G and Ryffel GU (2001) FLP and Cre recombinase function in *Xenopus* embryo. *Nucleic Acids Res,* **29**:E53.

White JA and Heasman J (2008) Maternal control of pattern formation in *Xenopus laevis*. *J Exp Zool B Mol Dev Evol,* **310**:73-84.

Wickens M (1990) In the beginning is the end: regulation of poly(A) addition and removal during early development. *Trends Biochem Sci,* **15**:320-324.

Yisraeli JK, Sokol S and Melton DA (1990) A two-step model for the localization of maternal mRNA in *Xenopus* oocytes: involvement of microtubules and microfilaments in the translocation and anchoring of Vg1 mRNA. *Development,* **108**:289-298.

Yost C, Torres M, Miller JR, Huang E, Kimelman D and Moon RT (1996) The axis-inducing activity, stability, and subcellular distribution of beta-catenin is regulated in *Xenopus* embryos by glycogen synthase kinase 3. *Genes Dev,* **10**:1443-1454.

Zhang J and King ML (1996) *Xenopus* VegT RNA is localized to the vegetal cortex during oogenesis and encodes a novel T-box transcription factor involved in mesodermal patterning. *Development,* **122**:4119-4129.

Zhou Y and King ML (1996a) Localization of Xcat-2 RNA, a putative germ plasm component, to the mitochondrial cloud in *Xenopus* stage I oocyte. *Development*, **122**:2947-2953.

Zhou Y and King ML (1996b) RNA transport to the vegetal cortex of *Xenopus* oocytes. *Dev Biol*, **179**:173-183.

Zhou Y and King ML (2004) Sending RNAs into the future: RNA localization and germ cell fate. *IUBMB Life*, **56**:19-27.

8. Seznam zkratek

Ago	Argonaute protein
MO	morpholino oligonukleotides
cdx1	caudal type homeobox 1
CPE	cytoplasmic polyadenylation element
dazl	deleted in azoospermia-like
ddx25	deadsouth
dvl	dishevelled
gdf1	growth differentiation factor 1
GRP	gastrocoel roof plate
gsk3β	glycogen synthase kinase 3 beta
hCG	human chorionic gonadotropin
HM	hlavový mezoderm
LPM	lateral plate mesoderm
MBT	mid-blastula transition
METRO	messenger transport organizer
miRNA	micro ribonucleic acid; microRNA
mRNA	messenger ribonucleic acid
mRNP	mRNA and protein complex
mtRNA	mitochondrial RNA
OCT	optimal cutting temperature
P-bodies	processing bodies
pgat	primordial germ cell-associated transcript

pitx2	paired-like homeodomain 2
qPCR	quantitative polymerase chain reaction
RISC	RNA-induced silencing complex
rRNA	ribosomal RNA
RT-miQPCR	reverse transcriptase miRNA quantitative polymerase chain reaction
RT-qPCR	reverse transcriptase quantitative polymerase chain reaction
RQI	RNA Quality Indicator
scaRNA	small cajal body-specific RNA
UTR	untranslated region
vegt	vegetal T-box transcription factor
Wnt	Wingless/Int-1
wnt11	wingless-type member 11
xbra	*Xenopus* brachyury
Xlsirt	*Xenopus laevis* short interspersed repeat transcripts
xnr	*Xenopus* nodal related